This is to certify that the

dissertation entitled

TWO-DIMENSIONAL QUASI-STATIC KNEE MODEL
FOR THE ESTIMATION OF LIGAMENT AND QUADRICEPS
FORCES AS A FUNCTION OF KNEE FLEXTION

presented by

Claudia Alejandra Angeli

has been accepted towards fulfillment
of the requirements for

Ph.D. degree in Kinesiology

Dianne Ulibarri
Major professor

Date May 14, 2001

TWO-DIMENSIONAL QUASI-STATIC KNEE MODEL FOR THE ESTIMATION OF LIGAMENT AND QUADRICEPS FORCES AS A FUNCTION OF KNEE FLEXION

By

Claudia Alejandra Angeli

A DISSERTATION

Submitted to
Michigan State University
In partial fulfillment of the requirements
For the degree of

DOCTOR OF PHILOSOPHY

Department of Kinesiology

2001

ABSTRACT

TWO-DIMENSIONAL QUASI-STATIC KNEE MODEL FOR THE ESTIMATION OF LIGAMENT AND QUADRICEP FORCES AS A FUNCTION OF KNEE FLEXION

By

Claudia Alejandra Angeli

The knee joint is one of the most commonly injured joints in sport activities. A two-dimensional quasi-static knee model was developed to estimate the forces sustained by the ligaments and generated by the quadriceps as a function of knee flexion. The tibio-femoral and patello-femoral joints were defined mathematically and modeled as frictionless joints. The anterior and posterior cruciate ligaments and the collateral ligament were modeled as single fiber extensible units. The instantaneous center of rotation was used in the estimation of the rolling and sliding characteristics of the knee joint. External forces were used as input parameters to the model. The model was tested using kinematic and kinetic data obtained during squatting for three different conditions: normal, ACL-deficient and ACL-reconstructed. The results obtained with the model showed the expected increase in anterior-posterior motion of the femur relative to the tibia in the ACL-deficient knee. Laxity values were higher for the ACL-deficient knee and had return to normal following the ACL-reconstruction.

To my family, for their constant support and encouragement.
And to Dr. Dianne Ulibarri, for inspiring me to reach for
excellence in every aspect of my life.

Special T

Dr. Robe

biomecha

Patricia S

All my co

times and

My comm

ACKNOWLEDGMENTS

Special Thanks to:

Dr. Robert Soutas-Little, for giving me the tools to be successful in the field of biomechanics.

Patricia Soutas-Little, for the constant support and encouragement.

All my coworkers and students at the Biomechanics Evaluation Laboratory, for the great times and constant support.

My committee members, for all the great advice.

TABLE OF CONTENTS

Table 1: St

Table 2: Le

Table 3: U

LIST OF TABLES

LIST OF FIGURES

Ix(t)
Iy(t)
b
t
Ix"
Iy"
θ
θ
Ixacl
Iyacl
Ixpcl
Iypcl
Ixcl
Iycl
Ixacl"
Iyacl"
Ixpcl"
Iypcl"
Ixcl"
Iycl"

KEY TO SYMBOLS

Ix(t)	X variable to define the involute circle
Iy(t)	Y variable to define the involute circle
b	radius of the involute circle
t	parameter of dependency for the contraint of the involute circle
Ix"	parametric equation of the involute with a prescribed rotation
Iy"	parametric equation of the involute with a prescribed rotation
ϕ	90 degree rotation of the involute
θ	angle of knee flexion
Ixacl	x-coordinate for the insertion point of the ACL on the femur at full extension
Iyacl	y-coordinate for the insertion point of the ACL on the femur at full extension
Ixpcl	x-coordinate for the insertion point of the PCL on the femur at full extension
Iypcl	y-coordinate for the insertion point of the PCL on the femur at full extension
Ixcl	x-coordinate for the insertion point of the CL on the femur at full extension
Iycl	y-coordinate for the insertion point of the CL on the femur at full extension
Ixacl"	x-coordinate for the insertion point of the ACL on the femur at θ degrees of flexion
Iyacl"	y-coordinate for the insertion point of the ACL on the femur at θ degrees of flexion
Ixpcl"	x-coordinate for the insertion point of the PCL on the femur at θ degrees of flexion
Iypcl"	y-coordinate for the insertion point of the PCL on the femur at θ degrees of flexion
Ixcl"	x-coordinate for the insertion point of the CL on the femur at θ degrees of flexion
Iycl"	y-coordinate for the insertion point of the CL on the femur at θ degrees of flexion

β	patellar tendon angle
β	
α	angle of inclination of the patella
α	
γ	angle between quadriceps tendon and patello-femoral force
γ	
δ	angle between the patellar tendon and patello-femoral force
δ	
F	ligament force
k	stiffness coefficient
Δ	change in length of the ligament
L	ligament length
Lo	original ligament length
Lacl	ligament length of the ACL
Lpcl	ligament length of the PCL
Lcl	ligament length of the CL
Oxacl	x-coordinate for the origin of the ACL on the tibia
Oxpcl	x-coordinate for the origin of the PCL on the tibia
Oxcl	x-coordinate for the origin of the CL on the tibia
Oycl	y-coordinate for the origin of the CL on the tibia
tp	y-coordinate for the position of the tibial plateau
ι	length ratio of the ligaments
j	subscript used to differentiate among ligaments
$\bar{r}$	position vector
$\bar{w}$	angular velocity
$\bar{v}$	linear velocity
$D_{sliding}$	sliding distance of the femur relative to the tibia
$D_{rolling}$	rolling distance of the femur relative to the tibia
Tr	transformation matrix
$\hat{n}$	normal unit vector
Racly	relative vector for the ACL along the y-axis
Rpcly	relative vector for the PCL along the y-axis
Rcly	relative vector for the CL along the y-axis
ACL_{angle}	angle between line of action of the ACL and the horizontal
PCL_{angle}	angle between line of action of the PCL and the horizontal
CL_{angle}	angle between line of action of the CL and the horizontal
Fl_{jx}	ligament force for jth ligament along the x-axis
Fl_{jy}	ligament force for jth ligament along the y-axis
dpy_{acl}	perpendicular distance for y-component of ACL force to ICR location
dpx_{acl}	perpendicular distance for x-component of ACL force to ICR location
dpy_{pcl}	perpendicular distance for y-component of PCL force to ICR location
dpx_{pcl}	perpendicular distance for x-component of PCL force to ICR location
dpy_{cl}	perpendicular distance for y-component of CL force to ICR location
dpx_{cl}	perpendicular distance for x-component of CL force to ICR location
M_{lj}	flexion/extension moment for the jth ligament

C

$\overline{M}$

$\overline{M}_p$

$\overline{M}_-$

Proj_F

$\overline{M}_x$

$\overline{M}_y$

$\overline{F}$

$\overline{F}_x$

$\overline{F}_y$

$\overline{F}_z$

h

X_{COP}

Y_{COP}

ICR_x

ICR_y

ICR_z

M_z

FQT

FQT_x

FQT_y

FPT

FPT_x

FPT_y

PFc

PFc_x

PFc_y

Ma_x

Ma_y

ΣF_x

ΣF_y

ΣM_z

$\hat{i}$

$\hat{j}$

$\hat{k}$

$\overline{Ra}$

C	contact point
$\overline{M}$	force plate moment
$\overline{M}_p$	moment parallel
$\overline{M}_\perp$	moment perpendicular
$Proj_F$	Projection of force vector
$\overline{M}_x$	forceplate moment about the x-axis
$\overline{M}_y$	forceplate moment about the y-axis
$\overline{F}$	resultant external force vector
$\overline{F}_x$	external force along the x-axis
$\overline{F}_y$	external force along the y-axis
$\overline{F}_z$	external force along the z-axis
h	height from the forceplate surface to the center of the forceplate
X_{COP}	location of the COP along the x-axis
Y_{COP}	location of the COP along the y-axis
ICR_x	location of the instantaneous center of rotation in the x-axis of the inertial coordinate system
ICR_y	location of the instantaneous center of rotation in the y-axis of the inertial coordinate system
ICR_z	location of the instantaneous center of rotation in the z-axis of the inertial coordinate system
M_z	flexion/extension external moment
FQT	quadriceps tendon force
FQT_x	quadriceps tendon force along the x-axis
FQT_y	quadriceps tendon force along the y-axis
FPT	patellar tendon force
FPT_x	patellar tendon force along the x-axis
FPT_y	patellar tendon force along the y-axis
PFc	patello-femoral contact force
PFc_x	patello-femoral contact force along the x-axis
PFc_y	patello-femoral contact force along the y-axis
Ma_x	moment arm along the x-axis
Ma_y	moment arm along the y-axis
ΣF_x	sum for forces along the x-axis
ΣF_y	sum for forces along the y-axis
ΣM_z	sum for forces about the z-axis
$\hat{i}$	unit vector along the x-axis
$\hat{j}$	unit vector along the y-axis
$\hat{k}$	unit vector along the z-axis
$\overline{R}a$	position vector for anatomical target

$\overline{R}d$	position vector for dynamic target
X_t	x-axis in segmental coordinate system of the thigh
Y_t	y-axis in segmental coordinate system of the thigh
Z_t	z-axis in segmental coordinate system of the thigh
X_s	x-axis in segmental coordinate system of the shank
Y_s	y-axis in segmental coordinate system of the shank
Z_s	z-axis in segmental coordinate system of the shnk
$Post_{axis}$	posterior axis of the shank
med_{cond}	position vector for the medial condyle
lat_{cond}	position vector for the lateral condyle
gr_{troc}	position vector for the greater trochanter
$prox_{leg}$	position vector for the proximal target on the shank
$dist_{leg}$	position vector for the distal target on the shank
$post_{leg}$	position vector for the posterior target on the shank
$\hat{e}_1$	floating axis base vector for the joint coordinate system
$\hat{e}_2$	base vector for the joint coordinate system
$\hat{e}_3$	base vector for the joint coordinate system

INTRODUCTION

Injuries to the knee joint are among the most common injuries sustained during sport activities. The ligaments of the knee joint are required to support high tensile loads, and are the most often injured soft tissues in the knee joint due to the high loads sustained during the restriction of excessive motion. Fifty percent of the knee injuries are due to trauma to the anterior cruciate ligament (ACL) and the medial collateral ligament (MCL) (Nicholas & Hershman, 1995).

Both cruciate ligaments are constraints for the rolling and sliding motion of the femur relative to the tibia. Even though the knee has been classified as a hinge joint, the articulation of the femur and the tibia allows for six degrees of freedom. The three rotational movements and the three translational movements are coupled throughout the full range of motion allowed by the joint. Complete loss of joint stability is observed with a third degree sprain of the ligament in which the ligament fibers are fully torn (Macnicol, 1986). The primary objective of treatment to an injured knee should be to restore the normal joint mechanics and stability and to prevent premature degeneration of the joint.

The soft tissues that cross the knee joint act as constraints to the kinematics of the joint. While the ligaments are considered the primary stabilizers of the knee joint, muscles also provide stabilization to the joint during dynamic activities. An injury to the ACL compromises the stability of the joint by allowing excessive anterior translation of the tibia with respect to the femur. Compromised stability due to an injury to the ACL may be controlled by increased muscle activity.

I. Need for the Study

The knee joint has been one of the most widely researched joints of the human body. Mathematical models have been developed to investigate various aspects of knee joint mechanics. The inclusion of muscle, ligamentous and cartilagenous tissue increases the number of unknown parameters in the model. This increase in unknowns is not matched by an increase in the number of motion or equilibrium equations. The limited number of motion equations with respect to the higher number of unknowns creates the complex situation of indeterminacy. Constraint equations can be developed to increase the number of equations and solve for some of the unknown variables; however, development of these equations becomes a complex task.

A number of mathematical models have been developed to evaluate the interaction of the cruciate ligaments as motion constraints. However, limited work has been performed in the evaluation of the interaction between ligamentous and muscle constraints to knee motion. An anterior load on the tibia has been shown to stress the ACL and produce an anterior displacement of the tibia relative to the femur. Contraction of the hamstrings group would produce a load in the posterior direction, reducing the stress on the anterior cruciate ligament and controlling the translational motion. The interactions of the ligamentous constraints with the constraints provided by muscle contraction are of great significance in the prediction of the rotational and translational motions of the knee joint. The abnormal joint mechanical behavior produced by an injured ACL can be compensated by the adaptation of the neuromuscular system to assist in the stabilization of the knee joint (Collins & O'Connor, 1991).

II. Purpo

Th

mechanics

dimension

relation to

forces on t

forces appl

III. Assump

Due

dynamic equ

the model. T

sagittal plane

two-dimensic

collateral liga

and only one

of the CL will

restraint of bot

Ligamentous c

of previous rese

prediction of th

(Figure 1). The

meniscii in the

II. Purpose of the Study

The wide range of research focused on the knee is indicative of the complex mechanics exhibited at the joint. The purpose of this study is to develop a two-dimensional quasi-static knee model for the prediction of quadriceps muscle forces in relation to ligament forces and angle of knee flexion. The model will predict the internal forces on the constraints of the joint, depending on the joint position and the external forces applied to the system.

III. Assumptions and limitations

Due to the complexity of the knee joint motion and the limited number of dynamic equations, several assumptions have been made to simplify the requirements of the model. The relative motion of the femur and the tibia will be examined only in the sagittal plane. The motion out of the sagittal plane is minimal and, therefore, an accurate two-dimensional model can be developed. For the two-dimensional model, the medial collateral ligament (MCL) will be combined with the lateral collateral ligament (LCL) and only one collateral ligament (CL) will be modeled. The origin and insertion locations of the CL will follow those of the LCL, due to the more important role of the LCL in the restraint of both anterior and posterior translations (Daniel, Akeson & O'Connor, 1990). Ligamentous constraints will be modeled as single nonlinear springs. From the evaluation of previous research, it was determined that a flat tibial plateau will allow for an accurate prediction of the translational values and the femur will be modeled as an involute circle (Figure 1). The joint will be assumed to be frictionless and any contributions of the meniscii in the joint mechanics will be ignored. The patella will be included in the model

for the pu

The patell

representat

flexion ang

be frictionl

inextensible

F

IV. Significan

The fin

aid to injury rel

stresses applied

for the purpose of transferring the force from the quadriceps tendon to the patellar tendon. The patella will be modeled as a rectangle with biarticulating surfaces, allowing the representation of the shift in contact surfaces between the femur and the patella at high flexion angles. Contact between the patella and the femoral condyles will be assumed to be frictionless. The quadriceps tendon and the patellar tendon will be considered inextensible cords.

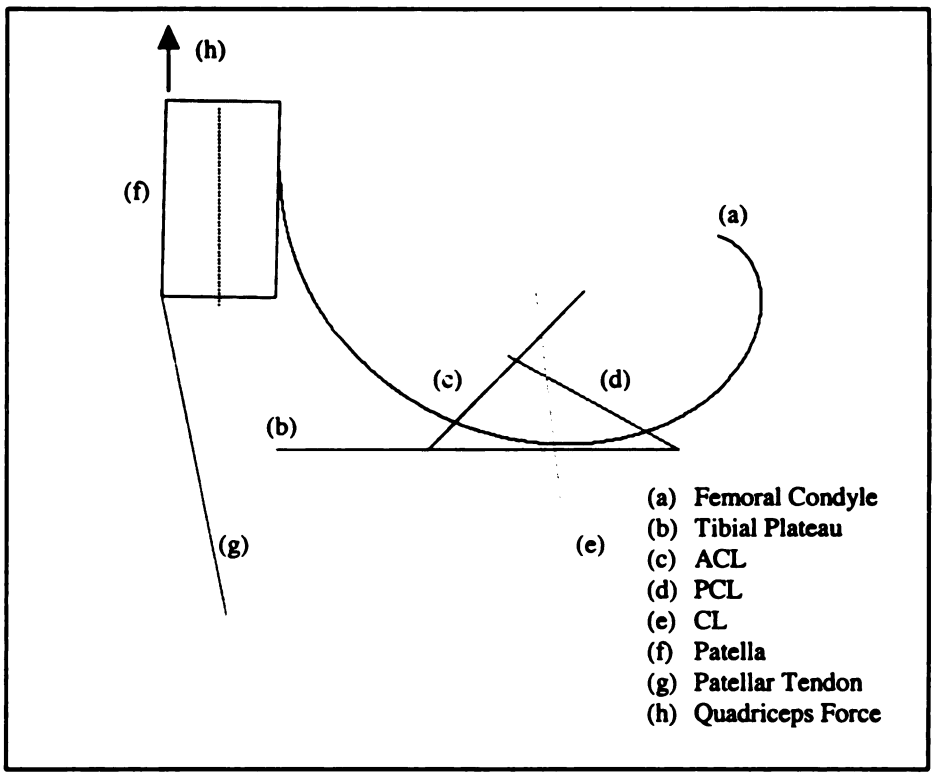

Figure 1: Graphical representation of the knee model.

IV. Significance of the study

The findings of this study will contribute to the field of orthopaedics as well as an aid to injury rehabilitation. The mathematical model will allow clinicians to determine the stresses applied to the injured ligament including the contribution of the quadriceps group

muscle co

forces act

rehabilitat

structures.

mechanics

the joint.

muscle contractions at specified flexion angles. The ability to determine the internal forces acting on the joint can aid in the identification of beneficial joint positions for rehabilitation exercises, as well as maximum loads that can be supported by the soft structures. The mathematical model also will help clinicians better understand the mechanics of the knee joint and the interactions of primary and secondary stabilizers of the joint.

REVIEW OF LITERATURE

The knee joint is one of the most commonly injured joints in athletic performance. The complexity of the kinematics associated with the knee joint has led to a large number of research studies conducted in this area. Mathematical models have been developed to describe the kinematics of the knee joint under simplified conditions. The mechanical properties and mechanical behavior of the joint constraints determine the overall kinematics of the joint. Injury to the joint constraints compromises the normal mechanics of the knee joint. Joint function has not been assessed in terms of the joint kinematics and interaction of soft tissue components. The objective of this literature review is to focus primarily on the mathematical modeling done on the knee joint and secondarily on the pertinent clinical research associated with ligamentous injuries and rehabilitation.

I. Mathematical Models

Two- and three-dimensional mathematical models of the knee joint have been widely used to describe the joint mechanics. Due to the complicated mechanics exhibited at the knee joint, mathematical models are simplified by describing limited aspects of the joint motion. Differences in the results obtained with similar analytical models are due to the wide variety of measurement techniques used to obtain the input parameters. These differences in results lead to the reconsideration of the importance of some parameters as predictors in the model. The literature review was focused on models that examined the mechanics of the knee joint and included the interaction of the ligaments and muscles surrounding the joint for stabilization purposes.

Si

two body

developed

system ch

plane. As t

tibia occur

validity of

Hirokawa &

the four-bar

ligament ba

inextensible

tibia and to r

extension of

The lo

to the externa

tibial plateau.

Simplified models have been successfully used to describe the interaction between two body segments. The four-bar kinematic linkage is one of the simplest models developed to describe knee joint motion (Daniel et al., 1990) (Figure 2). The linkage system changes geometry as the joint moves through the range of motion in the sagittal plane. As the knee flexes and extends, rolling and sliding actions of the femur over the tibia occur. This model gives an inextensible representation of the cruciate ligaments. The validity of the model has been questioned by other authors (Hefty & Grood, 1983; Hirokawa & Tsuruno, 1997; Lanir, 1983). Throughout the range of motion, the angles in the four-bar model change, and at any flexion angle the point of intersection of the two ligament bars is considered the instantaneous center of rotation of the joint. Due to the inextensible characteristics of the ligaments, the femur was shown to slide forward on the tibia and to roll backward as the knee flexes. The opposite actions were observed during extension of the knee joint (O'Connor, Shercliff, Biden & Goodfellow, 1989).

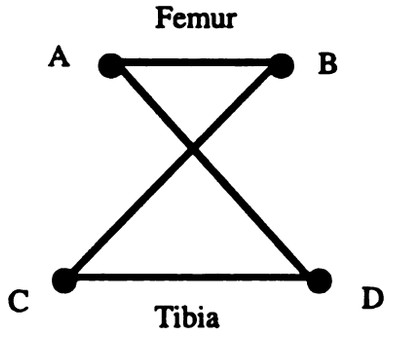

Figure 2: Four-bar linkage system

The load supported by the cruciate ligaments has been demonstrated to be linked to the external forces applied to the femur and tibia, as well as to the geometry of the tibial plateau. Chan and Seedhom (1995) investigated the effects of the tibial plateau's

geometry on t
cruciate ligam
P) force appli
combined wit
was performe
different geor
on the ACL a
reduction in th
application of
compressive f
for the convex
the same A-P
degree of flex
the cruciate lig
compartment a
plateau would

geometry on the prediction of forces on both cruciate ligaments. The ACL and posterior cruciate ligament (PCL) loads were examined under a pure external anterior-posterior (A-P) force applied to the tibia and also under a pure external axial compressive force combined with the A-P force using the four-bar kinematic linkage model. The analysis was performed for concave, convex and flat tibial plateau surfaces. The results of the different geometric configurations demonstrated that, for a concave surface, the loadings on the ACL and PCL were decreased when compared to those for the flat surface. This reduction in the forces sustained by the cruciate ligaments was due to the line of application of the tibio-femoral contact force (Figure 3). The addition of an axial compressive force would decrease the loading on the ligaments. The results were opposite for the convex surface, as the predicted forces for the cruciate ligaments were greater for the same A-P force. The line of application of the contact force is influenced by the degree of flexion at the knee joint. Therefore, knee flexion plays a role in the loading of the cruciate ligaments. The authors concluded that due to the concavity of the medial compartment and the convexity of the lateral knee compartment, a model with a flat tibial plateau would closely predict the actual forces on the cruciate ligaments.

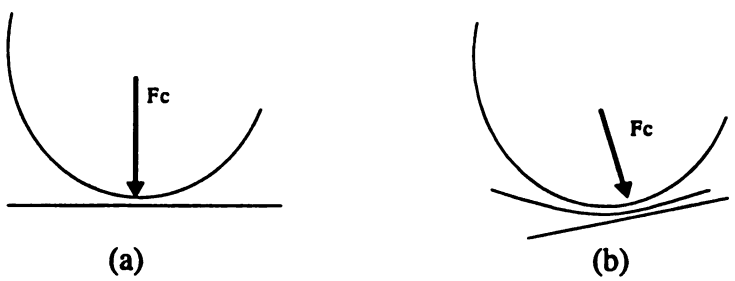

Figure 3: Line of application of the contact force for (a) flat tibial surface and (b) concave surface

data o

study.

impose

tensio

throug

limitati

surface

anteno

model

isometr

change

quadric

produce

contact

ligamen

The flat

not affec

K

orientatio

obtained

specimen

In a later study, Chan and Seedhorm (1999) obtained experimental and theoretical data on the effects of tibia geometry on ligament forces. The results supported their first study, concluding that a concave tibia provides protection by lowering the tension imposed on the ligaments during the application of an anterior-posterior force. The tension values obtained in the experimental results were lower than those obtained through theoretical methods. The discrepancy in the results was attributed to the limitations and simplifications of the theoretical model.

In a similar study, Imran and O'Connor (1997) examined the effects of tibial surface geometry and ligament orientations in the estimation of the forces produced at the anterior and posterior cruciate ligaments. In this study, the four-bar kinematic linkage model was analyzed under anterior-posterior loading and a loading condition simulating isometric quadriceps contraction. Ligament loading was found to be affected more by the changes in tibial surface geometry and the tilt of the tibial plateau in the isometric quadriceps exercises when than in the A-P loading condition. The curved tibial surfaces produced an increase in the ligament forces when the horizontal component of both the contact force and the ligament force acted in opposite directions, and decreased the ligament force when the two horizontal component forces acted in the same direction. The flat surface maintained a constant direction for the contact force and therefore, did not affect the ligament forces produced throughout the range of motion.

Knowledge of the origin and insertion sites for the ligaments is necessary, as fiber orientation and length are common input parameters to theoretical models. Fuss (1989) obtained the origin and insertion locations for the cruciate ligaments from cadaver specimens. The cruciate ligaments are multi-bundle fibers, which undergo tension under

differen

is suppo

maintai

same lig

changin

positior

in the li

the knee

ligamen

Limitat

inexter

joint m

pattern

during

attach

distan

attach

attach

flexio

would

separa

different stress conditions. The representation of these ligaments by a single bar segment is supported by the guiding bundle theory. The guiding bundles are the fibers that maintain the same distance between the origin and insertion sites. Other fibers within the same ligament will undergo tension under different conditions due to the constantly changing distance between the origin and insertion sites (Fuss, 1989). The functional position of the knee was described by Fuss as the position where the majority of the fibers in the ligament are under tension. The functional position for the ACL is full extension of the knee joint, while the PCL's functional position is full flexion of the knee joint.

The four-bar linkage system has been shown to be successful in the prediction of ligament forces and in the description of the interaction between the femur and tibia. Limitations of this model include the representation of the cruciate ligaments as inextensible bars as well as the omission of the collateral ligaments and their influence in joint motion and stability. Zavatsky and O'Connor (1992) investigated the recruitment pattern of ligament fibers based on the previously described four-bar linkage model during passive flexion. A neutral fiber was defined by joining a point on the tibial attachment with a similar point on the femoral attachment that remained at a constant distance through the range of motion. This representation allowed for a multiple fiber attachment site to be identified at each bone. Fibers then were mapped between the attachment sites. The translations and rotations of the bones relative to each other during flexion of the knee, resulted in shape changes of the ligaments within the joint, which would have an effect on the prediction of ligament loads.

The identification of multi-bundle ligaments adds accuracy to the model by separating ligament bundles with different mechanical characteristics. In an attempt to

examine

Blackwoo

model w

orientatio

three, an

lateral co

and orig

research

each of t

estimate

tibia, an

the same

ligamen

bundle

the diffe

al., 199

simultan

method

bundles

obtained

assumpt

and simu

examine the accuracy of the prediction of ligament forces, Mommersteeg, Huiskes, Blackvoort, Kooloos, Kauer and Maathuis (1996b) developed a three-dimensional knee model with multi-bundle ligaments. The bundles were defined according to the orientations of the ligament fibers in cadaver specimens. The authors defined seven, six, three, and three bundles for the anterior cruciate, posterior cruciate, medial collateral and lateral collateral ligaments, respectively. Optimization was used to determine the stiffness and original length of each ligament bundle. The optimization technique allowed the researchers to determined the number of bundles that best fit the constraint behavior of each of the four ligaments (Mommersteeg et al., 1996a). The ligament forces were estimated as a function of the relative position of the two rigid bodies, the femur and tibia, and the stiffness of the ligament fibers. The results from the experimental data were the same as those predicted from the mathematical model. In this study, the knee joint ligaments were modeled with non-uniform mechanical characteristics and different bundle orientations. Optimization techniques were used to determine the recruitment of the different ligament bundles during the range of motion of the joint (Mommersteeg et al., 1996b). A later study demonstrated the use of inverse dynamics to predict simultaneous forces sustained by the knee ligaments (Mommersteeg et al., 1997). The method of inverse dynamics allowed the prediction of the load carried by several fiber bundles of the main ligaments in the knee joint. Even though accurate results were obtained from this method, the limitations associated with the input parameters and assumptions would outweigh the advantages of using this method over more simplistic and similarly accurate methods.

The loads supported by the ligaments have been shown to be dependent on the geometric characteristics of the femur and tibia. The forces exerted on the ligaments also are dependent on the external loads generated by muscle contraction. A sagittal model of the knee joint was developed by Shelburne and Pandy (1997) to examine the effects of muscular contractions and bone geometry on the forces sustained by the ligaments of the joint. Eleven elastic bundles were used to model the ligaments of the joint. Hill-type contractile elements were used to model eleven muscles crossing the knee joint. The lines of pull of the muscles were represented as straight lines except for the gastrocnemious, semitendinosis and semimembranosis that wrap around the femoral condyles. The authors were able to determine the range of flexion over which ligaments were loaded relative to the amount of muscle contraction.

II. Knee Laxity and Restraints

A large number of studies have been performed on cadaver specimens to obtain a better understanding of the function of each ligament in the overall stabilization of the knee joint throughout the range of motion. In-situ evaluations of the restraining characteristics of ligaments are performed by sequentially cutting the ligaments and evaluating the joint under simulated loading conditions. A greater displacement of the adjacent bones following the removal of a ligament would imply a stabilization role of the ligament. Butler, Noyes & Grood (1980) proposed a method of measuring the force required to sustain a predetermined displacement following the cut of ligaments. The test simulated the anterior drawer clinical test, considering the cruciate ligaments as primary restraints and the collateral ligaments as secondary restraints. The authors found an

average restraining force of 333 N when the knee was positioned at 30° of flexion and 5 mm of anterior displacement of the tibia over the femur was allowed. During anterior drawer tests, the manual force applied is approximately 45 to 50 N. Approximately 85 % of the anterior displacement of the tibia over the femur is controlled by the anterior cruciate ligament. Following an injury to the anterior cruciate ligament, the anterior laxity is increased and the interaction between the secondary restraints is modified to provide stability to the joint.

In a similar study, Piziali, Seering, Nagel and Schurman (1980) tested the forces exerted on the knee ligaments during medial-latera placements. The results of this study indicated that the anterior cruciate ligament was the primary restraint for medial tibial displacement, while the lateral tibial displacement was primarily constrained by the collateral ligaments. The posterior cruciate ligament is also a restraint for lateral motion, becoming tense as a result of smaller displacements as compared to the ACL. Piziali et al. showed the significant coupling effects present during the application of medial-lateral external forces. Such coupling of ligament restraints is not apparent in the anterior-posterior displacement of the tibia over the femur, which supports the accuracy of models limited to motion in the sagittal plane.

III. Ligament mechanics

Quantification of the load-deformation curves of the ligaments of the knee is important in the understanding of the mechanical behavior of the joint. Most information on the mechanical behavior of ligaments has been obtained from cadaver specimens. Using strain gauges to evaluate the deformation of the ligaments, the ACL was found to

be mo

was ev

rotatio

to be

flexio

rotatio

Willis

been

Wood

acco

inter

be most lax at 35° of flexion (Figure 4). When the coupled motion of flexion and rotation was evaluated, at a flexion angle of 30° internal rotation tightened the ACL; external rotation produced the opposite result. The most lax position for the PCL was also found to be 35° of flexion (Figure 4). The tibial collateral ligament is most lax during complete flexion. With the knee positioned at 30° of flexion, the coupled motion of external rotation and/or abduction increased the strain on the ligament (Kennedy, Hawkins & Willis, 1977).

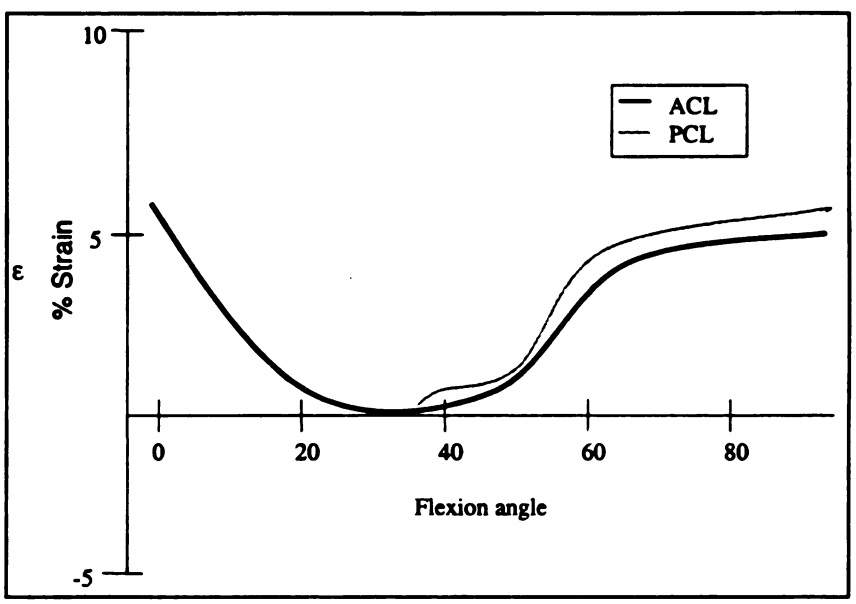

Figure 4: Cruciate ligament strains as a function of flexion angle.

The measurement of the cruciate ligament forces at different flexion angles has been of great interest to researchers (Sakane, Fox, Woo, Livesay, Li & Fu, 1997; Takai, Woo, Livesay, Adams & Fu, 1993). Studies of force distribution in the ACL take into account the ligament bundles and possible differences in mechanical properties. The anterior-medial fibers of the ACL show similar force distribution along the full range of

motion when tested under two different values of applied anterior force. However, the posterior-medial fibers are highly affected by the flexion angle, undergoing their highest stresses at 15° of flexion (Sakane et al., 1997). These results agree with results presented by Fuss (1989), where the anterior-medial fibers of the ACL were identified as the guiding fibers. When three ligament bundles were examined (Takai et al., 1993), the length of the anterior-medial fibers increased with knee flexion, while a decrease in length was seen in the posterior-medial fibers. A constant length was maintained by the intermediate fibers. In this study, Takai and coworkers (1993) used a six degrees of freedom linkage system to calculate the forces applied to the AC ligament bundles. At full extension, the load was distributed equally between the anterior and posterior ACL fibers. At knee flexion angles larger than 45°, up to 95% of the load was carried by the anterior fibers of the cruciate ligament.

The prediction of ligament force and ligament lengthening due to stress is critical in the overall description of joint mechanics and equilibrium. The nonlinearity associated with the ligamentous structures increases the complexity of the mathematical model. Several models have predicted changes in length by evaluating the relative motion between the insertion and origin sites during the joint's range of motion (Hefty & Grood, 1983). These models do not take into account the structural characteristics of the ligaments and the non-linearity associated with wrapping of the ligaments around bony structures. In the case of the cruciate ligaments, as the knee flexes and internally rotates the ligaments wrap around each other. The length of the ligaments can no longer be determined by the difference between the origin and insertion points. Considering ligament wrapping would affect the prediction of ligament length, ligament tension and

the direction of the force vector. The authors did not validate the importance of the three-dimensional model using experimental data; however, they stated that the wrapping effect would cause considerable changes to be observed in the predicted parameters (Hefty & Grood, 1983).

Hirokawa and Tsuruno (1997), considering the shear and twisting applied to the ligament bundles, also emphasized the restrictions associated with measuring ligament length by the relative position of the origin and insertion sites when analyzing the deformation of the ACL. Consideration of the wrapping of ligaments is of critical importance in the prediction of the MCL length (Blackevoort & Huiskes, 1991). The abduction/adduction rotations are affected by the incorrectly modeled ligament in the description of joint motion without consideration of the MCL wrapping around the bony edge of the tibia. Blackevoort and coworkers (1991) showed that including the interaction of the ligament and the bone allowed for greater stabilization when a valgus moment was applied.

Woo, Johnson and Smith (1993) presented a review of mathematical models developed to describe the mechanical behavior of tendons and ligaments. The nonlinearity associated with the behavior of ligaments under tension increased the complexity of the model. A linear load-deformation relationship is seen at large loads due to an increase in stiffness (Figure 5). The recruitment of fibrils under the application of load also affects the linear characteristics of the load-deformation curve. At maximum load, under the recruitment of all the fibrils, the ligament shows linear characteristics. Ligaments and tendons have been modeled as elastic as well as viscoelastic elements. The mathematical representation of the ligament is dependent on the complexity of the overall

knee model as well as the parameters to be predicted. A model of an incompressive hyper-elastic ligament was used by Hirokawa and coworkers (1997) in an attempt to analyze the deformation of the anterior cruciate ligament. The results of the experimental data indicated that the central portion of the ligament underwent the least amount of strain due to the limited shear, bending and twisting applied to the central fibers. The application of an anterior force on the tibia produced increased strain on the anterior fibers of the ligament. The results of this study also showed that the strain along the length of the ligament is nonuniform, indicating increased strain values near the insertion points.

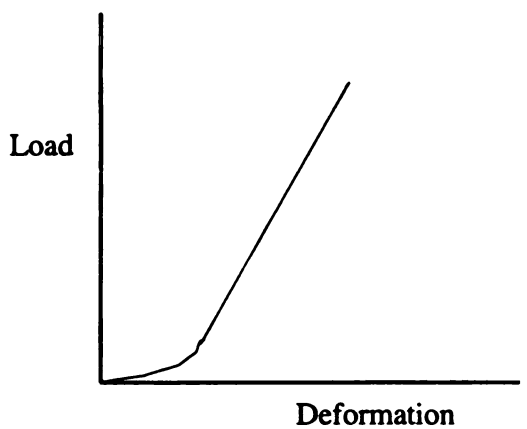

Figure 5: Load-deformation curve for ligaments

Ligaments and tendons are viscoelastic tissues. Repeated cyclic loadings induce a stable response, which resembles that of elastic material (Lanir, 1983). A recent study predicted the load-deformation behavior of ligaments when treated as quasi-linear viscoelastic materials, taking into consideration strain rate (Pioletti, Rakatomanana, Benvenuti & Leyvraz, 1998). Elastic and viscous potentials were expressed as functions

of stress and strain. The nonlinear characteristics of collagen fibers arise from the straightening of the crimped fibers during the initial three percent of the strain. Relaxation tests conducted at different levels of strain showed the stress to be a function of the strain squared (Haut & Little, 1972). The tissue's make up is assumed to be of fibrils at different states of crimp. As load is applied, the tissue straightens and becomes able to bear load. The load carried by the tissue is a function of the fiber's constitutive law (Hurschler, Loitz-Ramage & Vanderby, 1997).

Ligament failure can be modeled mathematically using selected stress-strain criteria. Hurschler et al. (1997) identified that failure occurs as a large number of fibers fail within the tissue as a result of tissue stretch. This increase in fiber failure results in a decrease in tissue stiffness. Mathematical models usually assume the same elastic modulus and strain limit for all fibers comprising the tissue. This assumption constrains the fibers to fail in the same sequence as they are recruited (Liao & Belkoff, 1999).

IV. Neuromuscular Activity

A complete analysis of knee joint mechanics and function includes the contribution of the muscles crossing the joint. Muscle contraction will produce joint motion or stabilization by compensating for internal and external forces. Muscles may be categorized as secondary stabilizing structures that assist the ligaments in the prevention of excessive motion when necessary. Knee joint function following an injury is evaluated by full range of motion, joint stability and muscle strength. The fact that muscle strength is considered part of the clinical evaluation should encourage the analysis of muscle forces in mathematical knee models.

Muscle forces as part of mathematical models add to the complexity of the computational methods. The number of muscles crossing a joint, which add to the number of unknown parameters, is a major limiting factor to simplifications in models. A large number of unknown muscle forces results in an indeterminant system. Optimization techniques have been used to predict accurate model solutions in the case of redundant systems. Electromyography also can aid in the determination of muscle activity and the reduction of the number of unknowns to allow solution of the dynamic equations. Collins and O'Connor (1991) developed a mathematical model to predict the muscle-ligament interaction during walking. A two-dimensional four-bar linkage system was used to determine the forces transmitted by three muscles, the two cruciate ligaments and the contact force. The constraints of the model reduced the redundancy of the twenty possible solutions. The researchers demonstrated single muscular activity at specific periods of the gait cycle thus raising questions concerning the assumption of multiple muscle contractions for joint stabilization. The results from the experimental testing would be assumed to be different in the case of injured subjects. Simultaneous muscle contractions are expected to assist in the stabilization of the knee joint. In a later study, Lu and O'Connor (1996) used the four-bar kinematic linkage model to calculate the moment arms of five muscles crossing the knee joint. Moment arms were calculated from a two-dimensional anatomically based model for the quadriceps, biceps femoris, semitendinosis, gastrocnemious and semimembranosis muscles. The ligaments were modeled as bands of fibers. The results of the model calculations showed a general agreement with experimental data reported by Collins and O'Connor (1991). The two-

dimensionality of the model did not pose any limitations to the moment arms and muscle line-of-action predictions.

Translations at the knee joint are mostly constrained by the cruciate ligaments. Hsieh and Draganich (1998) investigated the effects of quadriceps contraction on the rotational and translational movements at the knee joint. The researchers found a linear relationship between anterior translation, internal rotation and abduction of the tibia with respect to the femur, during an applied quadriceps load. The fiber length of the ACL, PCL and MCL also increased linearly with an increase in quadriceps load. The changes in joint kinematics due to quadriceps contraction were relatively small when compared to the changes experienced in ligament length. The effects of ligament loading due to muscle contraction would be of great importance in the rehabilitation process.

Aune, Nordsletten, Skjeldal, Madsen and Ekeland (1995) investigated the changes in mechanical properties of the ACL due to simultaneous contraction of the hamstrings and gastrocnemius during loading of the ligament. The ACL was loaded in tension while the ischiatic nerve was stimulated to obtain a tetanic contraction of the hamstrings and gastrocnemious. The results of this study showed that there was a 70% increase in the load needed to rupture the ligament and a 154% increase in the energy stored. Additionally, the protection mechanism provided by the muscles was dependent on the rate and magnitude of contraction. Contraction patterns of the hamstrings group have been studied using EMG analysis during isometric exercises (Solomonow, Baratta, Zhou, Shoji, Bose, Beck & D'ambrosia, 1987). These researchers focused on the load regulation characteristics of the hamstrings group when the ACL has a mechanical disadvantage and is unable to stabilize the joint. The importance of the hamstrings activity in reducing the

loads in the ACL and assisting in the anterior tibial translation constraint also was shown in a later study performed on cadaver specimens (Li, Rudy, Sakane, Kanamori, Ma & Woo, 1999). Mechanical advantage of the line of pull of the hamstrings, as well as the ACL, was shown to contribute to the ability to provide stability to the joint.

The rehabilitation process following an injury to the ACL is associated with hamstrings and quadriceps strengthening. Knowledge of the magnitude of strain placed on the joint ligaments as a result of muscle contraction could prevent excessive loading of the ligament during the early rehabilitation period. Modeling of ligament bundles and musculotendinous units assist in the determination of the effects of muscle contraction on the ligaments' mechanical properties (Shelburne & Pandy, 1997). Model calculations showed that due to the geometry of the knee joint alone, the ACL is loaded for the first 10° of flexion. Contraction of the flexor and extensor groups will assist in the reduction of ligament stress throughout the remainder of the flexion range.

Strain in the newly reconstructed ligaments should be minimized during rehabilitation exercises. Loading patterns in the ACL have been shown to be dependent on both knee flexion angles and load placement (Zavatsky, Beard & O'Connor, 1994). The authors calculated the "critical position" for load placement, which resulted in no ligament forces needed for equilibrium. Zavatsky et al. found that as the flexion angle increased the critical position moved distally along the shank segment. The maximum angle where a critical position could be found within the lower limb, was found to be 90° of flexion.

Simultaneous measurement of forces sustained by the constraints of the knee joint can aid in the full understanding of knee joint mechanics. In a study measuring the

contact forces and quadriceps tendon and patellar ligament forces, the authors found that the force sustained by the quadriceps tendon increased with increased angle of knee flexion (Singerman, Berilla, Archdeacon & Peyser, 1999). Similarly, the anterior-posterior patellar contact force increased with increased flexion. The tibiofemoral contact force acted posterior on the joint from full extension to approximately 52 degrees of flexion. The tibiofemoral contact force acted anteriorly at higher flexion angles. Singerman et al, (1999) cut the cruciate ligaments to evaluated the effects on the measured forces. Absence of the ACL resulted in a slight decrease of the quadriceps tendon force and an increase in the shear forces applied at the joint. The quadriceps force increased with dissection of the PCL.

ANALYTICAL METHODS

A model was developed for the prediction of ligament forces as a response of quadriceps muscle contraction and based on a quasi-static representation of the knee joint mechanics in two-dimensions. Three major ligaments were included in the model, the anterior and posterior cruciate ligaments and a collateral ligament. Due to the two dimensionality of the model, the medial collateral and lateral collateral ligaments were combined into one ligament. The ligaments of the knee joint were modeled as nonlinear springs to account for the viscoelastic properties of the tissue. Insertion and origin sites for the modeled ligaments were taken from the literature. Magnetic reasonance imaging (MRI) slides also were used to determine the anatomic insertion and origin sites for the modeled ligaments.

I. Tibio-femoral Joint Definition

The geometry of the femur and tibia have been shown to have an effect on the mechanics of the knee joint as well as the loads supported by the ligaments (Shelburne et al, 1997). In the model developed here, the femur was represented as an involute circle defined by two general parametric equations [1] and [2]. These equations describe a spiral, bounded by the parameter t. The value of t in the parametric equations [1] and [2] needed to be restricted to represent the portion of the involute circle that best fit the geometric characteristics of the femoral condyle. This restriction is dependent on the radius (b) of the circle in the two prescribed equations.

$$Ix(t) = -b \cdot \cos(t) - b \cdot t \cdot \sin(t) \qquad [1]$$

$$Iy(t) = b \cdot \sin(t) - b \cdot t \cdot \cos(t) \qquad [2]$$

A co

provides a

rotation Φ a

defining the

additional r

in equation

the tibia de

as shown by

$l_x = -b \cdot co$

$l_y = b \cdot \sin($

$\begin{bmatrix} l_x'' \\ l_y'' \end{bmatrix} = \begin{bmatrix} co \\ -s \end{bmatrix}$

A counterclockwise rotation (ϕ) of 90 degrees applied to the general equations provides a medial view of the femoral condyle as shown in Figure 6 (Balint, 1998). The rotation ϕ added to the general parametric equations would result in equations [3] and [4], defining the femoral condyle at the full extension position. To represent knee flexion, an additional rotational transformation was prescribed to the parametric equations as shown in equation [5]. The matrix multiplication associated with the rotation of the femur over the tibia defined a new set of equations dependent on a second rotational component (θ) as shown by equations [6] and [7].

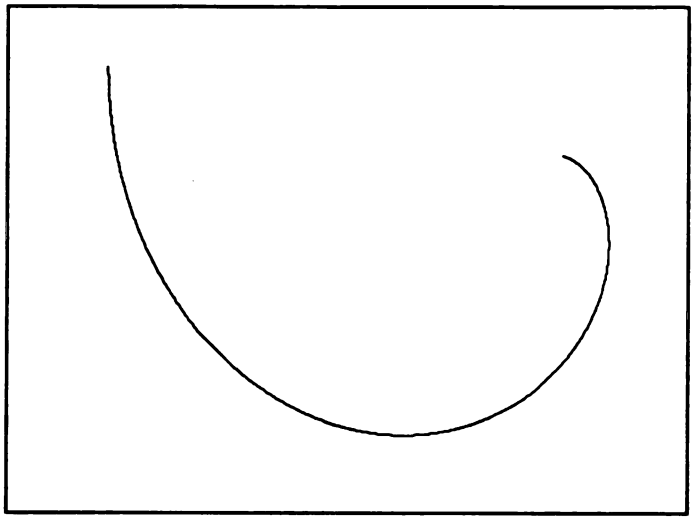

Figure 6: Involute circle with a 90 counterclockwise rotation, representing medial view of the femoral condyle

$$Ix = -b \cdot \cos(\phi + t) - b \cdot t \cdot \sin(\phi + t) \qquad [3]$$

$$Iy = b \cdot \sin(\phi + t) - b \cdot t \cdot \cos(\phi + t) \qquad [4]$$

$$\begin{bmatrix} Ix'' \\ Iy'' \end{bmatrix} = \begin{bmatrix} \cos(\theta) & \sin(\theta) \\ -\sin(\theta) & \cos(\theta) \end{bmatrix} \cdot \begin{bmatrix} Ix \\ Iy \end{bmatrix} \qquad [5]$$

$$Ix' = -b \cdot \cos(\phi + t + \theta) - b \cdot t \cdot \sin(\phi + t + \theta) \quad [6]$$

$$Iy' = b \cdot \sin(\phi + t + \theta) - b \cdot t \cdot \cos(\phi + t + \theta) \quad [7]$$

where, ϕ is the prescribed rotation to the original involute,

θ is the angle of flexion at the knee joint,

b is the radius of the involute circle

and t is the parameter in which x and y depend and the constraint to the involute.

The tibia was defined as the fixed segment in the model. The curved geometry of the tibial plateau influenced the distribution of load among the knee ligaments. In this model, the tibial plateau was represented as a flat surface, with a slope of zero degrees. A flat surface representing the tibial plateau was used due to the difficulty in modeling the simultaneous contributions of the concave medial and the convex lateral compartments. This simplification of the model has been shown to accurately predict the forces supported by the cruciate ligaments (Chan et al., 1995). Researchers have measured the slope of the tibial plateau and have found a 10° posterior slope (Meister, Talley, Horodyski, Indelicato, Hartzel & Batts, 1998; Matsuda, Miura, Nagamine, Urabe, Ikenoue, Okazaki & Iwamoto, 1999). This slope was assumed to have no direct effect on the design of this model; however, this assumption should be examined if the model is to be expanded into three-dimensions.

Three coordinate systems were used in the definition of the knee geometry and the joint kinematics. The unprimed coordinate system for the femur was defined at the full extension position of the knee joint. The location of the unprimed x-axis was derived from equation [5] at the point where the tangent to the line of the involute is equal to

zero. In the femoral condyle representation at full extension, two points with tangent zero can be found (Figure 7). The second point of slope zero (where $t = \pi\text{-}2\pi$) is representative of the contact point and the selected location of the unprimed x-axis of the femur.

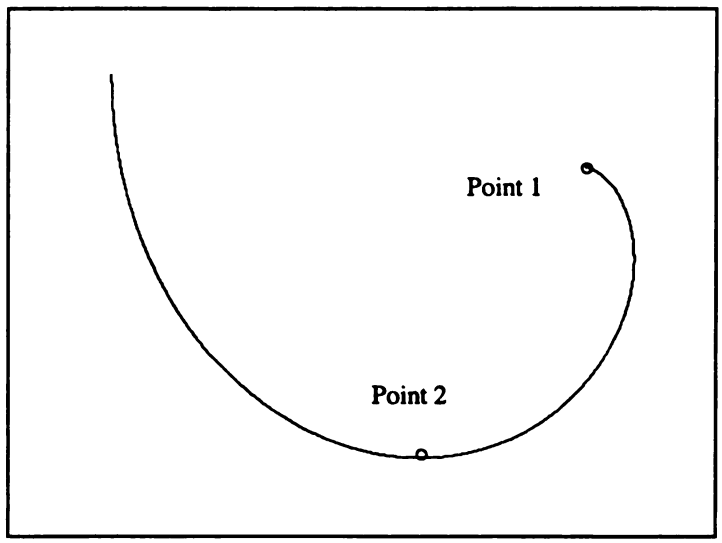

Figure 7: Involute circle with identification of slope zero positions.

The tibial plateau was modeled parallel but not coincidental with the femoral x-axis. The joint space between the femur and the tibia was taken into consideration in the development of the model. However, the articular cartilage and menisci were not included in the model. The tibio-femoral joint was considered frictionless during the allowed range of motion. The tibia's unprimed coordinate system had its origin at the anterior limit of the tibial plateau, and it was set parallel to the unprimed femoral coordinate system.

The unprimed y-axis of the femur was derived from equation [6]. The axis was defined at the tangent of the involute that is equal to infinity. For the specified involute

circle at the full extension position there were two points where the tangent to the line is equal to infinity (Figure 8). The second point defined by a t value of π- 5/2π corresponded with the location of the unprimed y-axis of the femur.

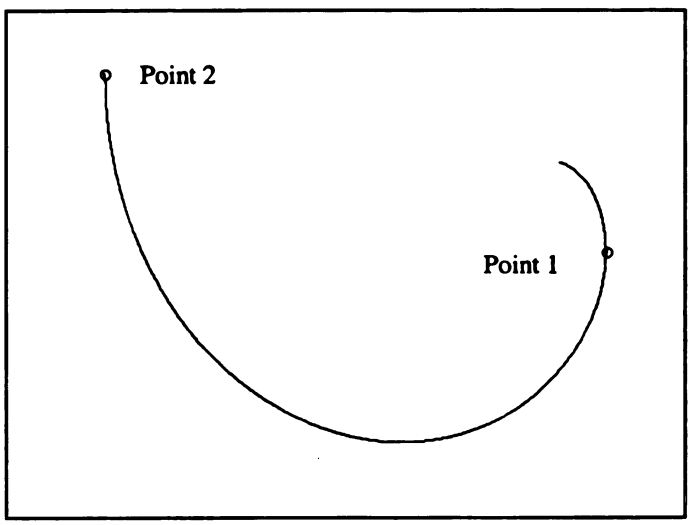

Figure 8: Involute circle with identification of infinity slope positions.

A second (primed) coordinate system, (x', y'), was defined at the origin point (0,0) of the involute at the full extension position. Anterior-posterior displacements of the femur relative to the tibia were estimated by the translation of the primed coordinate system in the x-direction relative to the fixed tibia. Position vectors were defined in the primed coordinate system for the full extension position unless otherwise specified.

Flexion at the knee joint was associated with rotation of the primed coordinate system of the femur relative to the tibia (Figure 9). The double primed coordinate system rotated with the body segment, while the unprimed and primed coordinate systems remained as reference frames.

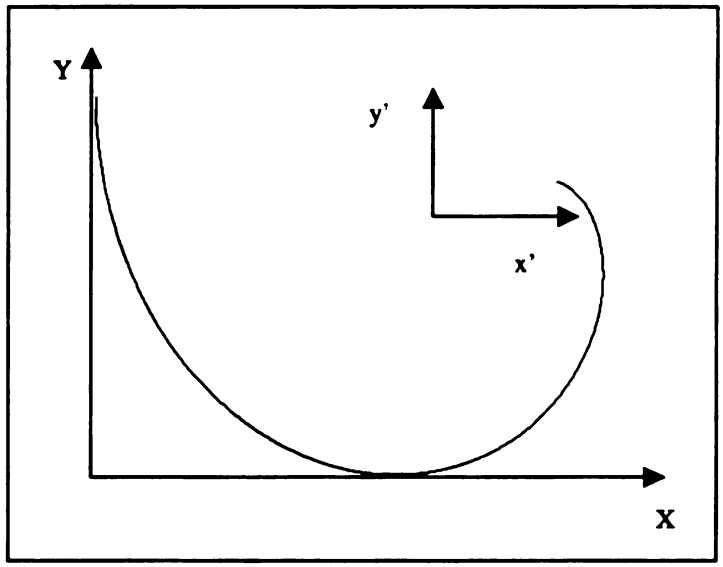

Figure 9: Representation of the femoral condyle in full extension in the unprimed and primed coordinate systems.

The insertion locations for the modeled ligaments were estimated from the unprimed coordinate system at full extension of the knee (Figure 10). The unprimed coordinate system also was used to estimate the location for the patella and patellar ligament insertion points. All ligaments in the graphical representation of the knee were drawn as lines; however, mathematically they were represented as non-linear springs. Position vectors from the unprimed x and y axes defined the origin and insertion points. The origin site of the collateral ligament was modeled in the estimated anatomical location, although the graphical representation of the tibia was not extended to encompass that area (Figure 11).

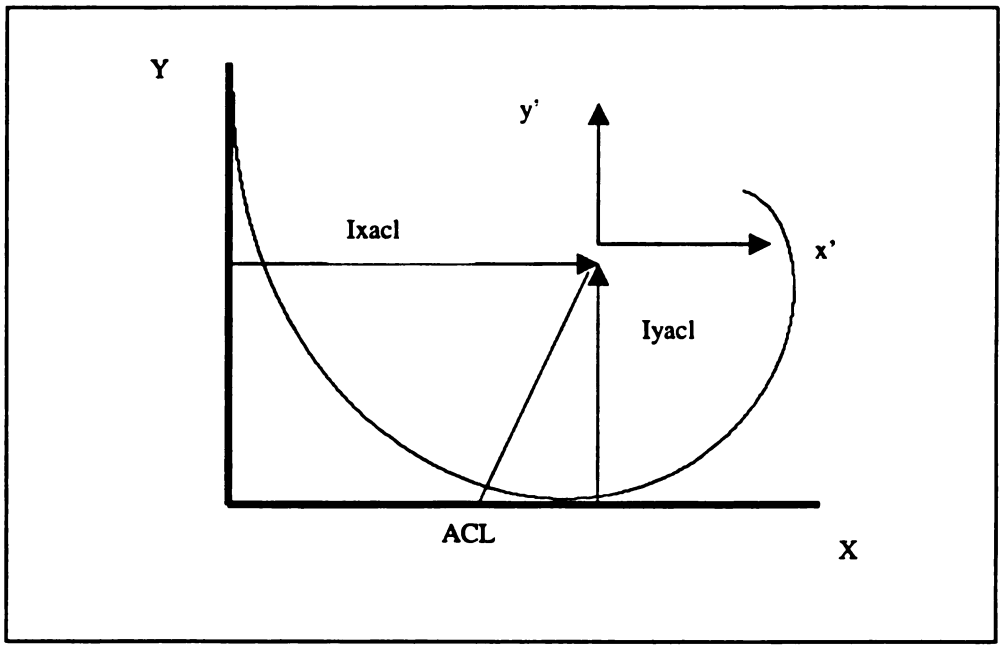

Figure 10: Representation of position vectors to locate the insertion of the ACL on the femoral condyle.

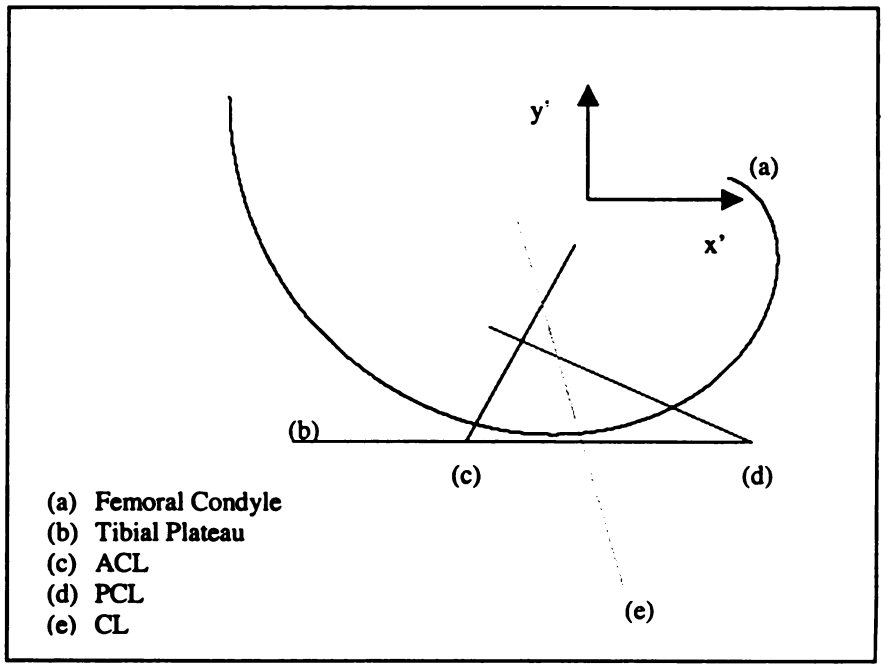

Figure 11: Graphical representation of the tibiofemoral joint with ligamentous constraints (Full extension).

To estimate the insertion and origin positions of the modeled ligaments during knee flexion, the relative insertion positions of the ligaments on the femur were prescribed the same rotational transformation as the involute (Equations 9 a-c). The positions of the ligament insertion points on the femur, relative to the geometric limits remained the same following the rotation of the femur. The origin locations of the modeled ligaments were not affected by the rotation because the tibia was defined as the fixed segment.

$$\begin{bmatrix} Ixacl' \\ Iyacl' \end{bmatrix} = \begin{bmatrix} \cos(\theta) & \sin(\theta) \\ -\sin(\theta) & \cos(\theta) \end{bmatrix} \cdot \begin{bmatrix} Ixacl \\ Iyacl \end{bmatrix} \qquad [9a]$$

$$\begin{bmatrix} Ixpcl' \\ Iypcl' \end{bmatrix} = \begin{bmatrix} \cos(\theta) & \sin(\theta) \\ -\sin(\theta) & \cos(\theta) \end{bmatrix} \cdot \begin{bmatrix} Ixpcl \\ Iypcl \end{bmatrix} \qquad [9b]$$

$$\begin{bmatrix} Ixcl' \\ Iycl' \end{bmatrix} = \begin{bmatrix} \cos(\theta) & \sin(\theta) \\ -\sin(\theta) & \cos(\theta) \end{bmatrix} \cdot \begin{bmatrix} Ixcl \\ Iycl \end{bmatrix} \qquad [9c]$$

A representation in the change of orientation of the knee ligaments at 60 degrees of flexion is presented in Figure 12. Note that the position of the femur relative to the tibia was arbitrarily set for the purpose of illustration, any linear displacements occurring as a result of knee flexion are parameters to be investigated in the model.

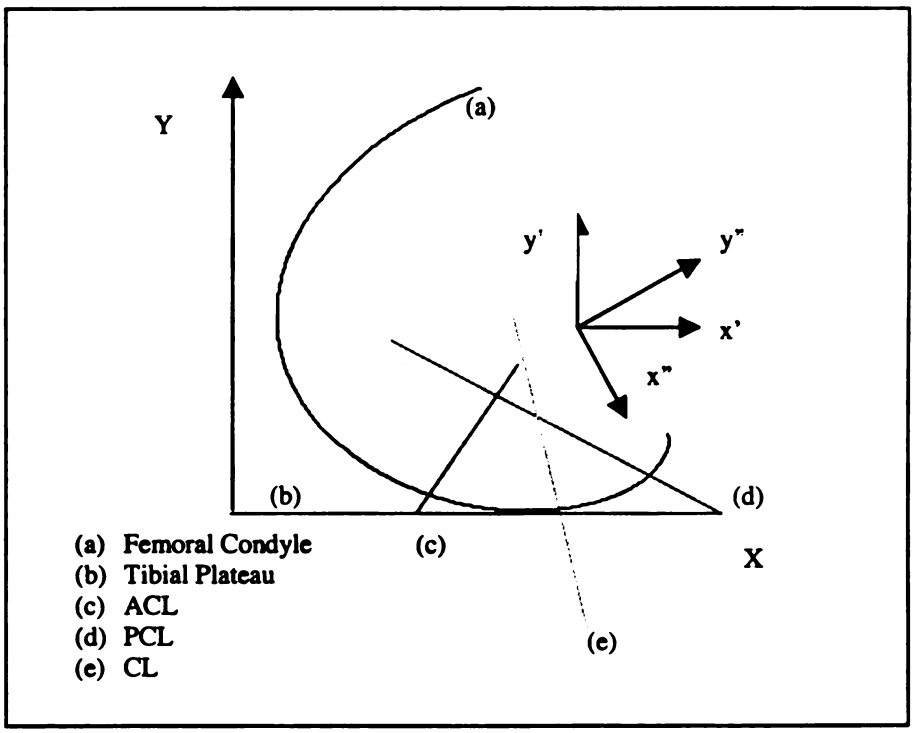

Figure 12: Graphical representation of the tibiofemoral joint at 60 degrees of flexion, and the relative position of the ACL, PCL and LCL.

II. Patello-femoral Joint Definition

The quadriceps group was the only muscle group included in the model. The four quadriceps muscles were combined into a single element inserting on the patella. The patella was modeled as a rectangle with two articulating surfaces. The biarticulating surfaces allowed the model to predict the patello-femoral mechanics more accurately at high flexion angles (Gill & O'Connor, 1996). At flexion angles larger than 100°, the contact surface of the femur shifts from the trochlea to the condyles. The patella sinks into the condylar groove to maintain contact with the femur. The model simulated this shift of contact surfaces by the shift in the articulating surface of the patella. The two articulating surfaces are represented more easily on the simplified rectangular

representation of the patellar than on the involute circle representing the geometry of the distal femur. The dimensions of the patella were taken from MRI slides to match the tibio-femoral joint geometry.

The normal ratio between the patellar dimensions and the patellar tendon length, a 1:1 ratio, was maintained in the model. Pathological conditions, such as patella alta, can be represented mathematically by adjusting the ratio between the patella and patellar tendon length. The insertion site of the patellar tendon in the tibia tuberosity was modeled according to the estimated anatomical location; however, as in the case of the insertion of the CL, the tibia was not graphically extended to encompass the insertion site.

With increased rotation of the femur relative to the tibia, the patella displaces approximately 7 cm proximal over the femoral condyles (Peterson & Frankel, 1986). The lengths of the quadriceps tendon and the patellar tendon are unchanged during tension. The inextensible properties of the patellar tendon added a constraint equation to the motion of the patella relative to the femur, thus defining the location of the anterior-distal point of the patella about an arc of radius PT. The angle of pull of both tendons changes as the knee flexion angle increases. The effect is to decrease the mechanical advantage of the patello-femoral mechanism at greater flexion angles. The angles β and α, as defined in Figure 13, determined the overall position of the patella relative to the femur at any given flexion angle. The constraints specified by the inextensible patellar tendon and the requirement of contact between the patella and the femoral condyles reduced the number of solutions for β and α angles. A third constraint to the patello-femoral motion was added by specifying a linear relationship between the angle of flexion (θ) and the angle of inclination of the patella (α). The last constraint necessary to define the patellar motion

relative to the femur was given by the orientation of the patello-femoral contact force. Since the patello-femoral joint was considered frictionless, the contact force had to be normal to the articulating surfaces of both the patella and the femoral condyle. The patello-femoral contact point was derived from the solution to the constraints of the motion and was not constant relative to either surface.

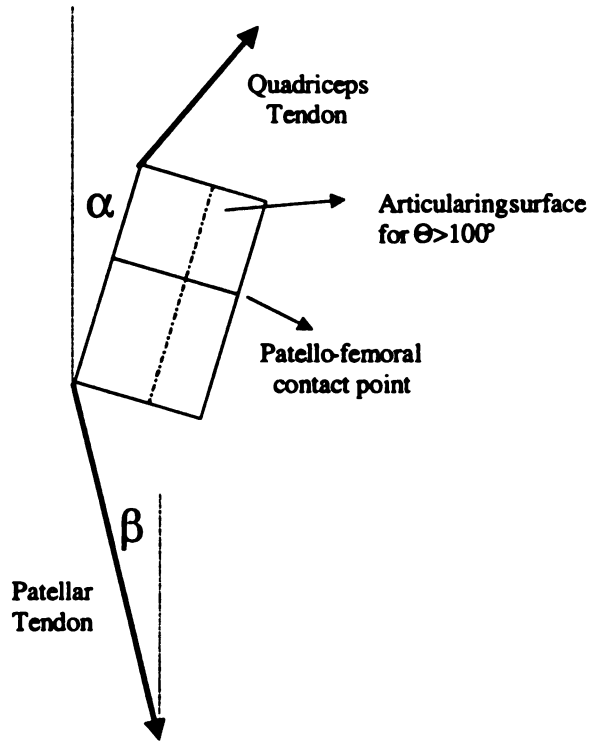

Figure 13: Patellar geometry.

Only the insertion position for the quadriceps tendon was of interest in the model. The origin of the quadriceps muscle group was not a necessary parameter to the model; however, the angle of pull of the quadriceps tendon relative to the patella must be included in the input parameters. The quadriceps tendon was modeled parallel to the longitudinal axis of the femur except at high flexion angles where wrapping of the tendon

occur

was

parel

Equi

is ne

parel

quadr

occurs over the femoral condyle. The constraint for the wrapping effect of the quadriceps was included at flexion angles larger than 90 degrees. The graphical representation of the patello-femoral and tibio-femoral joints at full extension is shown in Figure 14.

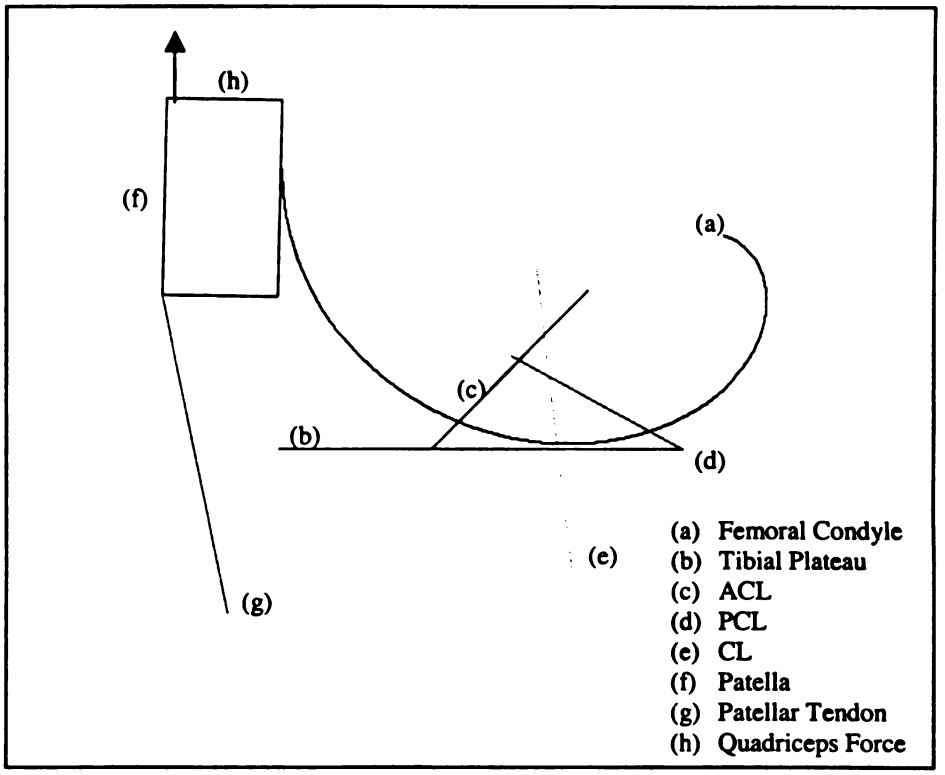

Figure 14: Patello-femoral and tibio-femoral joints at full extension.

The patello-femoral joint was not modeled as a simple pulley mechanism. Equilibrium between the quadriceps tendon force, patellar tendon force and contact force is necessary throughout the full range of motion (Figure 15). The equilibrium of the patello-femoral mechanism is dependent on the angles γ, the angle between the quadriceps tendon's line of pull and the patello-femoral contact force, and δ, the angle

between the lines of action of the patellar tendon force and the patello-femoral contact force. These angles are both dependent on the orientation of the patella relative to the femur and the angle of flexion of the knee.

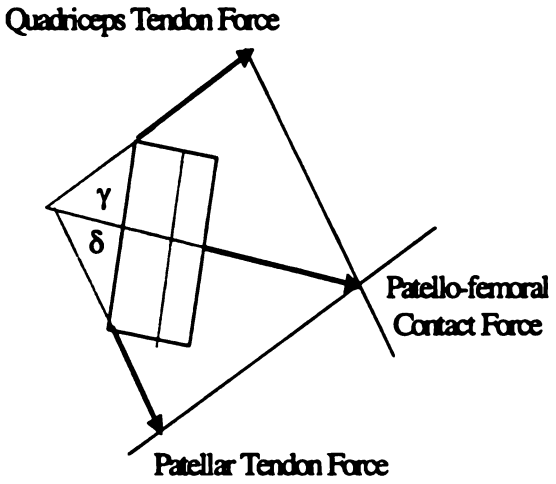

Figure 15: Patello-femoral equilibrium mechanism.

Once the inclination of the patella was defined by the angles α and β, the force equilibrium mechanism could be solved. In addition to the patellar tendon and quadriceps tendon being treated as inextensible units, they were constrained to carry only tensile loads. The ultimate goal of the model was the prediction of the force carried by the quadriceps tendon given the specific constraints determined by the tibio-femoral kinematics.

III. Ligament Forces

The anterior cruciate, posterior cruciate and collateral ligaments provide the primary constraints to the mechanics of the knee joint. The model was used to estimate the forces sustained by the ligaments and the force generated by the quadriceps muscle group to maintain equilibrium throughout the range of motion allowed by the knee joint. Mechanical properties of the ligaments reported in the literature served as input parameters in the estimation of ligament forces (Table 1). Equation [10] was used to calculate the forces sustained by the three ligaments as a function of length change throughout knee flexion.

Table 1: Stiffness coefficient for the modeled ligaments.

Ligaments	k (N/mm^2)
ACL	30
PCL	35
CL	15

$$\overline{F} = k\Delta^2 \qquad [10]$$

where k is the stiffness coefficient and Δ is the change in length as a function of angle of flexion.

The stiffness coefficient parameter allow for representation of a variety of injury conditions and the estimation of changes in ligament and muscle forces required to reach equilibrium. Changes in the stiffness coefficient contribute to a change in the force

produced by the ligaments and affect the mechanics of the knee joint. Adaptations in the knee joint mechanics, associated with changes in the mechanical properties of the ligaments, contribute to the better understanding of ligament injuries in the knee joint.

Ligament lengths were calculated by the difference between origin and insertion locations in the estimated position for any given flexion angle (Equations 11 a-c). The initial length of ligaments (L_o) was determined from the origin and insertion sites estimated in the model when the strains in the ligaments were equal to zero. The condition of $\varepsilon_o=0$ is not coincidental with full extension but occurs at approximately 35° of flexion for all ligaments (Adbel-Rahman & Hefzy, 1993). Strain values at full extension for each ligament were obtained from the literature and are shown in Table 2 (Adbel-Rahman et al., 1993). The initial length of each ligament was calculated using equation [12].

$$Lacl = \sqrt{(Ixacl'' - Oxacl)^2 + (Iyacl'' - tp)^2} \qquad [11a]$$

where $Ixacl''$ is the insertion of the ACL along the x-axis for the rotated femur.

$Oxacl$ is the origin position of the ACL along the x-axis.

$Iyacl''$ is the insertion of the ACL along the y-axis for the rotated femur.

tp is the location of the tibial plateau along the y-axis.

$$Lpcl = \sqrt{(Oxpcl - Ixpcl'')^2 + (Iypcl'' - tp)^2} \qquad [11b]$$

where $Ixpcl''$ is the insertion of the PCL along the x-axis for the rotated femur.

$Oxpcl$ is the origin position of the PCL along the x-axis.

$Iypcl''$ is the insertion of the PCL along the y-axis for the rotated femur.

$$Lcl = \sqrt{(Ixcl'' - Oxcl)^2 + (Iycl'' - Oylc)^2} \qquad [11c]$$

where $Ixcl''$ is the insertion of the CL along the x-axis for the rotated femur.

$Oxcl$ is the origin position of the CL along the x-axis.

$Iycl''$ is the insertion of the CL along the y-axis for the rotated femur.

$Oylc$ is the origin of the CL along the y-axis.

Table 2: Length ratio values for the modeled ligaments at full extension.

Ligaments	ι (mm/mm)
ACL	1.0215
PCL	1.050
CL	1.050

$$\iota_j = \frac{L_j}{Lo_j} \qquad [12]$$

where j represents the individual ligaments.

ι_j is the length ratio of the ligament, L_j is the length of the ligament, and L_{oj} is the initial length (resting length) of the ligament.

Ligaments were assumed to carry only tensile forces, which were specified by the boundary condition given by equation [13]. Changes in length due to wrapping of the

cruciate ligaments were not taken into consideration in the model. Each ligament's ultimate load, taken from the literature (Table 3), was set as the upper boundary condition. Any motion that would produce a ligament's force exceeding the ultimate load was not allowed and a change in the ligament's stiffness was required.

$$\overline{F} = 0 \text{ for } L_j < L_{oj} \qquad [13]$$

Table 3: Ultimate load of modeled ligaments and patella tendon.

Ligaments	Ultimate Load (N)
ACL	1700
PCL	2840
CL	945
PT	2900

IV. Mechanical Behavior of the tibio-femoral joint

Because in this model the knee joint was not classified as a hinge joint, the calculation of the instantaneous joint center more accurately defined the continuously changing knee center location due to rolling and sliding motions occurring at the joint. The instantaneous joint center can be calculated from the relative motion between the femur and tibia and their respective segment velocities (Figures 16 and 17).

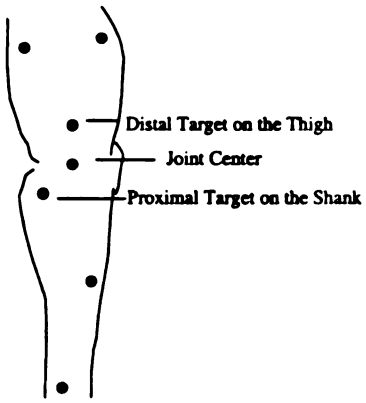

Figure 16: Targeting protocol for joint center calculation.

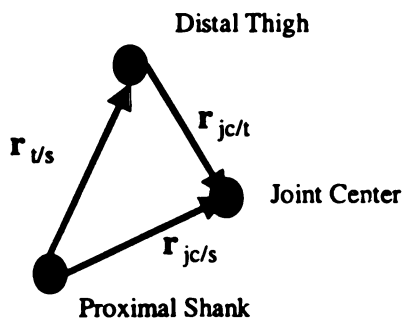

Figure 17: Position vectors involved in the calculation of the instantaneous knee joint center.

The thigh and shank segment angular velocities were derived from position vectors and linear velocities of two thigh targets and two shank targets respectively. The position vectors and linear velocities were forced to sagittal motion to simplify the calculation of the instantaneous joint center. The angular velocity for a segment is defined by equation [14].

$$\bar{\omega}_s \times (\bar{r}_2 - \bar{r}_1) = (\bar{v}_2 - \bar{v}_1) \qquad [14]$$

where ϖ_j i

targets in t

segment.

Th

zero relat

shank ex

velocity,

and a po

knee joi

angular

$\bar{v}_x = \bar{i}$

$\bar{v}_x = \bar{v}$

a

$\bar{r}_j$

jo

$\varpi_j = \varpi_i$

where ϖ_s is the angular velocity of the segment, $\bar{r}_1$ and $\bar{r}_2$ are the position vectors of two targets in the segment and $\bar{v}_1$ and $\bar{v}_2$ are the linear velocities of two targets in the segment.

The instantaneous joint center is defined to be a point in the thigh and shank with zero relative motion. The same point in the thigh or thigh extended and in the shank or shank extended will define the knee joint center. To obtain a point with zero relative velocity, the linear velocity of the knee joint center was calculated as a point in the thigh and a point in the shank (Equations 15 and 16 respectively). The angular velocity of the knee joint was defined by the relative angular velocity of the thigh with respect to the angular velocity of the shank as given by equation [17].

$$\bar{v}_{jc} = \bar{v}_{dt} + \bar{\omega}_t \times \bar{r}_{jc/dt} \qquad [15]$$

$$\bar{v}_{jc} = \bar{v}_{ps} + \bar{\omega}_s \times \bar{r}_{jc/ps} \qquad [16]$$

where $\bar{v}_{jc}$ is the linear velocity of the joint center, $\bar{v}_{dt}$ and $\bar{v}_{ps}$ are the linear velocities of the targets on the distal thigh and proximal shank respectively, ϖ_t and ϖ_s are the angular velocities of the thigh and shank respectively, and $\bar{r}_{jc/dt}$ and $\bar{r}_{jc/ps}$ are the position vectors from the thigh and shank targets to the joint center location.

$$\varpi_j = \varpi_t - \varpi_s \qquad [17]$$

From rigid bodies kinematics, the location of the joint center is given by equation [18]. The direct solution for the position of the joint center can be obtained by expansion of the vector equation into scalar components, or with a direct vector solution by using a triple vector product. The position of the joint center was obtained in the inertial coordinate system and was transformed to the segmental coordinate system of the femur for the purpose of calculating moments about this point. The ICR location in the segmental coordinate system was transformed to the primed coordinate system of the model.

$$\bar{\omega}_j \times \bar{r}_{jc/dt} = (\bar{v}_{dt/ps} - \bar{\omega}_s \times \bar{r}_{dt/ps}) \qquad [18]$$

The ICR location was used to define the joint kinematics as well as to predict the anterior displacement of the femur over the tibia. The geometric characteristics of the femoral condyles influence the rolling and sliding patterns of the femur over the tibia. During pure rolling of a circular disk, the center of rotation translates in the direction of motion (Figure 18a). During pure sliding of a disk, the center of rotation will not change position and coincides with the center of the disk (Figure 18b).

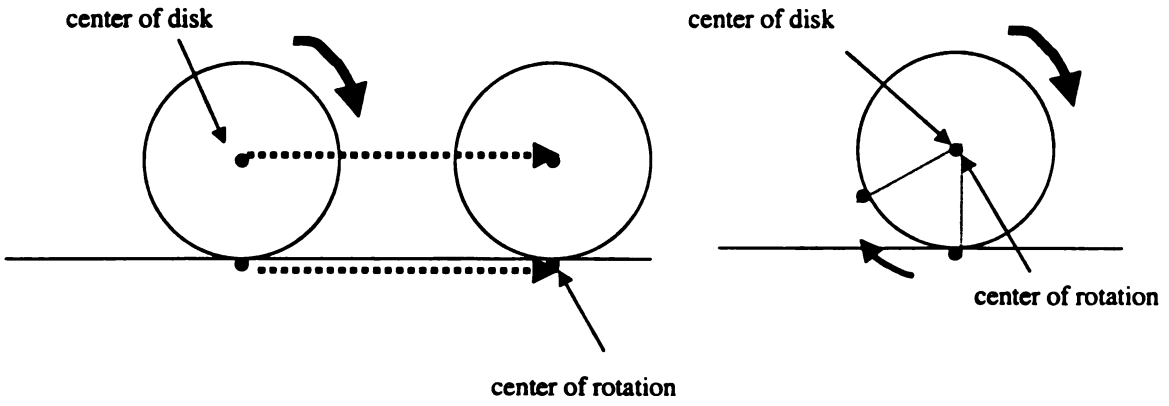

(a) (b)

Figure 18: Rolling and Sliding of a circular disk (a and b respectively).

The geometry of the femoral condyles can be assumed to be similar to two circles that match with the contact surface of the tibio-femoral joint and patello-femoral joints respectively (Figure 19). The center of the circle matching the posterior aspect of the femoral condyles was used as the initial center of rotation of the joint. The selection of this initial point of rotation was based on the fact that the initial rotation of the femur is dictated by the geometry of the posterior aspect of the femoral condyle (Wismans et al., 1980). Rolling of the femoral condyles with respect to the tibia occurred over the initial 25 degrees of knee flexion. The calculated instantaneous center of rotation then was used to define the change in position of the point of rotation and to define the rolling and sliding motion of the femur.

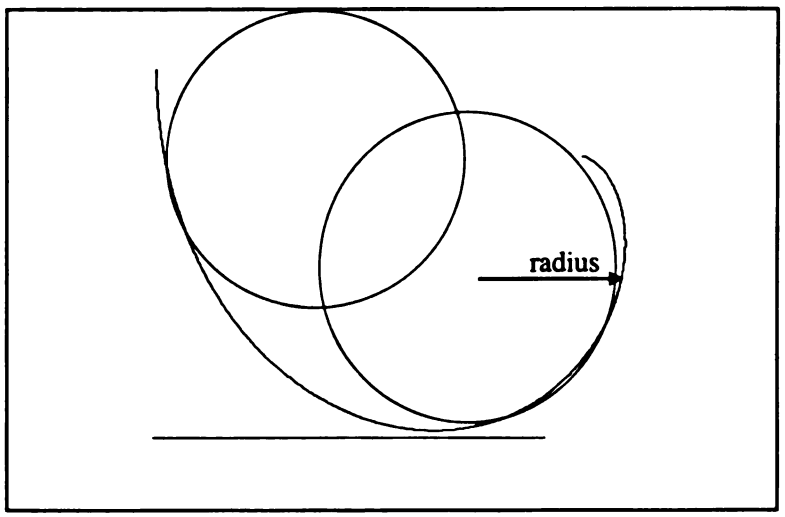

Figure 19: Assumption of circular discs representation of the femoral condyle geometry.

The change of position of the ICR allowed for the estimation of the anterior-posterior displacement of the femur relative to the tibia. The horizontal displacement of the femur was estimated from the difference in location of ICR between the flexed and fully extended positions. The prescribed rotation to the involute, associated with knee flexion, will cause an anterior-posterior displacement of the contact point from the initial to the final position. This displacement of the contact point is considered a normal translation dictated by the geometry of the surfaces in contact. The portion of the horizontal displacement purely caused by the sliding action of the femur was defined by equation [19]. The rolling component of the tibio-femoral motion was defined by equation [20] as the portion of the horizontal displacement that is not involved in the sliding action. The translation prescribed to the involute, as defined by the ICR, also was used to transform the location of any points associated with the femoral body segment (Equation 21).

D_{pla}

D_{mi}

$\bar{T}_{5}$ "

$\bar{T}_{yy}$

V. Ca

The po

Since th

condyle

flexion a

the invol

$$D_{sliding} = \int_{2\pi-\phi-\theta}^{2\pi-\phi} \left|\frac{d\bar{r}}{dt}\right| \cdot dt \qquad [19]$$

where $\bar{r} = Ix''(t)\hat{i} + Iy''(t)\hat{j}$

$$D_{rolling} = (ICR_\theta - ICR_o) - D_{sliding} \qquad [20]$$

where ICR_θ is the ICR location at θ degrees of flexion, and ICR_o is the ICR location at full extension.

$$\begin{bmatrix} \bar{r}_{xj}'' \\ \bar{r}_{yj}'' \end{bmatrix} = Tr \cdot \begin{bmatrix} \bar{r}_{xj}' \\ \bar{r}_{yj}' \end{bmatrix} + \bar{D}_{xy} \qquad [21]$$

where $\bar{r}_j'$ is the position vector for any given point in the femoral primed CS

Tr is the rotational transformation matrix, and $\bar{D}_{xy}$ is the translation vector (true ICR displacement).

V. Calculation of Tibio-femoral Contact Force

A contact condition between the femur and the tibia was assumed in the model. The point of contact was defined by the geometric characteristics of the femur and tibia. Since the tibial plateau was defined as a flat surface, the contact point at the femoral condyle was defined by the t value, giving the tangent line with zero slope for a specific flexion angle (Equation 22). As shown in Figure 7, two points satisfy this condition for the involute. The point used to define the x-axis of the unprimed coordinate system was

defin

all fi

- tai

posit

grou

$\vec{r}_{q'} =$

$\vec{r}_{q} =$

unit n

must

$\vec{n}_i \times \vec{r}$

C. Tha

kinem

VI. Ca

Due to

and use

defined by the t value of 2π. This t value will satisfy the condition of the contact point for all flexion angles.

$$-\tan(\theta + \phi + t) = 0 \qquad [22]$$

The contact point was derived by solving equations [6] and [7] using t = 2π. The position vector defined by this solution then was specified, for both the femoral and tibial articulating surfaces, in equation [23].

$$\begin{aligned} \bar{r}_{cf} &= Ix(2\pi)''\hat{i} + Iy(2\pi)''\hat{j} \\ \bar{r}_{ct} &= Ix(2\pi)''\hat{i} + tp\hat{j} \end{aligned} \qquad [23]$$

where $\bar{r}_{cf} = \bar{r}_{ct}$

The condition of tibio-femoral contact also must satisfy the assumptions that the unit normals to the femoral and tibial surfaces must be collinear and the cross product must be equal to zero (Equation 24).

$$\hat{n}_f \times \hat{n}_t = 0 \qquad [24]$$

The contact forces were defined by the $\overline{Fc}_x$ and $\overline{Fc}_y$ components acting at point C. These forces are considered internal or joint forces which influence the joint kinematics.

VI. Calculation of Internal Moments due to Ligament Forces

The estimated ligament forces produced internal moments about the joint center. Due to the simplifications of the model, only flexion/extension moments were calculated and used to estimate the equilibrium position. The internal moments were calculated

about the instantaneous joint center of the knee. The insertions and origins of the modeled ligaments defined the line of action of the calculated ligament forces. The angle between the line of action and the tibial plateau was used in the calculation of the component forces (Figures 20 & 21). In the case of the collateral ligament, a horizontal line at the insertion site in the tibia was used to define the ligament angle (Figure 22).

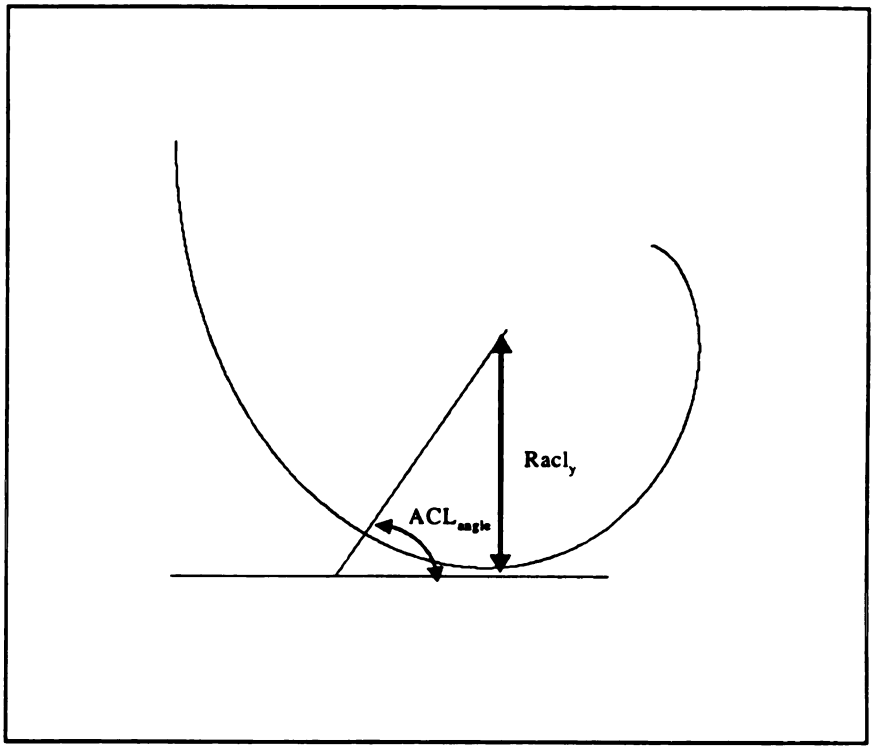

Figure 20: Representation of the ligament angle for the ACL.

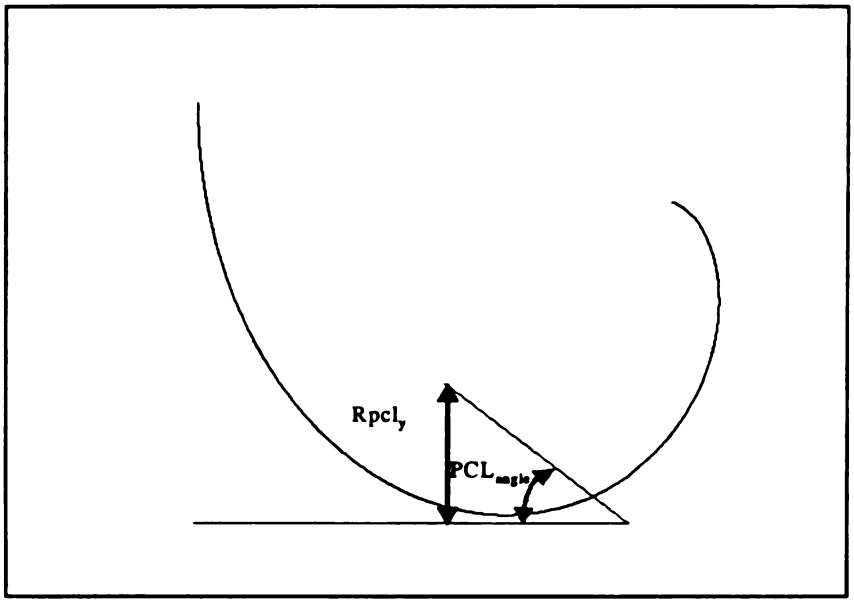

Figure 21: Representation of the ligament angle for the PCL.

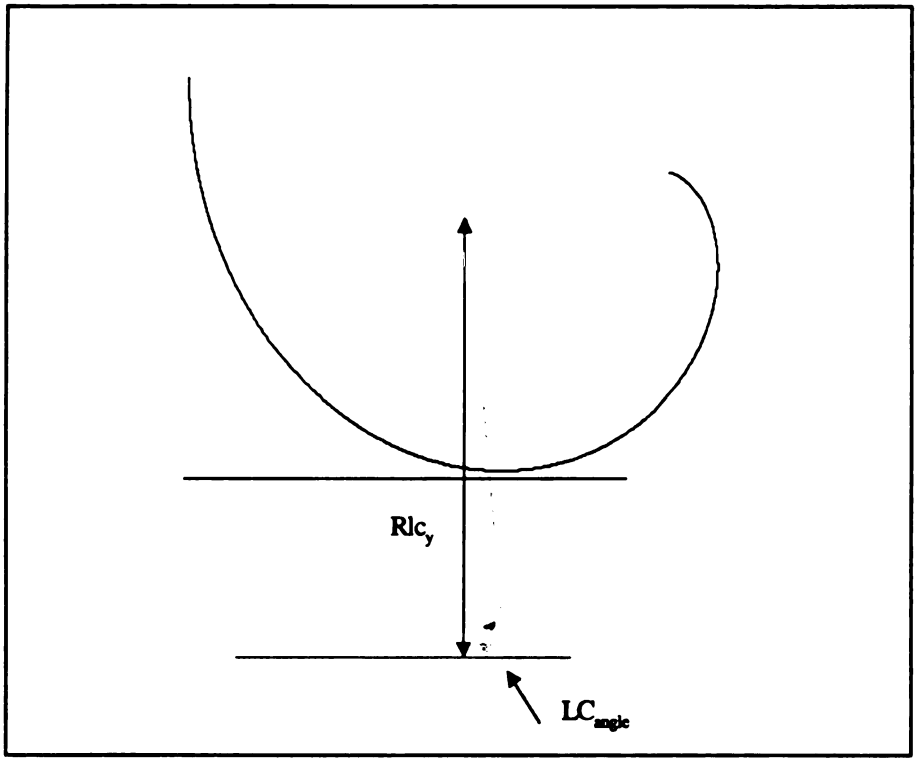

Figure 22: Representation of the ligament angle for the CL.

Equations [25a-c] were used in the calculation of ligament angles. In the case of the ACL and PCL, the angles formed with the tibial plateau always are acute. The model does not allow the femur to displace over the true anatomical constraints dictated by normal motion of the knee joint. Normal joint kinematics allow the collateral ligament to restrict excessive motion at both acute and obtuse angles. Given the geometrical parameters used to estimate the angle of pull and due to the properties of the sine function, equation [25c] will not accurately predict obtuse angles. When the sine function is used for angles greater than 180 degrees, the answer is the complement of the desired angle. To overcome this limitation, another equation [25d] was developed to use in the estimation of obtuse angles. A command to check the position of the ligament's insertion relative to its origin to determine which equation would give the appropriate CL angle was included in the model.

$$ACL_{angle} = \sin^{-1}\left(\frac{Racl_y}{Length_{acl}}\right) \qquad [25a]$$

$$PCL_{angle} = \sin^{-1}\left(\frac{Rpcl_y}{Length_{pcl}}\right) \qquad [25b]$$

$$CL_{angle} = \sin^{-1}\left(\frac{Rcl_y}{Length_{cl}}\right) \qquad [25c]$$

$$CL_{angle} = 180 - \sin^{-1}\left(\frac{Rcl_y}{Length_{cl}}\right) \qquad [25d]$$

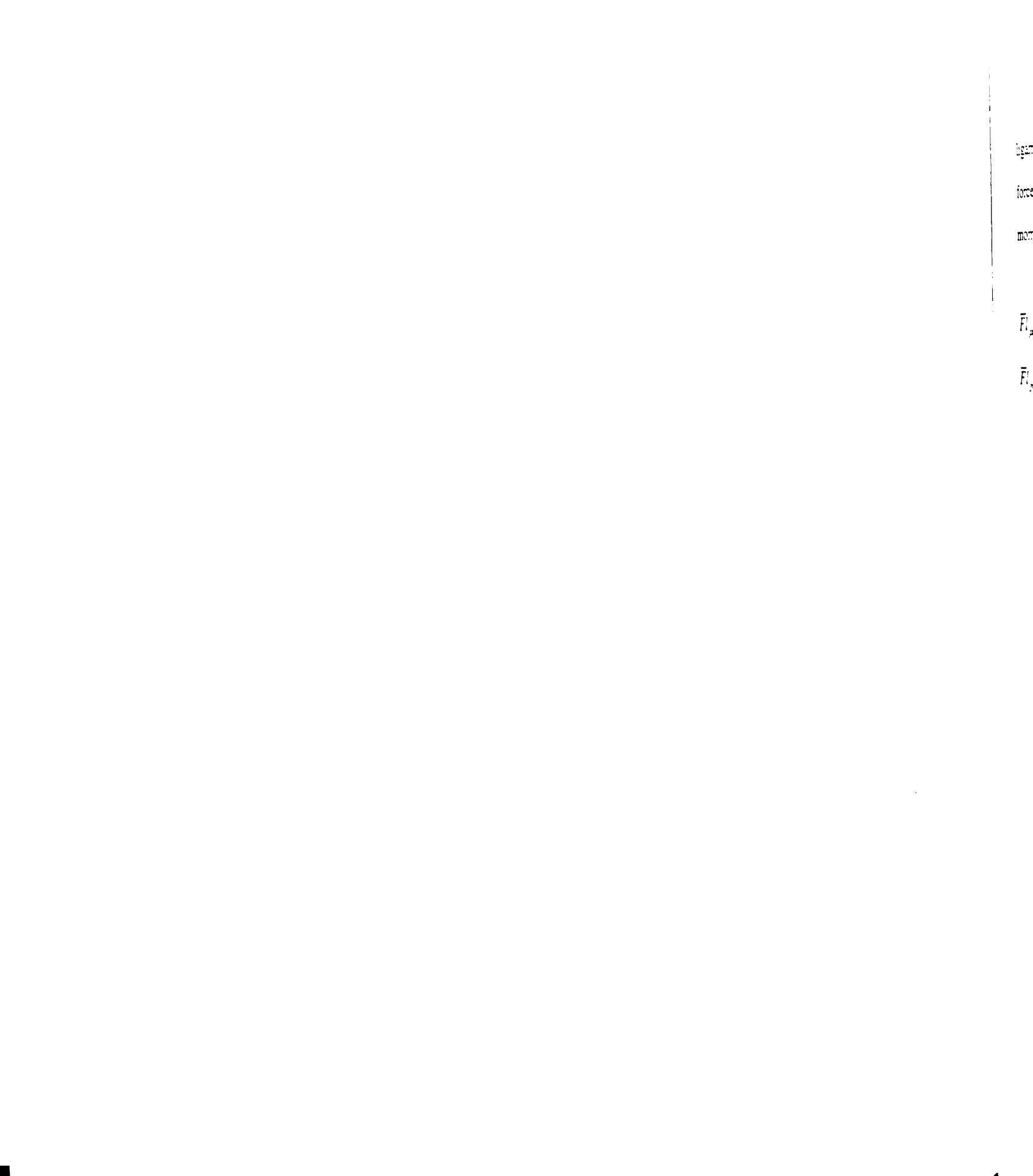

The component forces for each ligament were derived from the estimated ligament forces (Equation 26 a and b). The x and y components and the perpendicular force of each component, respectively, were used in the estimation of the internal moments (Figures 23-25).

$$\overline{Fl}_{jx} = \overline{Fl}_j \cdot \cos(lig_{angle}) \qquad [26a]$$

$$\overline{Fl}_{jy} = \overline{Fl}_j \cdot \sin(lig_{angle}) \qquad [26b]$$

where $\overline{Fl}_{jx}$ is the x-component of any ligament's force, $\overline{Fl}_{jy}$ is the y-component of any ligament's force, $\overline{Fl}_j$ is the resultant ligament's force, and lig_{angle} is the angle of pull of any ligament.

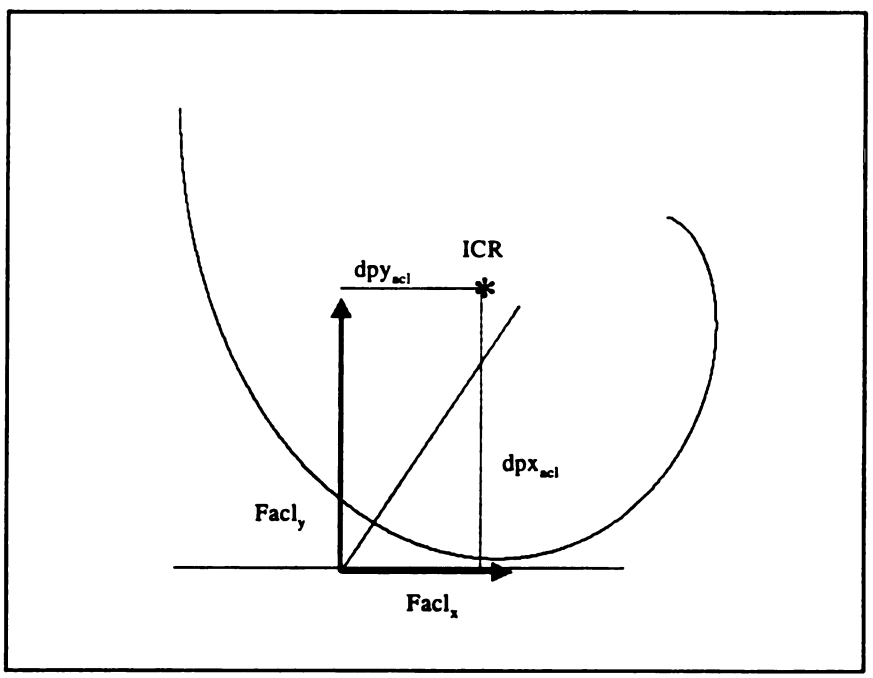

Figure 23: Graphical representation of the calculations of ACL internal moments.

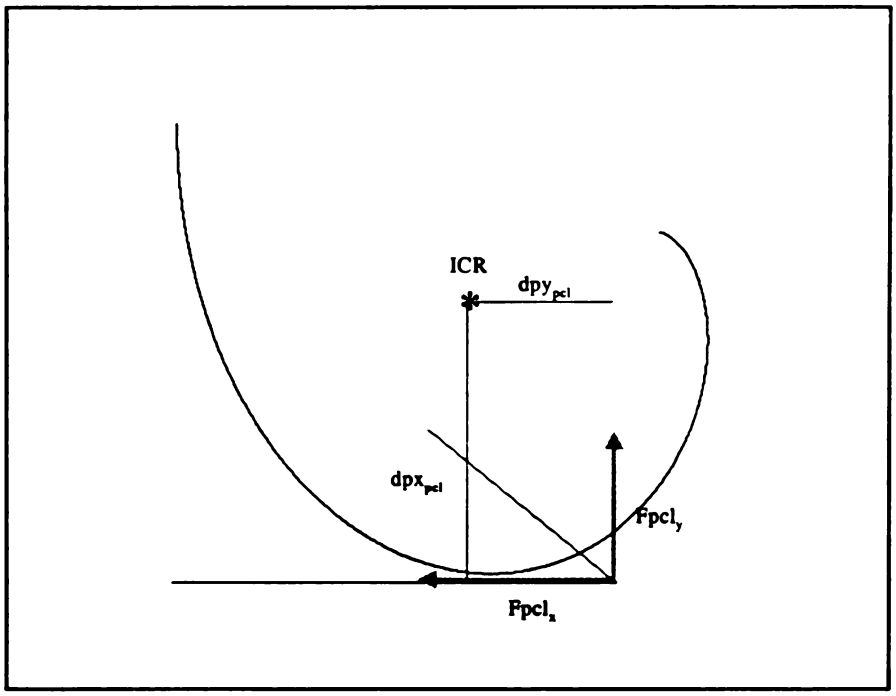

Figure 24: Graphical representation of the calculations of PCL internal moments.

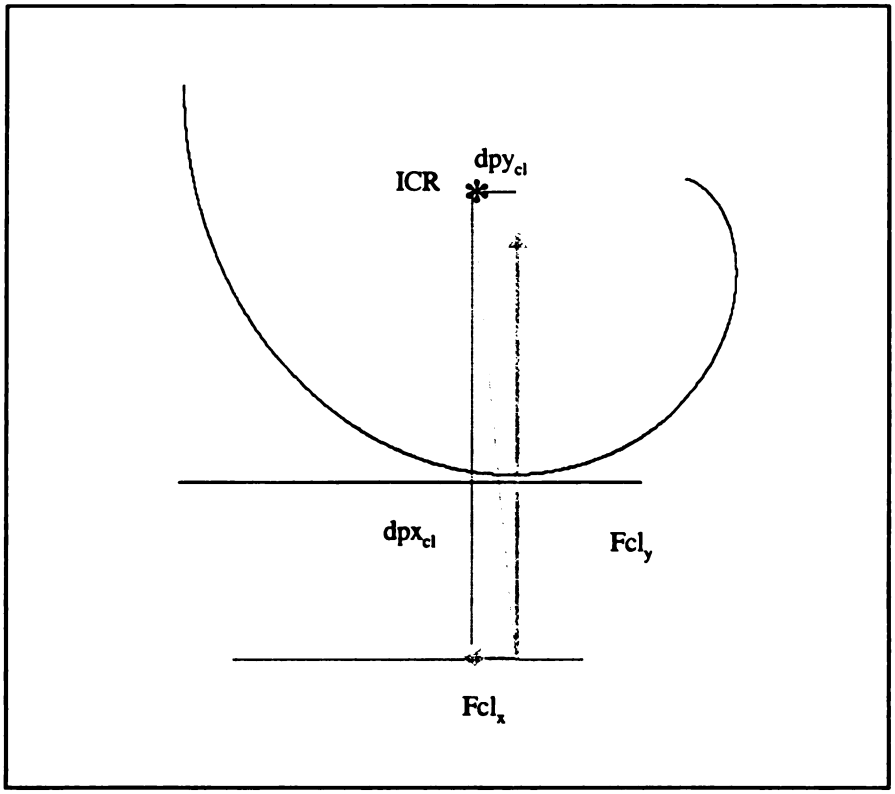

Figure 25: Graphical representation of the calculations of CL internal moments.

The ligament force components ($\overline{Fl}_{jx}$ and $\overline{Fl}_{jy}$) were used in the internal moment calculations. A flexion/extension internal moment was estimated for each ligament using equation [27]. The standard sign convention was used in the calculation of the moments, where counterclockwise is defined as negative and clockwise is defined as positive.

$$\overline{M}_{lj} = (\overline{Fl}_{jx} \cdot dpx_{lj}) + (\overline{Fl}_{jy} \cdot dpy_{lj}) \qquad [27]$$

where $\overline{M}_{lj}$ is the flexion/extension moment for ligament j

$\overline{Fl}_{jx}$ is the x-component of the force for ligament j

dpx_{lj} is the perpendicular distance to the ICR from the x-component of the force of ligament j

$\overline{Fl}_{jy}$ is the y-component of the force for ligament j

dpy_{lj} is the perpendicular distance to the ICR from the y-component of the force of ligament j.

In a similar manner, the internal moment generated by the contact forces was calculated about the ICR. The moment arms of the two components of the contact force was defined by the relative position of the contact point to the ICR, shown in equation [28]. The moments could then be calculated using equation [27].

$$R_{ICR/C} = ICR - C \qquad [28]$$

VII. Calculation of External Moments

External forces applied to the tibia and/or femur result in external moments about the knee joint. The model allows for input parameters of external forces in the form of ground reaction forces. Ground reaction force components and ground reaction moment components were used in the calculation of the flexion/extension external moments about the ICR. The resolved forces (COP) needed to be computed to obtain the point of application of the ground reaction forces relative to the ICR. The original moments obtained from the force platform measurement, and the ground reaction forces based on measurements about the center of the force platform, were used in this calculation. These parameters were reduced to a wrench system to determine the point where the line of application of the resultant ground reaction force crossed the surface of the plate. The component of the resultant moment parallel to the resultant force vector was first determined by equation [29]. The perpendicular component of the moment was then derived using equation [30]. The vector from the center of the force platform to the center of pressure point was defined by the assumption given by equation [31].

$$\overline{M}_p = \mathrm{Proj}_{\bar{F}} \cdot \overline{M} \qquad [29]$$

$$\overline{M}_\perp = \overline{M} - \mathrm{Proj}_{\bar{F}} \cdot \overline{M} \qquad [30]$$

$$\vec{r} \times \vec{F} = \vec{M}_\perp \qquad [31]$$

where $\vec{r}$ is the vector from the force plate center to the COP.

Equation [31] was expanded into scalar equations. Equations [32 a and b] were used when solving the scalar equations for the X and Y components of the COP.

$$X_{COP} = \frac{-h\overline{F}_x\left|\overline{F}\right|^2 - \overline{M}_y\left(\left|\overline{F}\right|^2 - \overline{F}_y{}^2\right) + \overline{M}_x\overline{F}_x\overline{F}_y + \overline{M}_x\overline{F}_x\overline{F}_z}{\overline{F}_x\left|\overline{F}\right|^2} \qquad [32a]$$

$$Y_{COP} = \frac{-h\overline{F}_y\left|\overline{F}\right|^2 - \overline{M}_x\left(\left|\overline{F}\right|^2 - \overline{F}_x{}^2\right) + \overline{M}_y\overline{F}_x\overline{F}_y + \overline{M}_z\overline{F}_x\overline{F}_z}{\overline{F}_z\left|\overline{F}\right|^2} \qquad [32b]$$

where h is the distance from the surface of the plate to the center of the plate.

The center of pressure location calculated as shown above was obtained in the force plate coordinate system. A transformation of coordinate systems was necessary to be able to obtain the position of the COP relative to the ICR. This transformation will be specified in more detail in the experimental methods chapter.

The calculation of the relative position vectors from the COP to the ICR is shown in equations [33 a-c]. The y-axis component (vertical component) of the COP location was assumed to be zero because most activities were performed on the surface of the force plate. Cases when this assumption was not met, will be addressed in the discussion of experimental methods.

$$\overline{R}_{ICR/COPx} = COP_x - ICR_x \qquad [33a]$$

$$\overline{R}_{ICR/COPy} = COP_y - ICR_y \qquad [33b]$$

$$\overline{R}_{ICR/COPz} = COP_z - ICR_z \qquad [33c]$$

The external moments were estimated from equations [33a-c] and the ground reaction forces components were recorded from the force platform. The estimation of the external moments was performed about the Z-axis of the lab coordinate system, which matches the out-of-plane axis in the model (Equation 34). To obtain the flexion/extension

external moment about the knee joint, the estimated moments were transformed to Euler axes.

$$\overline{M}_z = \overline{R}_{ICR/COPx} \cdot \overline{F}_y - \overline{R}_{ICR/COPy} \cdot \overline{F}_x \qquad [34]$$

VIII. Calculation of Patello-femoral Internal Moments

The forces generated within the patello-femoral mechanism produce moments about the center of the knee joint. All internal moments were calculated about the ICR point. The component forces were calculated for the quadriceps tendon, patellar tendon and patello-femoral contact forces, using equations [35] - [37] respectively.

$$\overline{FQT}_x = \overline{FQT} \cdot \sin(\theta) \qquad [35a]$$

$$\overline{FQT}_y = \overline{FQT} \cdot \cos(\theta) \qquad [35b]$$

where $\overline{FQT}$ is the resultant force of the quadriceps tendon, θ is the angle of flexion of the knee, and $\overline{FQT}_x$ and $\overline{FQT}_y$ are the component forces.

$$\overline{FPT}_x = \overline{FPT} \cdot \sin(\beta) \qquad [36a]$$

$$\overline{FPT}_y = \overline{FPT} \cdot \cos(\beta) \qquad [36b]$$

where $\overline{FPT}$ is the resultant force of the patellar tendon, β is the angle between the patellar tendon and the vertical, and $\overline{FPT}_x$ and $\overline{FQT}_y$ are the component forces.

$$P\overline{F}c_x = P\overline{F}c \cdot \cos(\alpha) \qquad [37a]$$

$$P\overline{F}c_y = P\overline{F}c \cdot \sin(\alpha) \qquad [37b]$$

where $\overline{PFc}$ is the patello-femoral contact force, α is the angle of inclination of the patella, and $\overline{PFc}_x$ and $\overline{PFc}_y$ are the component forces.

The moment arms for each of the force components were determined by a position vector between the point of application of the force and the ICR. The internal moments about the out-of-plane axis were calculated using equations [38-40]. The internal moments generated by the patellar tendon, quadriceps tendon and patello-femoral contact forces resist the sum of the internal moments produced by the ligament and tibio-femoral contact forces and the external moments produced by external forces.

$$\overline{MQT}_z = \overline{Ma}_x \cdot \overline{FQT}_y - \overline{Ma}_y \cdot \overline{FQT}_x \qquad [38]$$

$$\overline{MPT}_z = \overline{Ma}_x \cdot \overline{FPT}_y - \overline{Ma}_y \cdot \overline{FPT}_x \qquad [39]$$

$$\overline{MPFc}_z = \overline{Ma}_x \cdot \overline{PFc}_y - \overline{Ma}_y \cdot \overline{PFc}_x \qquad [40]$$

where $\overline{Ma}_x$ and $\overline{Ma}_y$ are the moment arms for the respective component force in the x and y directions respectively.

IX. Mathematical Solution

The input parameters to the model included the flexion angle, position data for the two targets on the thigh segment and the two targets on the shank segment that defined the ICR, and external forces and moments. Given the constraints and geometric compatibility equations, the number of unknowns was reduced and the equilibrium equations [41] were solvable.

$$\Sigma\overline{F}_x = 0$$
$$\Sigma\overline{F}_y = 0 \qquad [41]$$
$$\Sigma\overline{M}_z = 0$$

The mathematical solution of the model was found by combining the tibio-femoral forces/moments with the external forces/moments to solve for the requirements of equilibrium in the patello-femoral mechanism (Equations 42 a-c). The required quadriceps force for the specified kinematics of the tibio-femoral joint was obtained as the single number solution to the model.

$$\overline{FPT}_x = \overline{F}_x + \overline{Fc}_x + \overline{Facl}_x + \overline{Fpcl}_x + \overline{Fcl}_x \qquad [42a]$$

$$\overline{FPT}_y + = \overline{F}_y + \overline{Fc}_y + \overline{Facl}_y + \overline{Fpcl}_y + \overline{Fcl}_y \qquad [42b]$$

$$\overline{MPT}_z = \overline{M}_z + \overline{Mc}_z + \overline{Macl}_z + \overline{Mpcl}_z + \overline{Mcl}_z \qquad [42c]$$

The evaluation of a complete activity, such as squatting, with the quasi-static model allowed for the comparison of various parameters in terms of flexion angle changes. Therefore, the output of the model was not limited to a single parameter but, instead, supplied a number of parameters for the in-depth interpretation of knee joint kinematics.

EXPERIMENTAL METHODS

In the past, most experimental testing of knee joint models has been performed under constrained conditions that allow only flexion/extension at the joint. Some experimental testing using cadaver specimens allowed for unconstrained motion of the knee throughout the full range of motion. The action of squatting was chosen for the current investigation to experimentally test the accuracy of this model. The knee joint was unconstrained throughout each trial; therefore, the true mechanics of the knee joint were measured under normal loading.

I. Subjects and Data Collection

Squatting data collected from two subjects were used to test the accuracy of the computational model. A male subject, age 55, volunteered for the test. This subject was considered a control, with no known history of lower extremity injuries that could affect the knee mechanics. The model also was tested using data from a female subject, age 24. This subject was tested after having sustained a third degree ACL tear and then later three months after ACL reconstruction. The testing protocol was approved by the University Committee on Research Involving Human Subjects (UCRIHS) at Michigan State University under IRB number 93580.

The data used for the experimental testing was collected using the BTS Elite system and an AMTI force platform in the Biomechanics Evaluation Laboratory, College of Engineering at Michigan State University. The working volume was calibrated prior to data collection using a minimum of 27 known target locations. The calibrated volumes

for all tests were of similar dimensions; however, they were not necessarily the same. The four-camera system, sampling at 100 Hz., was used to follow the position of six targets (dynamic targets) placed on the lower leg during the squatting (dynamic) trial. A triad target configuration was used on each segment consisting of three targets on the thigh, and three targets on the shank segment respectively (Figure 26). The targets were covered with retro-reflective tape to allow each target to be recognized by the cameras. The BTS system calculates the barycentre of each marker and stores the two-dimensional x and y coordinates for each camera view in a file for later analysis.

II. Targeting Protocol

The dynamic targeting protocol, displayed in Figure 26, allowed for the definition of segmental coordinate systems in the thigh and shank respectively. Position vectors in the inertial (lab) coordinate system to each target in the thigh and shank segments were obtained from three-dimensional kinematic analysis. Relative positions between segment markers were used to define a plane on the body segment and subsequently construct a segmental coordinate system (Equations 43).

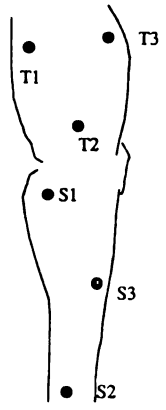

Figure 26: DynamicTargeting configuration for the thigh and shank segments.

$$\hat{i} = \frac{\vec{r}_{1/2} \times \vec{r}_{3/2}}{\left|\vec{r}_{1/2} \times \vec{r}_{3/2}\right|}$$

$$\hat{k} = \frac{\vec{r}_{1/2} \times \hat{i}}{\left|\vec{r}_{1/2} \times \hat{i}\right|} \qquad [43]$$

$$\hat{j} = \hat{k} \times \hat{i}$$

where $\vec{r}_{1/2}$ is the position vector from target 2 to target 1.

In addition to the dynamic trials, position data were collected during a standing file in which additional targets (virtual) were placed on anatomical landmarks. Virtual markers were used to define the anatomical axes and segment planes along the thigh and shank. The relative positions between the virtual markers and the dynamic targets in the segmental coordinate system are constant in magnitude and direction and are independent of the segment position in the inertial coordinate system. Therefore, it only is necessary to have both sets of targets (anatomical and dynamic) on the segment at the same time for one frame of data. Once the relative position was established in the segmental coordinate system, the location of the virtual targets were derived using an inverse translational transformation followed by a rotational transformation (Equation 44).

$$\vec{R}_a = \vec{R}_d + [T]^{-1} \vec{r}_{a/d} \qquad [44]$$

where $\vec{R}_a$ is the position vector to the anatomical target in inertial coordinates, $\vec{R}_d$ is the position vector to the dynamic target in inertial coordinates, T is the transformation matrix, and $\vec{r}_{a/d}$ is the relative

position vector between the anatomical and dynamic targets in segmental coordinates.

The greater trochanter and the medial and lateral epicondyles were used to define the mechanical axis and segmental plane for the thigh. The medial and lateral femoral epicondyles defined the medial-lateral axis, or Y_f axis. The longitudinal axis of the femur was defined using the relative position vector from the lateral femoral epicondyle to the greater trochanter. The Y_f axis and the longitudinal axis of the femur formed the segmental plane necessary to define the femoral coordinate system (Equations 45). X_t, Y_t and Z_t defined the coordinate axes fixed to the thigh segment.

$$Y_t = \frac{med_{cond} - lat_{cond}}{|med_{cond} - lat_{cond}|}$$

$$Longitudinal_{axis} = \frac{gr_{troc} - lat_{cond}}{|gr_{troc} - lat_{cond}|} \qquad [45]$$

$$X_t = \frac{Y_t \times Longitudinal_{axis}}{|Y_t \times Longitudinal_{axis}|}$$

$$Z_t = X_t \times Y_t$$

The shank coordinate system was defined in a similar manner. The tibial crest was used for the definition of the longitudinal axis of the tibia (Z_s), and a posterior target was used to define the para-sagittal plane of the lower leg. A position vector between the two targets on the tibial crest and a position vector between the distal target on the tibial crest and the posterior target on the leg defined the segmental plane. The development of the

coordinate system for the shank segment is shown by the set of equations 46. The fixed coordinate axes of the shank segment are X_s, Y_s and Z_s (Figure 27).

$$Z_s = \frac{prox_{leg} - dist_{leg}}{|prox_{leg} - dist_{leg}|}$$

$$Post_{axis} = \frac{dist_{leg} - post_{leg}}{|dist_{leg} - post_{leg}|}$$

$$Y_s = \frac{Z_s \times Post_{axis}}{|Z_s \times Post_{axis}|} \qquad [46]$$

$$X_s = Y_s \times Z_s$$

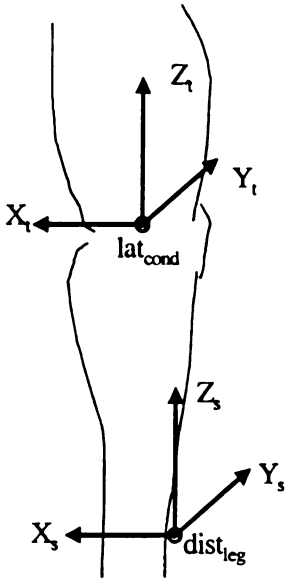

Figure 27: Thigh and shank segmental coordinate systems.

Euler angles were used to determine the angle of knee flexion throughout the squatting trial. Even though this method provided a three-dimensional analysis of knee joint motion, only the sagittal plane rotations were used as input parameters in the model.

The three-dimensional kinematic analysis of the knee joint motion provided a more accurate estimation of the flexion angle, as most rotations occurring at the knee joint are coupled. Knowledge of out of plane motion helped determine the validity of the simplifications made in the model.

The sequence of transformations required for the specification of Euler angles of the knee were the same as that reported by Grood and Suntay (1983). For the purpose of this calculation, and to maintain consistency with the clinical community, the calculation of Euler angles was performed for the motion of the tibia relative to the femur. This definition of relative motion did not influence the input parameter to the model or any other calculations performed within the model because $\theta_{f/e}$ will be the same in cases when either the femur or tibia is taken as the fixed segment. The first rotation was performed about the medial-lateral axis of the femur and specified knee flexion/extension. The second rotation was about the floating axis and defined adduction/abduction of the knee. The last rotation was about the inferior-superior axis of the tibia thus establishing internal/external rotation of the knee (Figure 28).

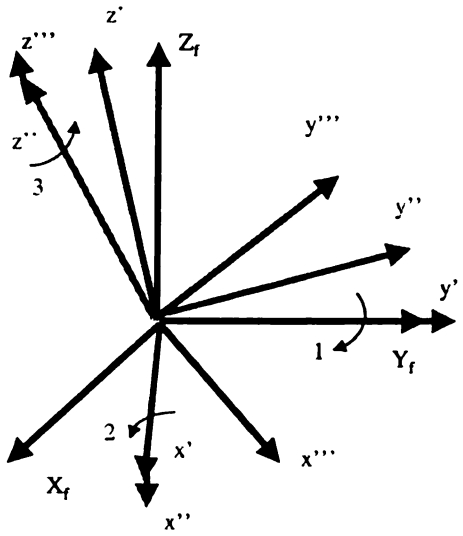

Figure 28: Rotational sequence for calculation of Euler angles.

The joint coordinate system was defined by two base vectors ($\hat{e}_2$ and $\hat{e}_3$), that corresponded to fixed axes, and a third mutually perpendicular base vector ($\hat{e}_1$). The relationship between the unit vectors and the corresponding segmental axis are illustrated in Equation [47] (Figure 29).

$$\hat{e}_2 = \hat{Y}_t$$

$$\hat{e}_3 = \hat{Z}_s \qquad [47]$$

$$\hat{e}_1 = \frac{\hat{e}_2 \times \hat{e}_3}{|\hat{e}_2 \times \hat{e}_3|}$$

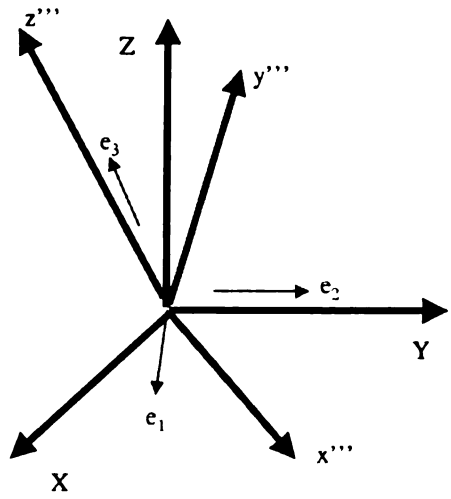

Figure 29: Joint coordinate system.

The calculation of the flexion/extension angle is shown in equation [48]. The rotation angles, as well as the abduction/adduction angles, have a side dependency. Right and left sides carry opposite signs, where external rotation and adduction are positive (negative) for a right (left) leg. The internal/external rotation angle and the abduction/adduction angle calculations are shown in equations [49] and [50] respectively. The flexion-extension angular motion, as defined by equation [48], was used as the input parameter (θ) in the model.

$$\theta = -\sin^{-1}(\hat{K}_f \cdot \hat{e}_1) \qquad [48]$$

$$\theta = -\sin^{-1}(\hat{e}_1 \cdot \hat{j}_t) \qquad [49]$$

$$\theta = -\sin^{-1}(\hat{e}_2 \cdot \hat{e}_3) \qquad [50]$$

III. Computational Model

The rest of the experimental methods will be presented in relationship to the computational model written in Matlab (version 6.0). The computer program (*k_exper.m)* is shown in its entirety in Appendix A. In this section, the functions called within the main program are identified and explained in more detail as necessary. Comments have been added throughout the program in Appendix A to aid in the understanding of the commands and to reduce the explanation necessary in this chapter. Mathcad (version 2000) was used in the computation of the ICR, in the calculation of the patella's position relative to the femur and in the final solution to the equilibrium equations. The templates used for these purposes are presented in Appendix B and Appendix C, respectively.

The instantaneous center of rotation was calculated using the position coordinates of two targets on the thigh and two targets on the shank segment. The calculation method was explained in detail in the analytical methods section. The ICR location was estimated relative to the superior target on the shank segment, which was treated as the fixed segment in the model. Linear parameters obtained from the experimental data and used as input variables in the model, such as the ICR location relative to the shank target, were converted to model units to allow for an anatomically correct representation of the knee motion in the model.

Model units were estimated using the true dimensions of the subject's knee as calculated with relative vectors between targets in the standing file. The depth of the knee, as defined by the anterior and posterior contours of the femoral condyles, was estimated using the anatomical ratio between depth and width of the epicondyles (Figure

30). The model calls the function *kneesize* to calculate the conversion variable. The relative position between the medial and lateral epicondyles in the standing file defined the width of the subject's knee. From this parameter, and with the known width to depth ratio, the depth was estimated and used in the representation of the knee model.

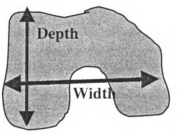

Figure 30: Graphical representation of the transverse view of the femoral condyles and depth-width relationship.

The anterior-posterior linear displacement of the femur over the tibia was defined using the location of the ICR relative to the superior target on the fixed tibia. Pure sliding of the femur relative to the tibia would occur about the center of curvature of the femur (Figure 19), which was estimated to be approximately 24 mm anterior to the posterior aspect of the femoral epicondyle. Any difference in the position between the ICR and the center of curvature of the femur would indicate the existence of rolling in the joint motion. The model calls the *contact_point* and *tct_pt* functions for the estimation of the location of the contact points of the femur and tibia respectively. Equations [19-21] are used to define the contact point between the femur and the tibia in pure rolling and pure sliding conditions.

Once the position of the femur relative to the tibia was estimated using the ICR position, the ligament length was calculated using the difference between the insertion and origin locations. As explained in the analytical methods, the ligaments were treated as extensible units, but wrapping was not considered in the calculation. The change in length of each ligament was taken as the difference between the ligament length at the specific flexion angle and the original ligament length. The function *change_length* is called to calculate Δ_{acl}, Δ_{pcl} , Δ_{lc} and ligaments strains. All three ligaments were assumed to be taut at full extension. The original length was calculated from known strain parameters of the ligaments at full extension. According to the literature, the ligaments would be under no strain at approximately 30° of flexion, assuming no imposed displacement of the femur over the tibia.

The stiffness coefficient (k) for each ligament was treated as an input parameter to the model. In the non-injured case, k was assigned normal values taken from the literature (Winsman et al., 1980). In the experimental case of an injured ligament, the k variable was adjusted accordingly to represent the pathology. The changes in this parameter did not affect the estimated ligament length, however, changes were noticeable in the forces sustained by the ligaments during the activity. The *lig_force* function was called to calculate the forces sustained by the ligaments as a function of knee flexion. The experimental model included a constraint check to limit all forces within the physiological range of each ligament. If the force estimated at any ligament exceeded the ultimate failure value for the ligament, the model reduced the stiffness coefficient by a value of 0.01 until the force generated was within the normal range. In cases when the

ligament is assumed to be completely torn, this constraint check would be omitted, and the k value would be zero.

Internal moments were calculated about the ICR using the estimated ligament forces and ligament angles. The function *moments* calculates the ligament moments about the ICR. The moments were calculated about the $\hat{e}_2$ base vector of the joint coordinate system. The transformation of the M_z moment about the Euler axis defined the moment about the true flexion/extension axis and not the Z-axis of the inertial coordinate system. Internal moment values were converted to N*m units and normalized to percent body weight, to allow for easy comparison across subjects.

The ground reaction forces and moments acquired with the AMTI force platform sampling at 1000 Hz. were used as the external input parameters in the model. The assumption that in a quasi-static situation all internal forces equal all external forces had to be met for equilibrium to exist. The model approached this assumption from the stand point of the known external forces generated during the squatting trial and the estimated ligament forces. The unknown forces of interest were the ones necessary to create equilibrium by the patello-femoral mechanism. The function *e_moments* was called to calculate the external moments about the ICR. The ICR location in the inertial coordinate system was used for the calculation of the external knee moments. The center of pressure calculation, as explained in the analytical methods, was included in this function. The moments were calculated about the x, y, and z axes of the inertial coordinate system. These external moments were then transformed to the Euler axes defined by the joint coordinate system. Only the flexion/extension external moment was used in the model.

The external moment was normalized to percent body weight for purpose of data analysis.

Tibio-femoral contact forces were estimated in the Mathcad template during the solution of the equilibrium equations. The moments about the flexion/extension axis passing through the ICR were also calculated within this template. The tibio-femoral joint was assumed to be frictionless, therefore the contact force must satisfy the condition of normality to the surfaces in contact. The horizontal force was also calculated with the purpose of analysis and interpretation of the internal forces generated on the ligaments.

Prior to the estimation of the quadriceps group force necessary to satisfy the equilibrium condition, the position of the patella relative to the femur needed to be known. The patella position is dependent on the overall position of the femur relative to the tibia as defined by the flexion angle and the antero-posterior displacement. The inextensibility of the patellar tendon was used as another constraint to the motion of the patella. Appendix B contains the Mathcad template used in the solution of the simultaneous set of equations as defined by the constraints for the motion of the patello-femoral joint. The patella was assumed to rotate about the trochlear groove. The center of rotation is approximately 22 mm from the anterior aspect of the trochlear grove of the femur. The center of rotation of the patella was defined as a constant parameter in the model. The biarticulating patella model allowed the shift of contact of the patella from the trochlear groove to the condyles occurring at flexion angles greater than 100 degrees.

The solution to the quasi-static model was obtained with the Mathcad template presented in Appendix C. Parameters from the patella position were used to solve the equilibrium mechanism of the patello-femoral joint and then used in the estimation of the

quadriceps forces necessary to balance the external and internal forces and moments calculated in the model. The position of the patella as defined by the angles α and β was used in the estimation of the unit vectors for the patellar tendon, quadriceps tendon and the patello-femoral contact force as shown in Figures 31 and 32.

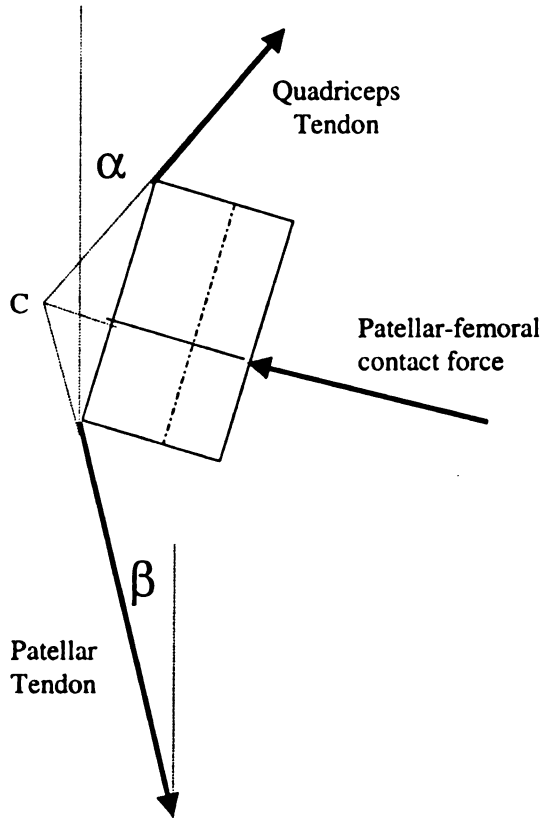

Figure 31: Patello-femoral equilibrium mechanism.

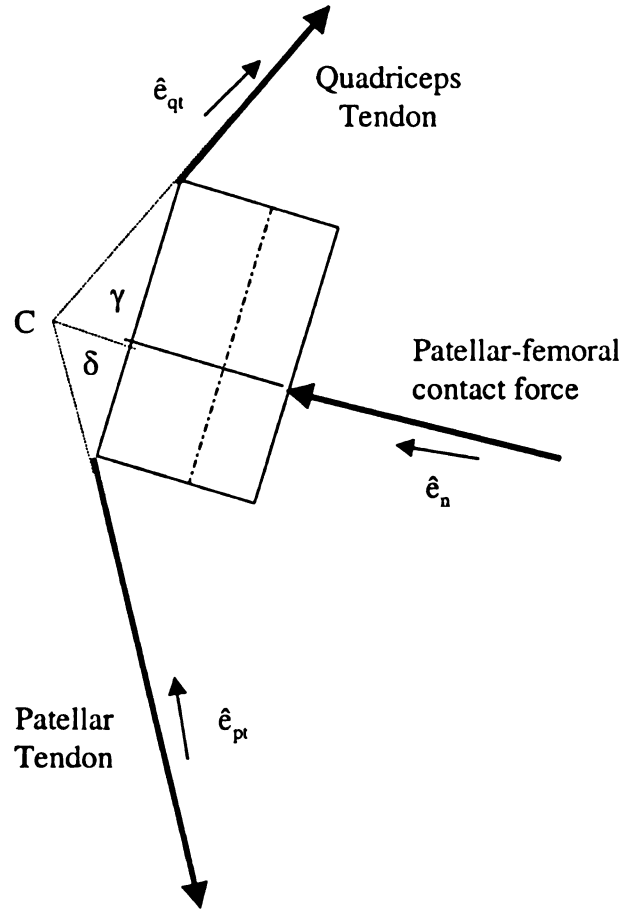

Figure 32: Unit vector representation in the patello-femoral mechanism.

RESULTS AND DISCUSSION

Many mathematical models of the knee joint have been developed to predict the mechanical behavior of the joint. Most experimental testing of these models has been performed on cadaver specimens under constrained conditions. The mathematical model presented in the analytical methods was tested using biomechanical data obtained during squatting. The results of the experimental tests for the initial half squat cycle, are presented in this chapter and some comparisons with other proposed models are included.

Researchers have demonstrated that the knee joint is not a true hinge joint. Normal knee mechanics include a combination of rolling and sliding of the femur over the tibia. These two actions are influenced by the geometry of the femoral and tibial condyles and are believed to be constrained primarily by the cruciate ligaments. Even though the knee joint is no longer classified as a hinge joint, the quantification of rolling and sliding has been difficult. As presented in the review of literature a variety of models have been used to define the knee joint mechanics; however, very few models have been tested in-vivo while performing unconstrained movements.

In this model the ligaments were treated as extensible units allowing a measure of ligament laxity as determined by joint motion. The instantaneous center of rotation was calculated and used in the estimation of the rolling and sliding characteristics of the joint. Following the determination of joint position, the equilibrium equations were used to estimate the muscle and internal forces necessary to maintain the joint in that position.

Differences in the mechanical behavior of the knee joint were evident in the comparison of the data for the three subjects tested. These results also showed some

variations when compared to results presented in the literature. However, the differences in values and patterns of the data were found to be consistent with the known mechanical characteristics of the tested knees. Only the more important parameters are discussed in this chapter.

The equilibrium condition that needed to be satisfied by the system is dependent on the relative position between the femur and the tibia. As the position changes, the constraints to the motion change, influencing the internal forces of the system. The predicted displacement of the femur relative to the tibia illustrated by the change in position of the contact point of the femoral condyle is shown in Figure 33. The comparison in the displacement pattern of the contact point for the three tested subjects shows that in all cases the knee behaves under a combination of rolling and sliding motions. The pure rolling pattern is included in Figure 33 as a point of comparison.

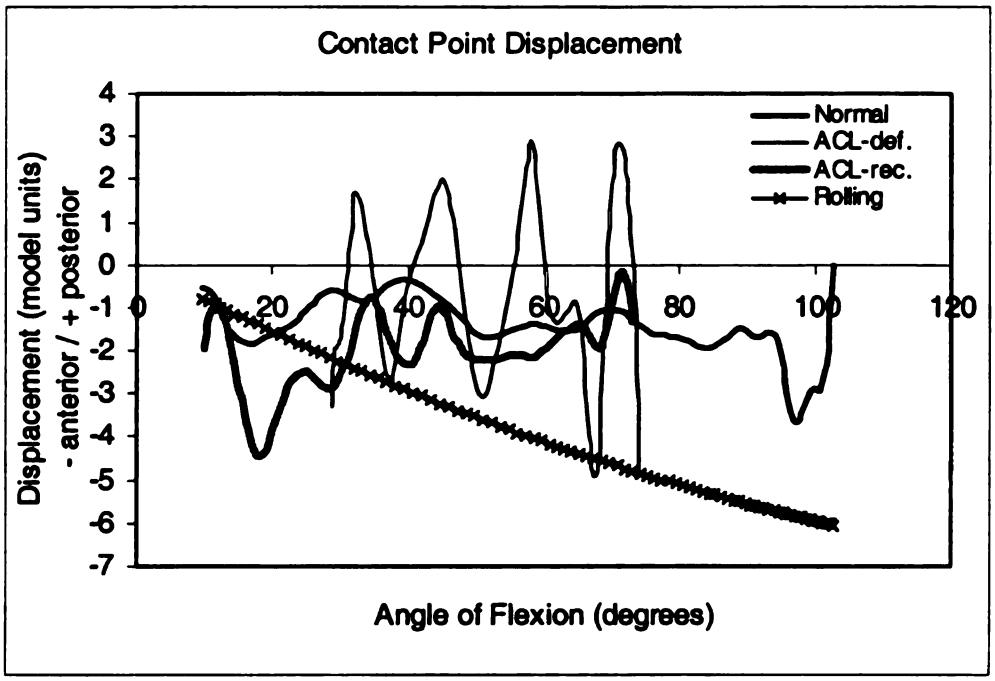

Figure 33: Contact point displacement comparison.

The displacement pattern for the ACL deficient patient gave an indication of the instability present at the knee joint. The increase in the amount of translation allowed in the joint demonstrates the importance of the cruciate ligaments acting as the primary constraints to rolling and sliding of the knee joint. One of the objectives of ACL reconstruction is to return the joint to its normal mechanical behavior. The comparison between contact point displacement for the ACL deficient knee and the ACL reconstructed knee indicates that the reconstruction was successful in meeting this objective. The translational motion of the femur relative to the tibia was decreased following the ACL reconstruction; and the pattern was similar to that of the normal knee, except for that observed during the initial 20° of flexion.

The differences in pattern observed between the displacements presented in Figure 33 and those previously presented in the literature are due to the unconstrained motion of the joint under the current testing conditions. A more predictable rolling and sliding pattern can be expected when the knee joint motion is not influenced by external forces and is moved through a controlled range of motion. For equilibrium to exist, the internal and external forces and moments have to cancel out. The internal forces and moments are dependent on the relative position of the femur and the tibia. Therefore, the mechanics of the joint cannot be compared between constrained and unconstrained motions.

The amount of laxity of the joint is a direct indicator of the mechanical behavior of the constraints. An anterior displacement of the femur relative to the tibia has to be controlled by the PCL, while a posterior displacement of the femur relative to the tibia is

controlled by the ACL. The cruciate ligament angles determine the amount of horizontal force contributed by each ligament in the constraint of the horizontal translation at the knee joint. Due to the orientation of the collateral ligaments, the contribution to anterior-posterior constraint of motion by this ligament is limited when compared to that of the cruciate pair.

The laxity curves for each subject are presented in Figures 34-36. The horizontal forces of the ACL, PCL and CL were summed and graphed as a single horizontal force which acted as the constraint to the motion. A negative horizontal force would represent a force acting anteriorly on the joint, and a positive horizontal force acted posteriorly on the joint.

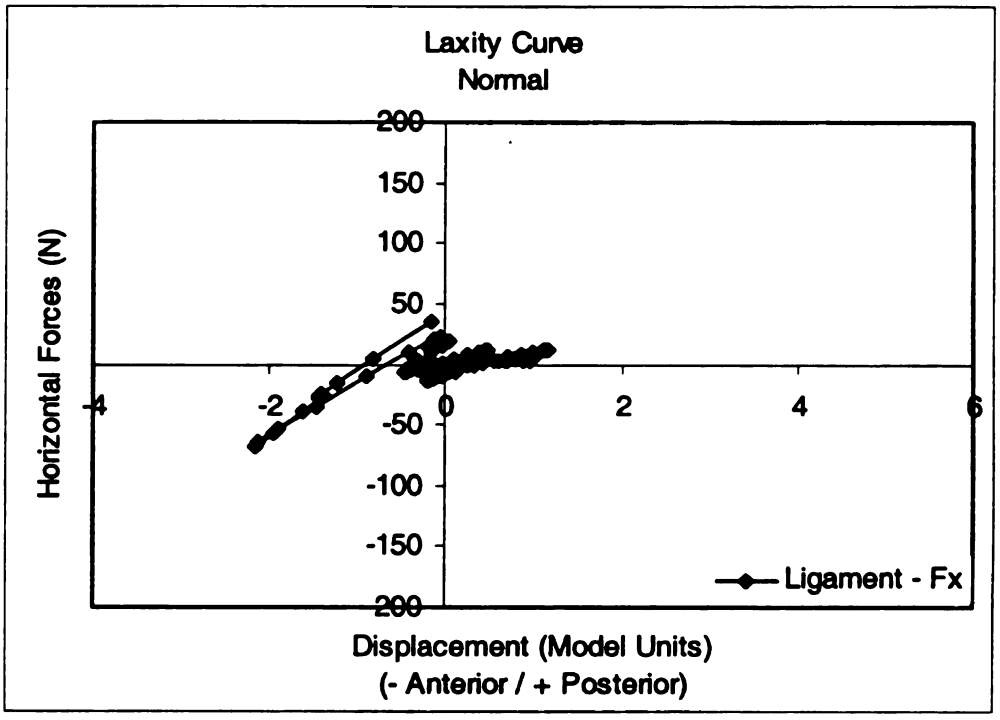

Figure 34: Laxity Curve: Ligament horizontal force vs. Anterior-posterior displacement for a normal knee.

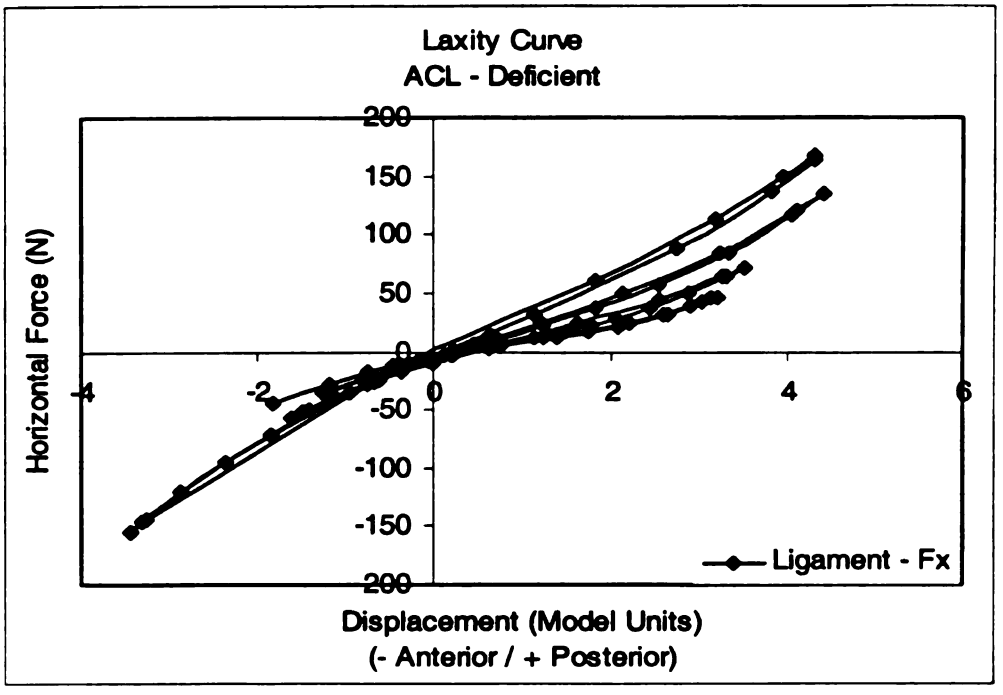

Figure 35: Laxity Curve: Ligament horizontal force vs. Anterior-posterior displacement for an ACL deficient knee.

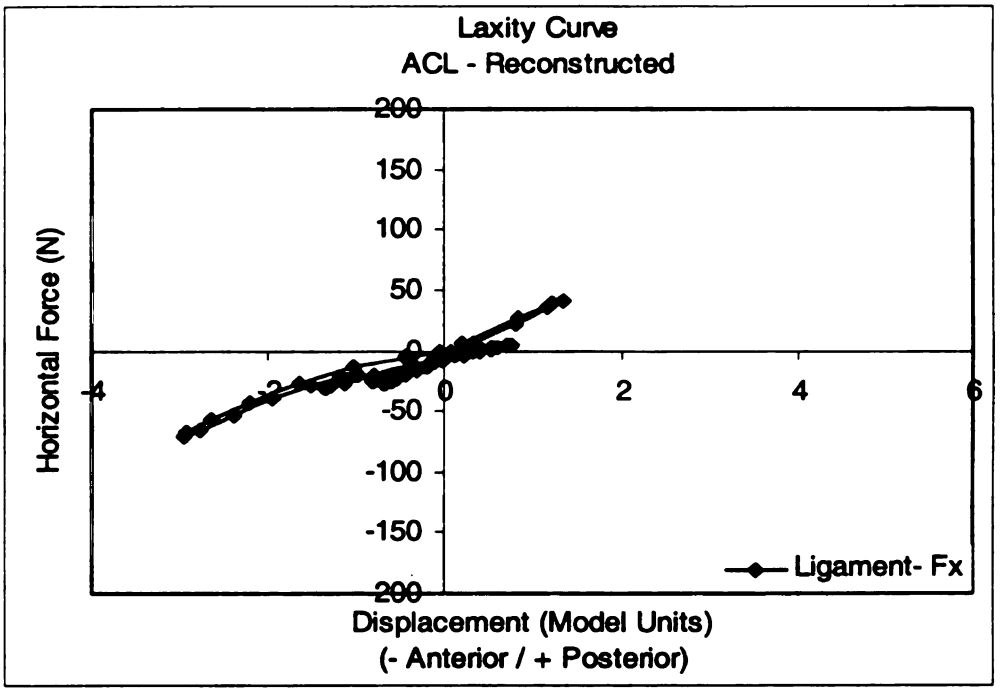

Figure 36: Laxity Curve: Ligament horizontal force vs. Anterior-posterior displacement for an ACL reconstructed knee.

The tighter the pattern represented by the laxity curve, the less motion that is allowed in the joint; and, therefore, the lower the amount of force necessary to constrain the motion. Figure 35 is a representation of the amount of horizontal force produced by the ligaments in an unstable knee. The amount of laxity in the unstable knee due to the deficient ACL, was considerably greater than that observed in the normal knee. This increase in laxity was primarily in the posterior direction, which is regularly controlled by the ACL. There was also an apparent increase in the laxity in the anterior direction. However, when comparing the ACL-deficient and ACL-reconstructed graphs (Figures 35 and 36 respectively), the same anterior displacement can be observed. The laxity in the anterior direction suggests that the anterior laxity was not a result of the ACL injury, but a natural difference in ligament laxity between this subject and the subject used as the norm.

Following the ACL reconstruction, the laxity of the knee was decreased and the forces sustained at the ligaments also were decreased. The tightness of the laxity curve demonstrated the ability of the new tissue to act as a good constraint to posterior motion of the knee joint. Differences between the laxity curve from the uninjured subject and that of the post reconstruction subject can be explained by the differences in contact point displacement presented earlier.

The position of the femur relative to the tibia and the internal forces produced by the ligaments determined the position of the patella relative to the femur and consequently the patello-femoral equilibrium mechanism. Two angles described by the patello-femoral mechanism are of particular interest in this model: β, which is the angle between the patellar tendon and the vertical, and α, which is the angle between the

anterior aspect of the patella and the vertical. These two angles affect the forces necessary for equilibrium which are produced by the quadriceps and are transmitted through the patellar tendon. The differences in α and β between the normal, ACL-deficient and ACL-reconstructed conditions can be observed in Figures 37-39, respectively.

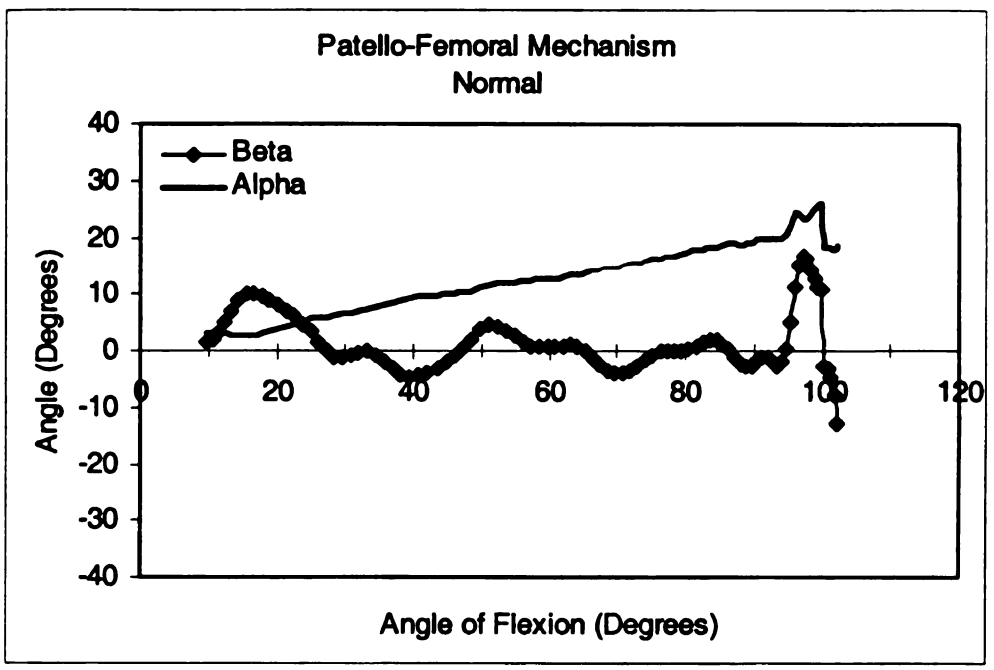

Figure 37: Patello-femoral Mechanism angles vs. Knee flexion. Normal knee.

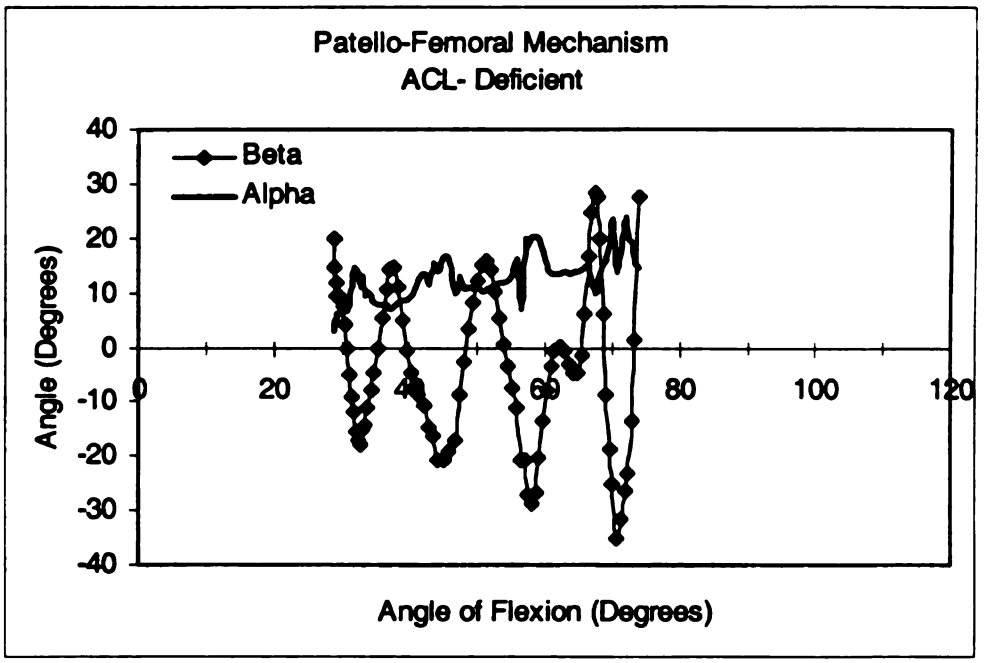

Figure 38: Patello-femoral Mechanism angles vs. Knee flexion. ACL-deficient knee

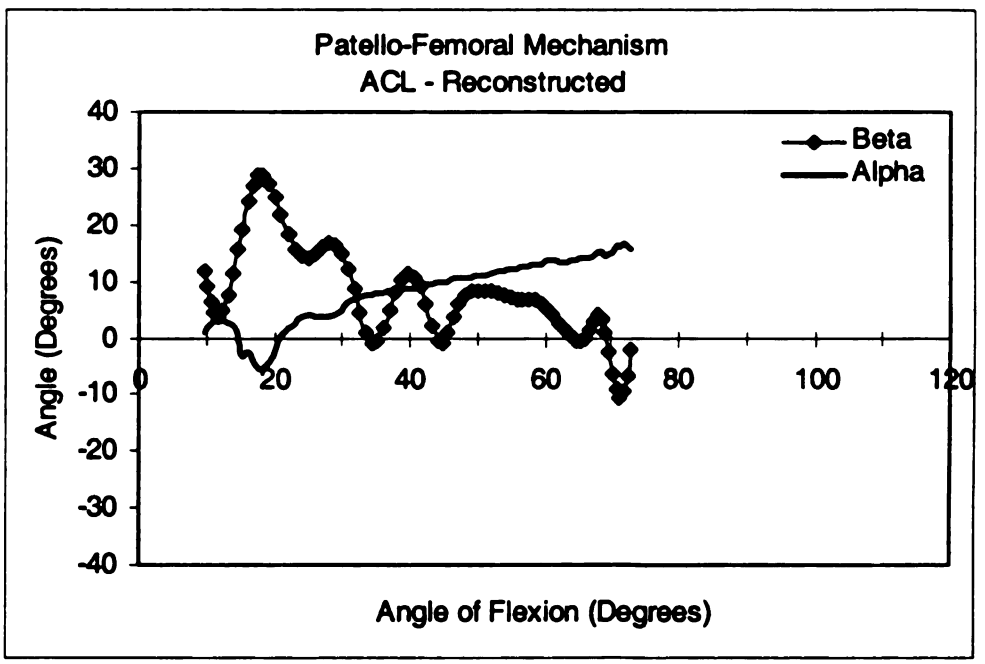

Figure 39: Patello-femoral Mechanism angles vs. Knee flexion. ACL-reconstructed knee.

The magnitude of α, or degree of inclination of the patella, increased with knee flexion. This pattern agreed with the results presented by Gill et. al. (1996). However, the overall range of α in the normal knee condition was lower for the current study. The sharp decrease in magnitude seen at 100° of flexion corresponded with the change in contact surface that was allowed by the biarticulating model. In Figure 38 there was an apparent dependency between α and β magnitudes. In the ACL-deficient knee, the angle of inclination of the patella was not dependent on the angle of flexion of the knee joint but was dependent on the position of the patellar tendon. Following ACL reconstruction (Figure 39), the dependency between α and β disappeared for most of the range of motion, and there was a return to the normal increase in α with an increase in knee flexion. The initial 20° of knee flexion still showed a dependency between α and β angles in the ACL-reconstructed condition. This pattern matched the difference in the displacement pattern observed in Figure 33 when the normal and ACL-reconstructed conditions were compared.

When examining the pattern defined by the line of action of the patellar tendon, the results of the present study did not agree with previous research. The results presented by Gill et al. (1996) showed a constant decrease of β from 20° to -10° with increased knee flexion. The results presented in Figures 37-39 showed a greater dependency between the position of the patellar tendon and the position of the femur relative to the tibia. The differences in results can be explained by assuming that the dependency of the line of pull of the patellar tendon on the angle of knee flexion has to be accompanied by a similar dependency with the relative position of the femur in the horizontal direction. This dependency was particularly evident in Figure 38 for the ACL-deficient knee. As

was previously shown, the knee joint with a deficient ACL was more lax. This increased motion of the femur over the tibia affected the overall position of the patella relative to the femur.

One of the constraints used in the solution of the patello-femoral equilibrium equations was the requirement of contact between the femur and the patella throughout the range of motion. Adjustments in the angles β and α contributed to partially satisfying this constraint. The greater adjustments necessary were accomplished by changing the orientation of the patellar tendon, which changed the overall position of the patella relative to the femur; then smaller adjustments to alpha were made to satisfy the contact point condition.

In the ACL reconstructed condition, the angle β (Figure 39) followed a similar pattern to that of the displacement of the femur over the tibia; however, α followed a pattern that was considered normal. This dependency can be compared to the ACL deficient condition (Figure 38) where both α and β were dependent on the displacement pattern. Greater adjustments in the position of the patella were necessary to satisfy the condition of contact between the patella and the femur.

The forces produced by the quadriceps are influenced by the internal and external forces at the tibio-femoral joint as well as by the condition of equilibrium in the patello-femoral mechanism. Changes in the orientation of the patella will influence the transmission of forces from the quadriceps tendon to the patellar tendon. The ratio between patellar tendon (PT) and quadriceps tendon (QT) forces is a simple indication of the mechanical behavior of the patello-femoral mechanism. This ratio is illustrated in

Figures 40-42 for the normal, ACL deficient and ACL reconstructed conditions, respectively.

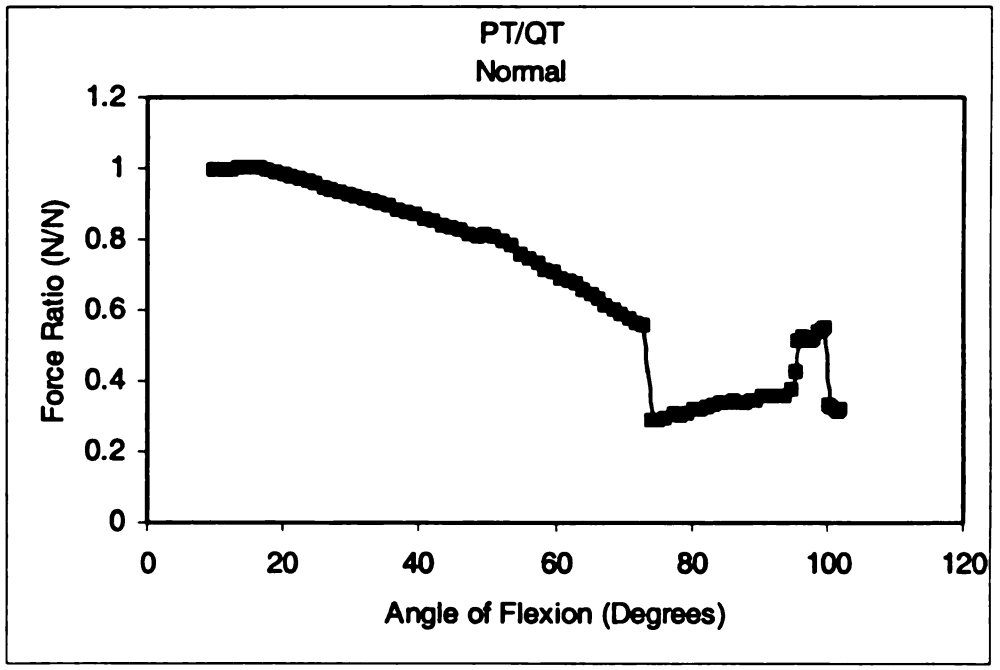

Figure 40: Patellar Tendon to Quadriceps Tendon force ratio for the normal knee.

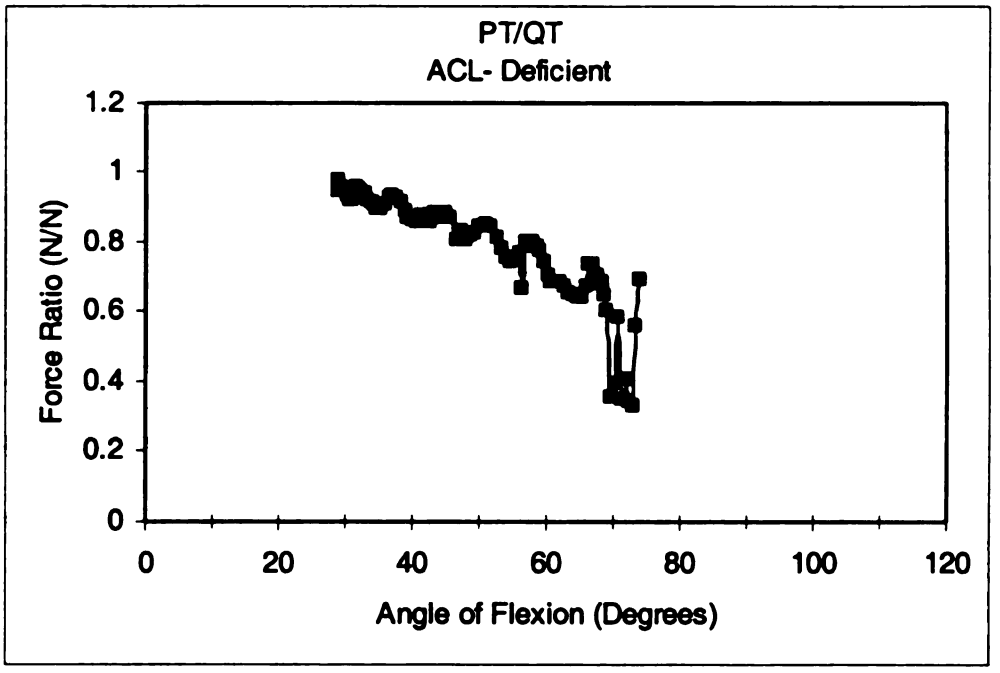

Figure 41: Patellar Tendon to Quadriceps Tendon force ratio for the ACL-deficient knee.

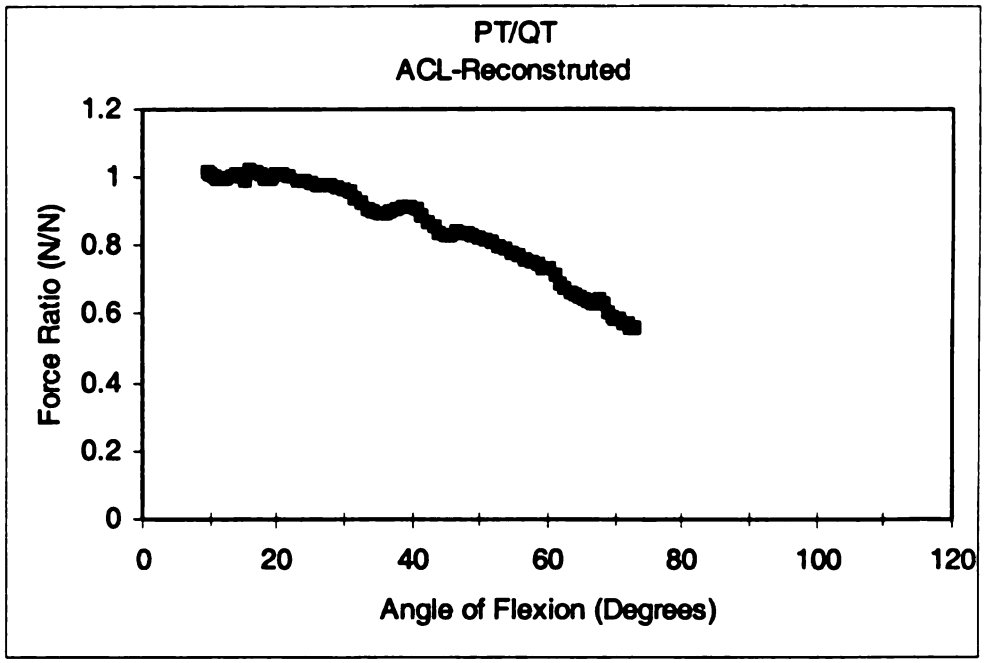

Figure 42: Patellar Tendon to Quadriceps Tendon force ratio for the ACL-reconstructed knee.

The ratio between the patellar tendon force and the quadriceps tendon force was similar in all tested conditions and followed closely that described by Gill et al. (1996). The two points of interest in Figure 40 were the start of the wrap of the quadriceps tendon and the switch in contact surface between the patella and the femur. As the quadriceps tendon started to wrap around the femoral trochlea at approximately 75° of flexion, there was a marked decreased in the ratio between the PT and QT forces. At 100° of flexion when the contact between the patella moved from the trochlea to the condyles, there was another marked decrease in the ratio of forces between the two tendons.

Even though the ratio between the PT and QT forces followed a similar pattern for the ACL-deficient knee followed a pattern similar to that observed in the normal knee, there were some additional small fluctuations that could be observed (Figure 41).

The smaller changes in the slope of the line could be matched with the large changes observed in the translation of the femur over the tibia (Figure 38). As a result of the more predominant changes in the α and β angles, the line of pull of both the patellar tendon and the quadriceps tendon were affected. The mechanical advantage of each of these tendons was affected at different times throughout the range of flexion, which affected the ratio of forces.

The purpose of this mathematical model was to develop a tool for the prediction of ligament strains and forces during dynamic activities without the need for an invasive technique. The strains on the ligaments were calculated using the difference in length of the fibers throughout the range of motion of the knee. Change in ligament length was directly affected by the position of the femur relative to the tibia and by the distance between origin and insertion sites. The forces generated by the ligaments are presented in Appendix D, and more attention is given to the strain patterns obtained from the model. Since the displacement characteristics of the joint were found to be different from previous studies, the strain patterns shown in Figures 43-45 also showed differences when compared to previously reported data.

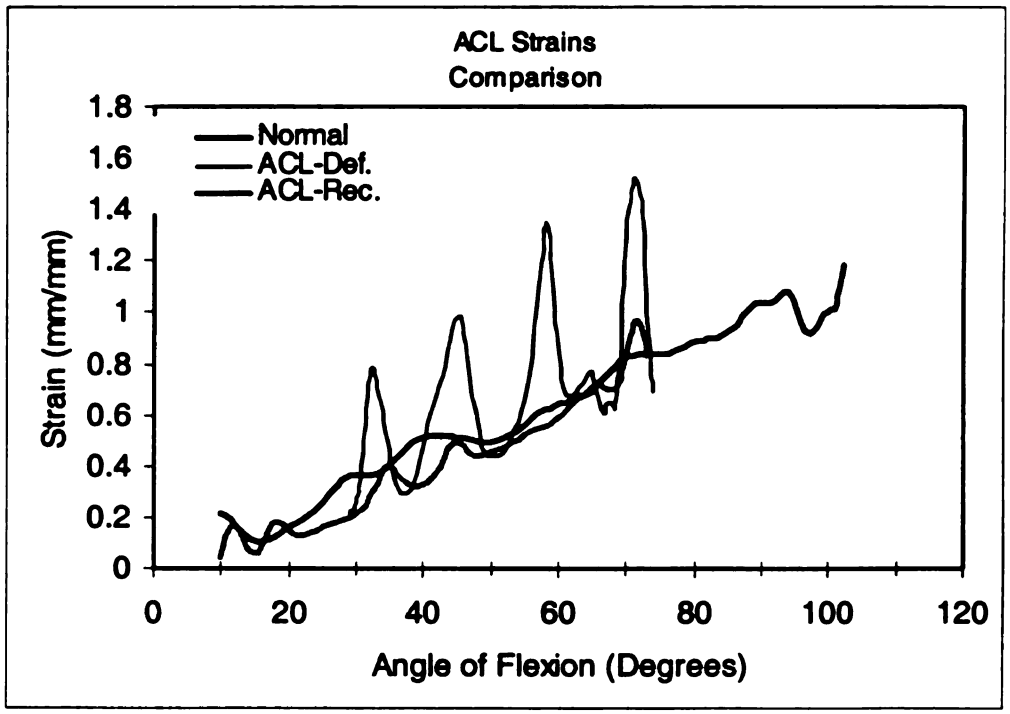

Figure 43: Strain comparison for the ACL.

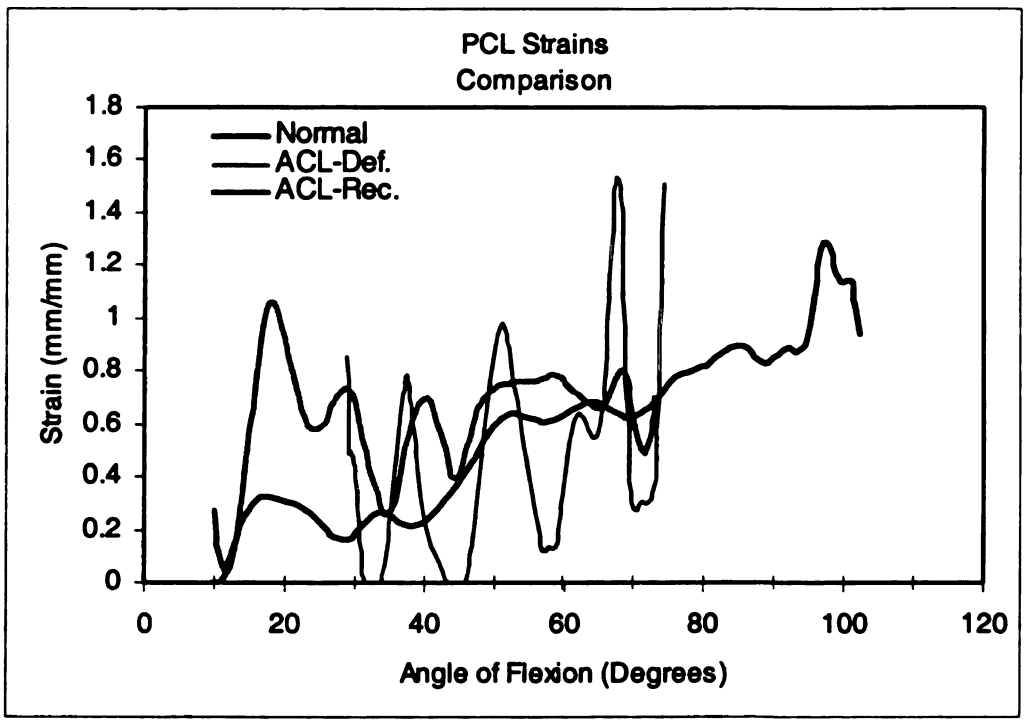

Figure 44: Strain comparison for the PCL.

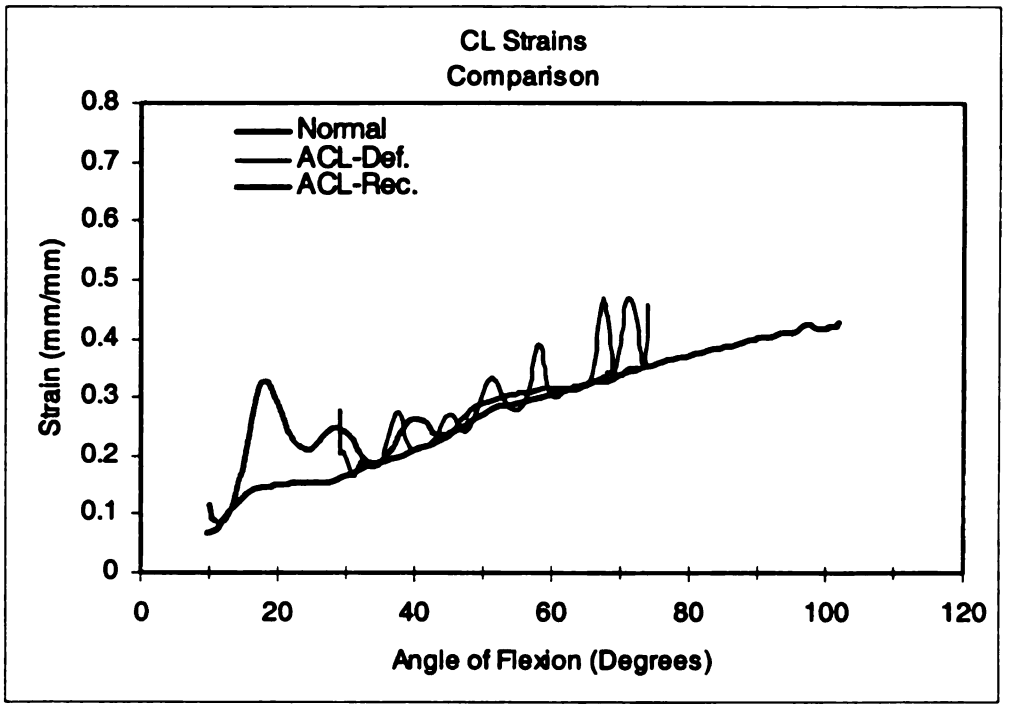

Figure 45: Strain comparison for the CL.

Winsman et al. (1980) indicated that the ACL is under-strain from 0 to 20° of knee flexion. The ACL is considered to be slack from approximately 20° to 40° of flexion, at which point there is a constant increase in strain of the ligament with increased knee flexion. The pattern for ACL strain obtained with the current model for the normal knee (Figure 43) demonstrated the lowest strain level at approximately 15° of flexion and a constant increase in strain with increased flexion. The absence of the period when the ligament is unstrained, expected in the normal pattern, can be explained by the slight posterior displacement of the femur over the tibia which occurred from 20° to 45° of flexion (Figure 33). This posterior displacement of the femur relative to the tibia very likely produced the observed strain on the ACL.

The overall strain pattern for the other two conditions, ACL-deficient and ACL-reconstructed, was similar to that obtained for the normal subject (Figure 43). The expected peaks in strain were observed for the ACL-deficient condition where the femur was abnormally displaced over the tibia. A higher knee flexion angle combined with a larger posterior displacement of the femur relative to the tibia, generated a larger strain when compared to similar translations at lower flexion angles. When designing rehabilitation exercises for ACL-deficient patients, the range of motion allowed at the knee joint should be taken into consideration due to the strains placed on the ACL with increased knee flexion.

Following ACL-reconstruction, the strain pattern at the ACL was similar to that obtained for the normal knee. The differences in the displacement patterns of the femur relative to the tibia, between the two conditions, did not influence the strain patterns for the ACL. This fact also was apparent when comparing the laxity curves for the two conditions.

Winsman et. al (1980) showed that the PCL was strained from 40° of flexion to full flexion. The data obtained for the normal knee with the present model showed an increase in the PCL strain from 5° to full flexion (Figure 44). The differences between strains obtained with the present model and those previously reported data are believed to be predominantly due to of possible errors associated with the insertion and origin locations of the ligament. The selected insertion and origin sites for the present model might not have been representative of the overall behavior of the ligament fibers.

Deviations from the normal pattern for the PCL strains obtained from the ACL-deficient knee data could be explained in the same manner as the differences obtained

with the ACL strain patterns. The instability of the knee joint affects not only the injured tissue, but also the surrounding structures. The anterior laxity observed in the data for the ACL-reconstructed knee placed increased strains on the PCL during the initial 30 degrees of knee flexion. Slightly higher strains were observed for the ACL-reconstructed knee throughout the range of flexion than for the normal knee when both were tested with the present model.

There was a constant increase in strain for the CL throughout the range of flexion for the normal knee (Figure 45). Increases in strain obtained for the ACL-deficient and ACL-reconstructed knees were due to the displacement patterns that accompanied knee flexion. At lower flexion angles, an anterior displacement of the femur over the tibia increased the strain on the CL. The opposite was true at higher flexion angles where a posterior translation had a greater influence on the strain pattern of the CL.

Following the calculation of the relative position between the femur and the tibia and the calculation of ligament strains and forces, the solution to the equilibrium equations was obtained by calculation of the quadriceps force necessary to balance the system. Equilibrium of the patello-femoral mechanism, quadriceps tendon, patellar tendon and patello-femoral contact forces had to be satisfied before the final solution could be obtained. The forces obtained for the QT and PT were dependent on the angle of flexion as well as the internal and external forces applied to the system. Due to the influence of the displacement of the femur, relative to the tibia, to the angle of pull of the patellar tendon, the horizontal and vertical components of the QT and PT forces are presented separately. The QT and PT forces obtained for the normal knee are presented in Figures 46a-b.

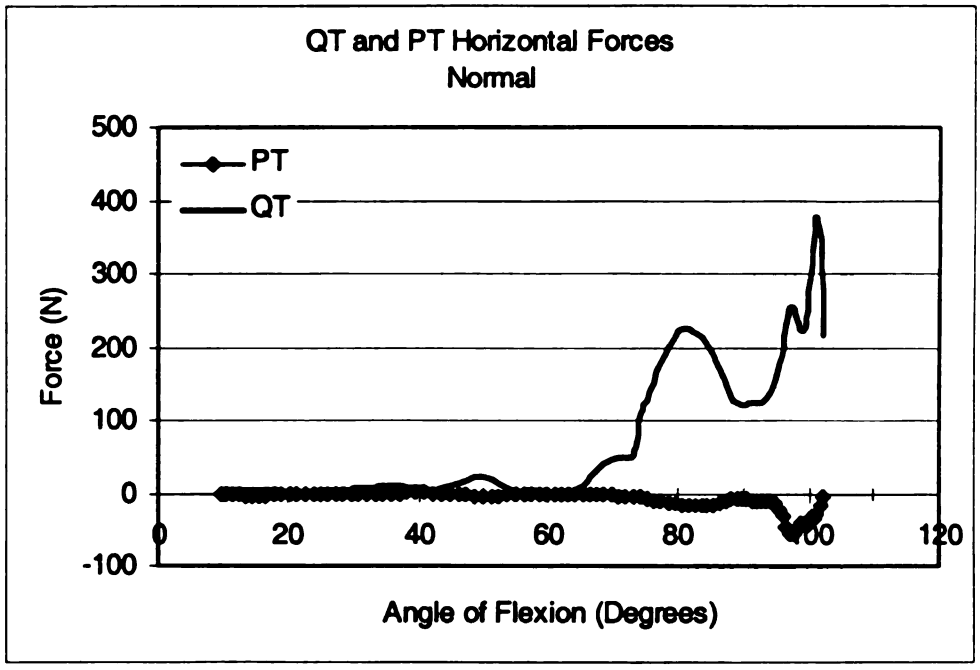

(a)

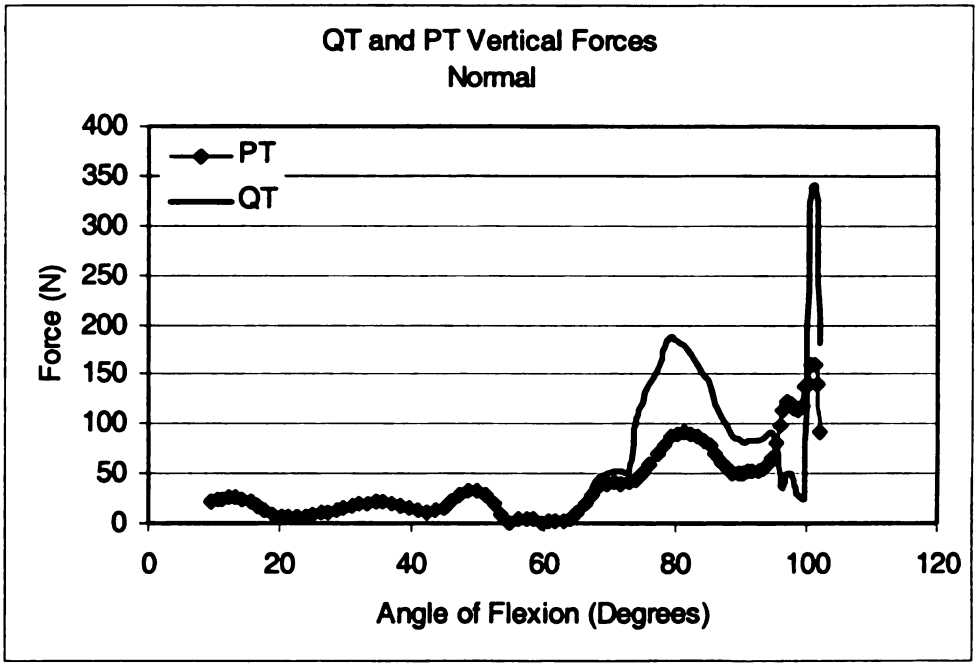

(b)

Figure 46: Quadriceps and Patellar Tendon forces for the normal knee.
(a) Horizontal Forces (b) Vertical Forces.

The resultant QT and PT forces increase with an increase in knee flexion angle. The horizontal force transmitted to the PT is limited when compared to the horizontal force generated by the QT. As observed by changes in β, the range of the angle of pull of the patellar tendon was limited in the normal knee when compared to the results of previous studies. The greatest contribution to knee motion for the PT comes from the vertical force.

In the ACL-deficient knee, the quadriceps was found to be more active in the initial period of knee flexion (Figure 47). This contribution can be explained by the stabilization role that the muscle has to perform in the absence of healthy primary constraints. When compared to the normal knee, higher forces for the QT and PT were found in both the horizontal and vertical components. The horizontal forces transmitted through the PT followed the pattern of displacement of the femur over the tibia (Figure 47a). The horizontal pull of the PT being in the same direction as the displacement of the femur relative to the tibia supported the role of the quadriceps muscle as a stabilizer of the joint. An anterior pull of the PT on the tibia, combined with an anterior displacement of the femur over the tibia, reduced the relative displacement between the two bones. The increase in the vertical forces of both the PT and QT was a result of the increase in the resultant force.

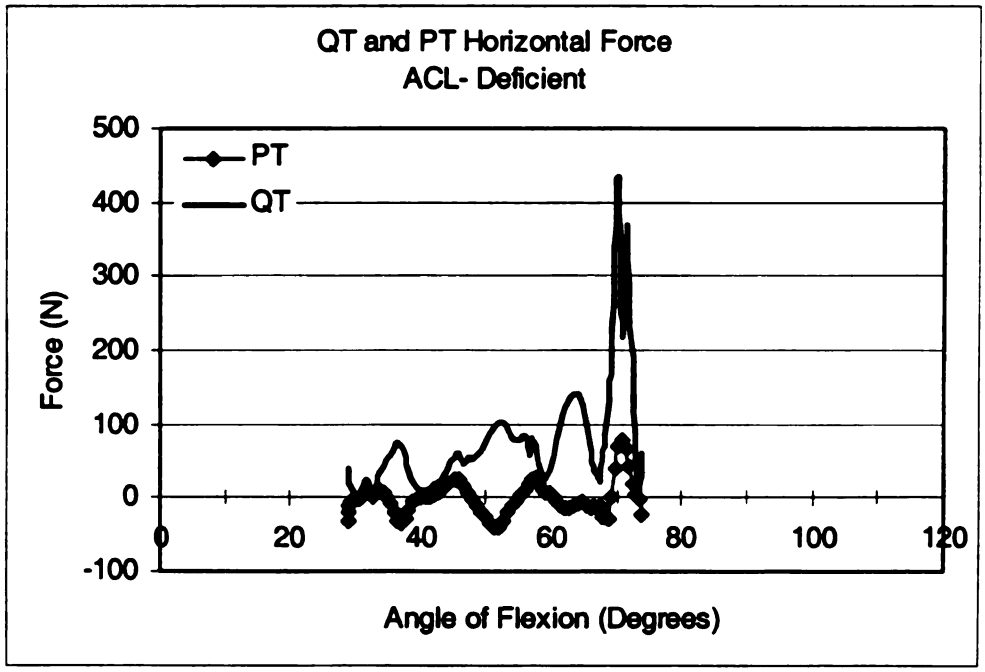

(a)

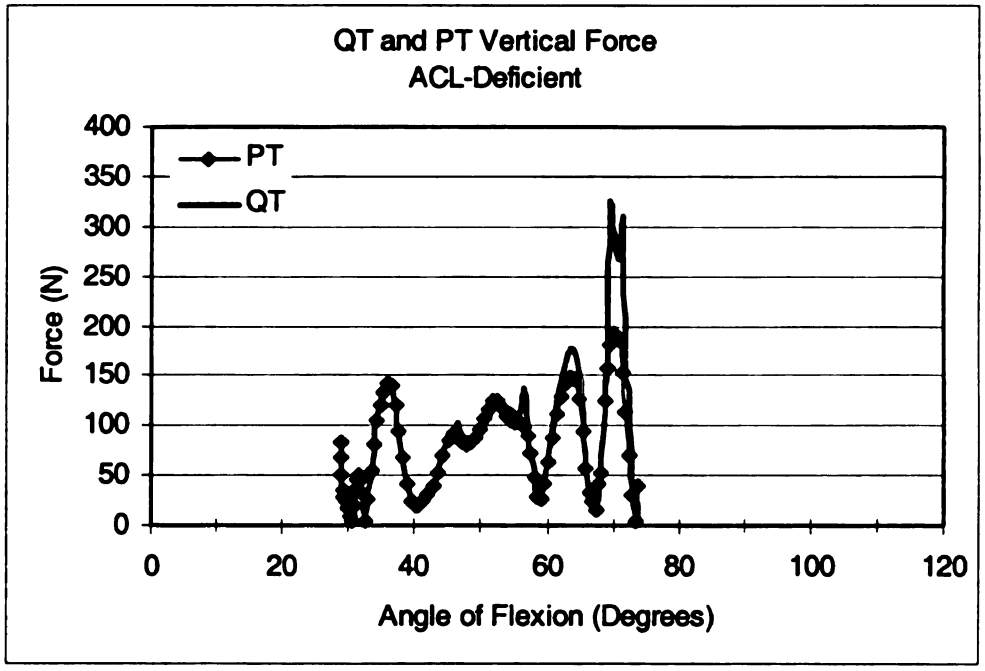

(b)

Figure 47: Quadriceps and Patellar Tendon forces for the ACL-deficient knee. (a) Horizontal Forces (b) Vertical Forces.

The forces obtained for the ACL-reconstructed knee were of particular interest in the analysis of the results (Figure 48). A common adaptation during gait for subjects with ACL-deficiency, or following an ACL-reconstruction, is known as quadriceps avoidance gait. When quadriceps avoidance gait is present there is a reduction in the quadriceps muscle activity. This reduction in muscular contraction is believed to be due to the possible anterior displacement of the tibia relative to the femur caused by excessive force transmitted to the PT. The reduction in QT and PT forces observed in the ACL-reconstructed knee could be interpreted as a similar type of adaptation being present during the squat. The quadriceps contraction is not needed as a secondary stabilizer to the knee following reconstruction of the ligament. However, the subject might still feel cautious about contracting the quadriceps for fear of causing an excessive translation of the tibia over the femur. A weaker quadriceps group might also influence the forces generated during the squat.

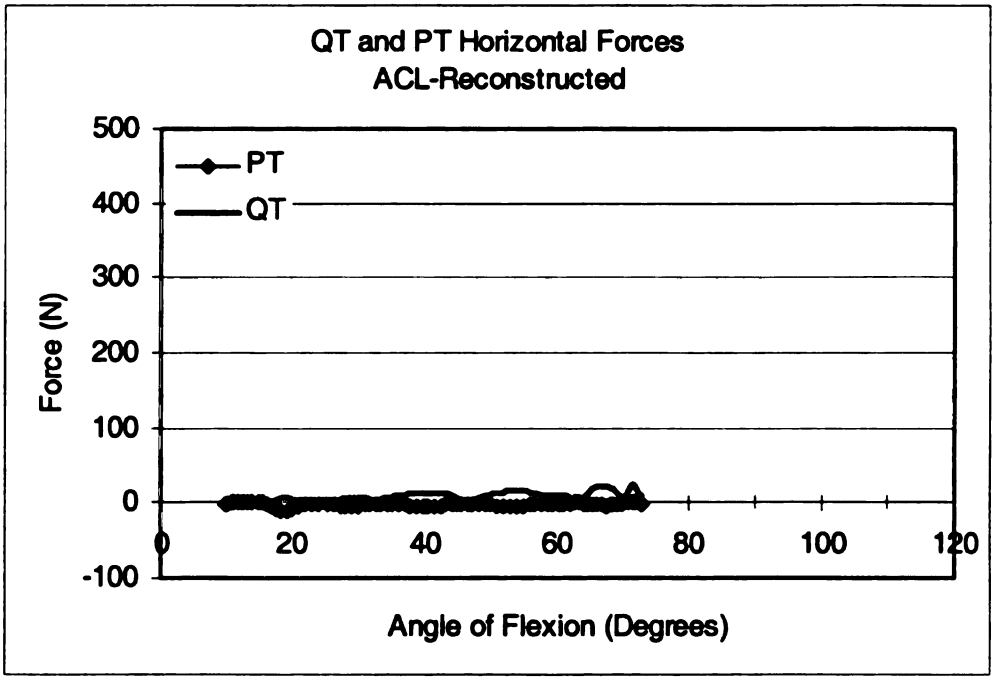

(a)

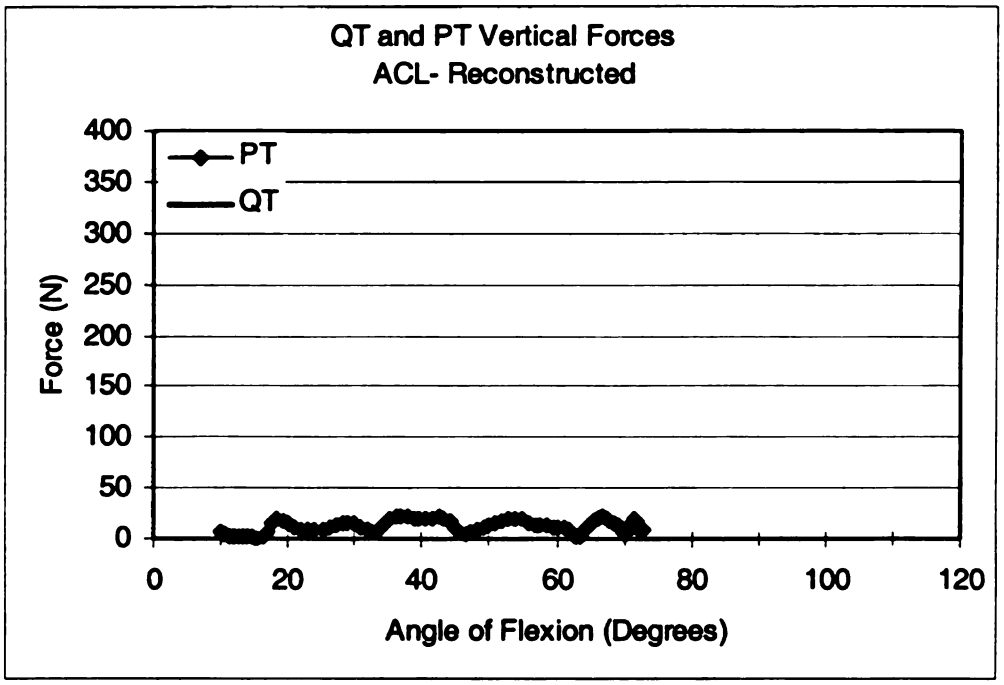

(b)

Figure 48: Quadriceps and Patellar Tendon forces for the ACL-reconstructed knee. (a) Horizontal Forces (b) Vertical Forces.

The results obtained from the mathematical model followed the expected trends for the data sets used in the experimental testing. Subjects with known differences in the mechanical behavior of the knee joint were selected to test the accuracy of the model in predicting such differences. Data from the uninjured subject were used as the norm for comparison against the other two conditions tested with the model as well as for comparison with previously reported data.

The ICR was determined to be a good estimator for the relative position between the femur and the tibia. The linear translation between the two bones was found to be consistent with the known laxity of the knee joint. Even though the rolling and sliding pattern did not directly match those of previous research, the differences in the testing protocols supported the differences in results.

Laxity of the joint and ligament response was measured and illustrated using laxity curves. The results of the forces sustained by the ligaments in response to the laxity of the knee joint were accurate. The expected differences between the norm, ACL-deficient and ACL-reconstructed conditions were shown in the data from the model. These results add to the usefulness of the model in the rehabilitation and injury prevention fields.

In combination with the laxity curves, information about ligament strain versus angle of flexion and quadriceps force versus angle of flexion provide important tools that will add to the better development of rehabilitation exercises. Estimation of quadriceps forces and ligament forces during dynamic activities also can help identify possible injury situations.

CONCLUSIONS

The knee joint has been one of the most researched joints in the human body. The complicated joint mechanics have led to the development of a number of mathematical models. In the review of literature, a two-dimensional quasi-static mathematical model was presented for the estimation of ligament and quadriceps forces as a function of knee flexion. The model used the ICR for the estimation of the amount of rolling and sliding present at the knee joint. The anterior cruciate, posterior cruciate and collateral ligaments were modeled as extensible units. The patella was modeled as a rectangle allowing the transmission of the quadriceps force to the patellar tendon assuming equilibrium of the patello-femoral mechanism.

Although some of the results did not match the trends presented in the literature, the model was based on some underlying differences which might have led to such differences in results. The model was developed with the purpose of being used in conjunction with kinematic and kinetic data obtained during an unconstrained activity. To test the accuracy of the model, data from squatting trials were used as the input parameters. Most of the previously reported data were from tests performed in-vitro and under constrained motions. Therefore, any comparison of results has to be done keeping these differences in mind.

The simplifications of the model were found to be valid by the accuracy of the results obtained. The model was able to predict the expected differences in mechanical behavior between the three tested conditions without being affected by the simplifications imposed in the mathematical development. Limiting the model to two-dimensions did not

have an influence on the accuracy of the results. Further validation of the model might be supported with multiple tests for similar conditions.

I. Limitations

The following limitations need to be taken into consideration when analyzing the results of the model. First, due to the use of two different mathematical software packages, the solution of the equilibrium equations was performed on a frame-by-frame basis thus making the process time consuming, especially for long files. This led to the decision only to present one half cycle of the squat for each tested condition. Programming the model in one software package would allow a faster execution of the code and the ability to use the entire data set. Second, due to the characteristics of the data and the low number of subjects used to test the model, a statistical comparison of the results was not performed. The results obtained were reported in a descriptive manner. Third, the model was designed to take into consideration only the forces generated by the quadriceps muscle. The importance of the hamstrings group and the gastrocnemious as contributors to the knee mechanics was ignored. Strain and joint displacement patterns might have been affected by the contraction of the other muscle groups which were omitted during the model's use and interpretation of the results.

II. Suggestions for future studies

Further investigation in this area is recommended. The model could be modified to calculate the forces of the hamstrings instead of the quadriceps and to study the effects

of the knee flexors on the joint mechanics. Further improvement of the model could lead to the inclusion of both muscle groups.

Further research would be beneficial in determining the exact attachment sites for the modeled ligaments. More accurate results also might be obtained by modeling the ligaments as multi-bundle fibers. The ability to calculate strains for more than one fiber per ligament would give a better indication of the mechanical behavior of the ligament bundle.

The mathematical approach to the calculation of the internal forces sustained by the soft tissue of the knee joint allowed the examination of different mechanical and structural adaptations to the knee joint to be performed in a non-invasive manner. Kinematic and kinetic data collected during any activity could be used as the input to the model, with the ability to mathematically induce changes in the structural and mechanical properties of the knee joint. The model offers a unique contribution to the fields of orthopaedics and sports medicine. The results obtained with the model will delineate the mechanical behavior of the knee joint and could be used to address treatment or surgical questions. The model also provides insight as to the behavior of the ligaments and quadriceps muscles, which could be applied to the development of safe and efficacious rehabilitation protocols.

APPENDIX A

APPENDIX A

Main Program Code

This appendix presents the code written in Matlab computational software. Comment lines have been included in the program to clarify the definition of variables, or guide the reader in the flow of the program. These comments are enclosed on percentage signs (%). Any wording preceded by a % is not an executable line in the program. The name of functions called by the main program have been highlighted. These functions have been added to the end of the main code.

```
%%%%%%%%%%%%%%%%%%%%%%%%%%%%%%%%%%%%%%%%%%%%%%%%%%%%%%%%%%%%%%%%%%%%%%%%%%%%%%%%%%%%%%%
% k_exper  Matlab script - Uses the Instantaneous                  %
% center of rotation to determine the relative position             %
% between the femur and tibia, calculates the change in             %
% length of the ACL, PCL and LCL, and calculated the Force          %
% on each ligament.                                                 %
%%%%%%%%%%%%%%%%%%%%%%%%%%%%%%%%%%%%%%%%%%%%%%%%%%%%%%%%%%%%%%%%%%%%%%%%%%%%%%%%%%%%%%%

% The program has been tested for the "normal" motion of the
% femur relative to the fixed tibia using made up parameters
% for the position of 2 points in the femur and 2 points in
% the tibia for the calculation of the ICR. The calculation
% was made on Mathcad and the values are input parameters to
% this program. The Experimental testing of this program
% will be tested later using data collected during squatting
% trials.
%
% Author: Claudia A. Angeli
%
%
% Model reads ICR file for theta, ICR r.t.shank and ICR in
% lab C.S. Output file has: theta, APdisp, roll and dispx
% parameters
% The position of the Sa target relative to the center of
% the tibial plateau and the ICR location in model units
% taken from the normal ratio between the length and the
% width of the femoral condyles.
```

```
%%%%%%%%%%%%%%%%%%%%%%%%%%%%%%%%%%%%%%%%%%%%
% Definition of model parameters taken from MRI images
% values in mm (MRI image sizes)
%%%%%%%%%%%%%%%%%%%%%%%%%%%%%%%%%%%%%%%%%%%%
Tratio=1.644;            % True ratio - ratio between the MRI image and the
                          "normal" knee
addline=19-5;            % Distal segment to adductor line
heightcond=19;           % Height of the condyle
widthcond=37;            % Width of the condyle
mecaxis=20;              % Distance from anterior aspect of the condyle to the
                          mechanical axis of the femur
tbwdthratio=3/3.5;        % Width ratio of the tibial plateau

maxy=2*pi;               % t value - defining the distal limit of the femur
minx=5*pi/2;             % t value - defining the anterior limit of the femur
maxx=3*pi/2;             % t value - defining the posterior limit of the femur
miny=pi;                 % t value - defining the proximal limit
                          of the femur femur
midx=2*pi;               % t value - used to specify the location
                          of the Tb target
midy=1.5*pi;             % t value - used to specify the location of the Tb
                          target

%%%%%%%%%%%%%%%%%%%%%%%%%%%%%%%%%%%%%%%%%%%%
% Read file with ICR location and theta angle
%%%%%%%%%%%%%%%%%%%%%%%%%%%%%%%%%%%%%%%%%%%%

ICR_f=fopen('ICR_m.prn');
[p,pf]=fscanf(ICR_f,'%f',[6,498]);
pc=p/10;

tmax=p(1,:);
ICRsx=p(3,:);
ICRsy=p(4,:);
ICRix=pc(5,:);
ICRiy=pc(6,:);
```

```
%%%%%%%%%%%%%%%%%%%%%%%%%%%%%%%%%%%%%%%%%%%%
% Definition of the involute circle
%%%%%%%%%%%%%%%%%%%%%%%%%%%%%%%%%%%%%%%%%%%%

b=1.5;                          % radius
phi=pi;                         % phi value
for it=1:max(size(tmax))
  d=tmax(it);                    % loop for range of knee flexion
  theta=d*(pi/180);              % Convert angles from radians to degrees
  Tr=[cos(theta) sin(theta); -sin(theta) cos(theta)];
                                 % Transformation matrix

      for i=1:1          % Loop to define the involute (all x and y values
                         within the involute)
   T(i)=(i-1)*0.002;
   tc(1)=T(i);
   ti=0;
   tf=5*pi/2-T(1)-phi;
   tftrunc=str2num(num2str(tf));
   t=ti:0.001:tftrunc;

%%%%%%%%%%%%%%%%%%%%%%%%%%%%%%%%%%%%%%%%%%%%
% Definition of femoral geometric surface
%%%%%%%%%%%%%%%%%%%%%%%%%%%%%%%%%%%%%%%%%%%%

lx=-b.*cos(T(1)+phi+t+theta)-b.*t.*sin(T(1)+phi+t+theta);
           % X values of involute for rotated femur (at angle theta)

ly=b.*sin(T(1)+phi+t+theta)-b.*t.*cos(T(1)+phi+t+theta);
           % Y values of involute for rotated femur (at angle theta)

lxo=-b.*cos(T(1)+phi+t)-b.*t.*sin(T(1)+phi+t);
           % X values of involute at full extension

lyo=b.*sin(T(1)+phi+t)-b.*t.*cos(T(1)+phi+t);
           % Y values of involute at full extension

%%%%%%%%%%%%%%%%%%%%%%%%%%%%%%%%%%%%%%%%%%%%
% Definition of limits of condyles
%%%%%%%%%%%%%%%%%%%%%%%%%%%%%%%%%%%%%%%%%%%%

lydist=b.*sin(T(1)+phi+(-phi-theta+maxy)+theta)-b.*(-phi-theta+maxy).*cos(T(1)+
phi+(-phi-theta+maxy)+theta);
           % Distal limit for rotated femur
```

```
lyprox=b.*sin(T(1)+phi+(-phi-theta+miny)+theta)-b.*(-phi-theta+miny).*cos(T(1)+
        phi+(-phi-theta+miny)+theta);
            % Proximal limit for rotated femur

lxant(it)=-b.*cos(T(1)+phi+(-phi-theta+minx)+theta)-b.*(-phi-theta+minx).*sin(T(1)
        + phi+(-phi-theta+minx)+theta);
            % Anterior limit for rotated femur

lxpost=-b.*cos(T(1)+phi+(-phi-theta+maxx)+theta)-b.*(-phi-theta+maxx).*sin(T(1)
        + phi+(-phi-theta+maxx)+theta);
            % Posterior limit for rotated femur



%%%%%%%%%%%%%%%%%%%%%%%%%%%%%%%%%%%%%%%%%%%%%%%%%%%%%%%%%%%%%%%%%%%%%%%%%%%%
% Definition of fixed limits
%%%%%%%%%%%%%%%%%%%%%%%%%%%%%%%%%%%%%%%%%%%%%%%%%%%%%%%%%%%%%%%%%%%%%%%%%%%%

lyfdt=b.*sin(T(1)+phi+(-phi+maxy))-b.*(-phi+maxy).* cos(T(1)+phi+(-phi+maxy));
            % Distal limit for femur at full extension

lyfpx=b.*sin(T(1)+phi+(-phi+miny))-b.*(-phi+miny).* cos(T(1)+phi+(-phi+miny));
            % Proximal limit for femur at full extension


lxfant=-b.*cos(T(1)+phi+(-phi+minx))-b.*(-phi+minx).* sin(T(1)+phi+(-phi+minx));
            % Anterior limit for femur at full extension

lxfpst=-b.*cos(T(1)+phi+(-phi+maxx))-b.*(-phi+maxx).* sin(T(1)+phi+(-
        phi+maxx));
            % Posterior limit for femur at full extension

lypfc=b.*sin(T(1)+phi+(-phi+minx))-b.*(-phi+minx).* cos(T(1)+phi+(-phi+minx));
            % Y location of patello-femoral contact point at full extension

%%%%%%%%%%%%%%%%%%%%%%%%%%%%%%%%%%%%%%%%%%%%%%%%%%%%%%%%%%%%%%%%%%%%%%%%%%%%
% Definition of the Initial point of rotation. A circle with
% a 24mm radius was taken to fit the posterior aspect of the
% femoral condyle and taken as the initial rotation point
% when the knee starts to flex. The Tb target (or point)
% will be define as this initial point of rotation. The 24mm
% is converted to model units (modelratio=6.6285) and then
% the point is found by subtracting/adding this value to the
% previously specified limits of the femoral condyle. During
% knee flexion this point is located by rotating the Tb
% (original) point with the transformation matrix, ONLY to
```

```
% specify the coordinated of the point as given by the
% transformation of the involute. The true coordinates of
% this point are found using the ICR calculations.
%%%%%%%%%%%%%%%%%%%%%%%%%%%%%%%%%%%%%%%%%%%%%%%%%%%%%%%%
lxtbo=lxfpst-3.62;              % X coordinate of the Tb target at full
                                extension
lytbo=lyfdt+3.62;               % Y coordinate of the Tb target at full
                                extension
ltb=Tr*[lxtbo; lytbo];          % Transformation of the Tb target position to
                                define the MODELS rotated position
lxtb=ltb(1);                    % Separation of the X-Y coordinates
lytb=ltb(2);
end

  for m=0:100
    c=1;
  end

  if c==0
    d=11;
  else
  end



lxo=lxo(1);             % Definition of the first X value in the involute at FULL
                        EXTENSION
lyo=lyo(1);             % Definition of the first Y value in the involute at FULL
                        EXTENSION

%%%%%%%%%%%%%%%%%%%%%%%%%%%%%%%%%%%%%%%%%%%%%%%%%%%%%%%%
% Call function to find the true ratio between the subject's
% knee and the model
%%%%%%%%%%%%%%%%%%%%%%%%%%%%%%%%%%%%%%%%%%%%%%%%%%%%%%%%

[pmratio, Smax, Smay]=kneesize;

%%%%%%%%%%%%%%%%%%%%%%%%%%%%%%%%%%%%%%%%%%%%%%%%%%%%%%%%
% Definition of model parameters dependent on lx and ly
%%%%%%%%%%%%%%%%%%%%%%%%%%%%%%%%%%%%%%%%%%%%%%%%%%%%%%%%

modelratio=heightcond*Tratio/norm(lyfpx-lyfdt);
                        % Model ratio using the height of the condyle and the
                        True ratio from MRI images
```

```
wdthtibia=widthcond*Tratio*tbwdthratio/modelratio;
                        % Definition of the width of the tibial plateau

jtspace=0.3*Tratio/modelratio;
                        %Definition of the joint space taken from MRI images


%%%%%%%%%%%%%%%%%%%%%%%%%%%%%%%%%%%%%%%%%%%%%%%%%%%%%%%%%%%%%%%%%%%%%%%%
% Model parameters for the tibia
%%%%%%%%%%%%%%%%%%%%%%%%%%%%%%%%%%%%%%%%%%%%%%%%%%%%%%%%%%%%%%%%%%%%%%%%

lxotibia=lxfant;        % Anterior limit of the tibial plateau at full extension

lyotibia=lyfdt;         % Y position of the tibia relative to the femoral condyle distal
                        limit
tibia=[lxotibia; lxotibia+wdthtibia];
                        % definition of the tibial plateau

jp=lyotibia;            % jp variable


%%%%%%%%%%%%%%%%%%%%%%%%%%%%%%%%%%%%%%%%%%%%%%%%%%%%%%%%%%%%%%%%%%%%%%%%
% Calculate relative position between ICR and Involute
% origin
%%%%%%%%%%%%%%%%%%%%%%%%%%%%%%%%%%%%%%%%%%%%%%%%%%%%%%%%%%%%%%%%%%%%%%%%

%%%%%%%%%%%%%%%%%%%%%%%%%%%%%%%%%%%%%%%%%%%%%%%%%%%%%%%%%%%%%%%%%%%%%%%%
% Calling function to calculate contact point at rotated
% position of the femur (from full extension --> transformed
% by Tr)
%%%%%%%%%%%%%%%%%%%%%%%%%%%%%%%%%%%%%%%%%%%%%%%%%%%%%%%%%%%%%%%%%%%%%%%%
[Rfcp, lxct, purer]=contact_point(theta, T, phi, maxy, maxx, minx, miny, b, Tr);

Xc=Rfcp(1);             % Definition of the rotated contact point (from full
                        extension transformed by Tr)
Yc=Rfcp(2);

lyct=lydist;            % lxct & lyct are the contact points at theta degrees of
                        flexion.
                        % lxct is used in the definition of the displacement of
                        the contact point.
```

```
%%%%%%%%%%%%%%%%%%%%%%%%%%%%%%%%%%%%%%%%
% Calling function to calculate contact point at rotated
% position of the femur.
%%%%%%%%%%%%%%%%%%%%%%%%%%%%%%%%%%%%%%%%

Rtcp=fct_pt(T, phi, maxy, maxx, minx, miny, b, jtspace, lydist);

Xtc=Rtcp(1);             % Contact point at full extension, prior to the
                         application of the translation of disp x.
Ytc=Rtcp(2);



%%%%%%%%%%%%%%%%%%%%%%%%%%%%%%%%%%%%%%%%
% Instantaneous Joint center relative to the SA shank target
%%%%%%%%%%%%%%%%%%%%%%%%%%%%%%%%%%%%%%%%

ICRx=-28.9757;     %Using values from Mathcad pure rolling/sliding and/or
                   combination files

ICRy=26.6107;      % (rjcs)

% Convertion of the ICR relative to SA to model units

ICRxsa=ICRsx(it)/pmratio;
ICRysa=ICRsy(it)/pmratio;

Sax=lxotibia+(wdthtibia/2)+Smax;
                         % location of the Sa target calculated from the
                         difference in the X direction between femoral condyle
                         and the Sa target position in the standing file. Units
                         have been converted to model units using a 9.641
                         convertion factor. This factor was calculated using a
                         "normal" .8636 ratio between the length/width of the
                         femoral condyles and the known width of the femoral
                         condyle from the standing file. The modelratio
                         parameter specified in this program only applies to
                         the convertion between the MRI image estimated
                         parameters to model units.

Say=lyotibia-Smay;       % location of the Sa target relative to the tibial plateau
                         in the Y-direction.

JCx(it)=Sax+ICRxsa;      % Estimation of the Joint center position. Taken from
                         the Sa target and adding the
```

```
JCy(it)=Say+ICRysa;            % relative positon of the ICR.

%%%%%%%%%%%%%%%%%%%%%%%%%%%%%%%%%%%%%%%%%%%%%%%%%%%%%%%%%%%%%%%
% Estimation of the Tb target given the position of the
% joint center (previously defined) and subtracting the
% relative position of the ICR (femoral component). This
% value is the predicted location of the Tb target as
% ESTIMATED from TRUE data, not the simple rotation of the
% involute
%%%%%%%%%%%%%%%%%%%%%%%%%%%%%%%%%%%%%%%%%%%%%%%%%%%%%%%%%%%%%%%

diff2=-purer-Xtc;          % difference between the Contact Point at full
                           extension and the contact point of the theta rotated
                           femur.

diff3=Ix(1)-Ixo;           % Difference between the origin location of the
                           rotated femur and the femur at full extension.

diff1=Ixtb-Ixtbo;

diff4=JCx(it)-Ixtbo;

%%%%%%%%%%%%%%%%%%%%%%%%%%%%%%%%%%%%%%%%%%%%%%%%%%%%%%%%%%%%%%%
% Calculation of the difference between the ESTIMATED Tb
% target position and the CALCULATED tb target position
% given the rotation of the involute. The dispx and dispy
% parameters specify the translation of the femoral condyle,
% at point Tb between the two methods of calculation.
%%%%%%%%%%%%%%%%%%%%%%%%%%%%%%%%%%%%%%%%%%%%%%%%%%%%%%%%%%%%%%%

di=diff4-diff1;            % The difference between the distance given by the
                           true motion (ICR-Ixtb) and the distance between the
                           two contact point parameters. This defines the
                           necessary displacement of the femoral condyle over
                           the tibial plateau specified by the true motion of the
                           femur over the tibia.

dispy(it)=-(Iyo-Iy(1));
                           % Translation of the involute to the CORRECTED
                           position. The difference calculated above is used to
                           translate the entire involute. Rigid body mechanics
                           prescribes the translation of the entire involute given
                           the especified translation of one point.

dispx(it)=di;
```

```
Ix=Ix+dispx(it);          % Translation of the involute by parameter dispx
Iy=Iy+dispy(it);          % Translation of the involute by parameter dispy

ICPx=Xtc;                 % definition of new variable to allow the untranslated
                          value of the contact point at full extension to be used
                          in subsequent calculations.

Xtc=Xtc+dispx(it);        % Translation of the contact point according to the
                          involute translation
Ytc=Ytc+dispy(it);

Xc=Xc+dispx(it);          %Translation of the contact point according to the
                          involute translation
Yc=Yc+dispy(it);

roll_disp=purer;          % Definition of true rolling given by the x-distance
                          between the rotated contact point and the contact
                          point at full extension.

roll(it)=roll_disp*pmratio;
                          % Definition of pure rolling displacement in mm units.
                          Converted back.


APdisp(it)=(Xc+roll_disp)*pmratio;
                          % APdisp is define as the slipping component of the
                          translation of the femur over the tibia. The
                          displacement of the contact point is subtracted
                          from the pure rolling component associated with knee
                          flexion. Parameter in True mm units.
 end


%%%%%%%%%%%%%%%%%%%%%%%%%%%%%%%%%%%%%%%%%%%%%%%%%%%%%%%%%%%%%%%%%%%%%%%%%%%%
% Definition of the Ligament parametes taken from MRI
% images. Ratio parameters are values taken from the MRI
% images. Insertion parameters are calculated using the
% model values (limits specified earlier) to define the x
% and y coordinates of the insertion points.
%%%%%%%%%%%%%%%%%%%%%%%%%%%%%%%%%%%%%%%%%%%%%%%%%%%%%%%%%%%%%%%%%%%%%%%%%%%%

ratioaclt=15/modelratio;
ratiolcltx=23*Tratio/modelratio;
ratiolclty=11*Tratio/modelratio;

Insertiontacl=Ixotibia+ratioaclt;
```

```
Insertiontpcl=lxotibia+wdthtibia;
Insertiontlcl=lxotibia+ratiolcltx;
Insertiontlcly=jp-ratiolclty;

%%%%%%%%%%%%%%%%%%%%%%%%%%%%%%%%%%%%%%%%%%%%%%%%%%%%%%%%%%%%%%%%
% Model parameter for the femur
% Definition of the Ligament parameters taken from MRI
% images. Ratio parameters are values taken from the MRI
% images. Insertion parameters are calculated using the
% model values (limits specified earlier) to define the x
% and y coordinates of the insertion points.
%%%%%%%%%%%%%%%%%%%%%%%%%%%%%%%%%%%%%%%%%%%%%%%%%%%%%%%%%%%%%%%%

Insacl=3.226;
Inspcl=2.2081;
ratioacl=1.6477;
ratiopcl=2.6315;
ratioxlcl=1.76294;
ratioylcl=6.5794;

Insertionxacl=Insertiontacl+ratioacl;
Insertionxpcl=Insertiontpcl-ratiopcl;
Insertionxlcl=Insertiontlcl-ratioxlcl;

Insertionyacl=jp+Insacl;
Insertionypcl=jp+Inspcl;
Insertionylcl=Insertiontlcly+ratioylcl;

%%%%%%%%%%%%%%%%%%%%%%%%%%%%%%%%%%%%%%%%%%%%%%%%%%%%%%%%%%%%%%%%
% Call function to calculate of external moments
%%%%%%%%%%%%%%%%%%%%%%%%%%%%%%%%%%%%%%%%%%%%%%%%%%%%%%%%%%%%%%%%

[M_flex, M_flex2, BW, ec, Fy, Fz]=e_moments(ICRix, ICRiy);

e3y_all=ec(:,2);          % Definition of column vector with e3 values to be
                          used in calculation of internal moments.


for it=1:max(size(tmax))
  d=tmax(it);             % Loop (same as defined earlier) to go through range
                          of flexion
  theta=d*(pi/180);
  Tr=[cos(theta) sin(theta); -sin(theta) cos(theta)];
                          % Redefinition of the transformation matrix
```

```
%%%%%%%%%%%%%%%%%%%%%%%%%%%%%%%%%%%%%%%%%%%%%%%%%%
% Transformation of ligament insertions on the femur to
% follow the rotation of the knee. ALL previously
% defined values were taken from the full extension
% position.
%%%%%%%%%%%%%%%%%%%%%%%%%%%%%%%%%%%%%%%%%%%%%%%%%%

  [RIpcl]=Tr*[Insertionxpcl; Insertionypcl];

  [RIacl]=Tr*[Insertionxacl; Insertionyacl];
  [RIlcl]=Tr*[Insertionxlcl; Insertionylcl];

%%%%%%%%%%%%%%%%%%%%%%%%%%%%%%%%%%%%%%%%%%%%%%%%%%
% Separation of the matrix components for each ligament
% insertion, and translation of the points according to
% the previously specified displacement of the entire
% involute.
%%%%%%%%%%%%%%%%%%%%%%%%%%%%%%%%%%%%%%%%%%%%%%%%%%


RIpcl(1)=RIpcl(1)+dispx(it);      RIpcl(2)=RIpcl(2)+dispy(it);

RIacl(1)=RIacl(1)+dispx(it);      RIacl(2)=RIacl(2)+dispy(it);

RIlcl(1)=RIlcl(1)+dispx(it);      RIlcl(2)=RIlcl(2)+dispy(it);


%%%%%%%%%%%%%%%%%%%%%%%%%%%%%%%%%%%%%%%%%%%%%%%%%%
% Definition of the Length of the ligament (AT THE
% SPECIFIED FLEXION ANGLE). Pythagorian Theorem
%%%%%%%%%%%%%%%%%%%%%%%%%%%%%%%%%%%%%%%%%%%%%%%%%%

  Lpcl=sqrt((Insertiontpcl-RIpcl(1))^2+(RIpcl(2)-jp)^2);
  Lacl=sqrt((RIacl(1)-Insertiontacl)^2+(RIacl(2)-jp)^2);
  Llcl=sqrt((Insertiontlcl-RIlcl(1))^2+(RIlcl(2)-Insertiontlcly)^2);



%%%%%%%%%%%%%%%%%%%%%%%%%%%%%%%%%%%%%%%%%%%%%%%%%%
% Definition of the angle between the ligament and the
% horizontal. All angles were taken as acute angles
% during FULL FLEXION. The following values are during
% the specified theta.
%%%%%%%%%%%%%%%%%%%%%%%%%%%%%%%%%%%%%%%%%%%%%%%%%%
```

```
    angacl=asin((RIacl(2)-jp)/Lacl);

    if RIacl(1)<Insertiontacl
                        % Necessary to control for angle greater than 90

  angacl=pi-asin((RIacl(2)-jp)/Lacl);

end


angpcl=asin((RIpcl(2)-jp)/Lpcl);

if RIpcl(1)>Insertiontpcl
                        % Necessary to control for angle greater than 90
  angpcl=pi-asin((RIpcl(2)-jp)/Lpcl);
end


anglcl=asin((RIlcl(2)-Insertiontlcly)/Llcl);
if RIlcl(1)<Insertiontlcl
                        % Necessary to control for angle greater than 90
  anglcl=pi-asin((RIlcl(2)-Insertiontlcly)/Llcl);
end


%%%%%%%%%%%%%%%%%%%%%%%%%%%%%%%%%%%%%%%%%%%%%%%%%%%%%%%%%%%%%%%%%%%%%%%
% Conversion of ligament angle values to degrees
%%%%%%%%%%%%%%%%%%%%%%%%%%%%%%%%%%%%%%%%%%%%%%%%%%%%%%%%%%%%%%%%%%%%%%%



ta(it)=angacl*180/pi;

tp(it)=angpcl*180/pi;
tl(it)=anglcl*180/pi;
```

```
%%%%%%%%%%%%%%%%%%%%%%%%%%%%%%%%%%%%%%%%%%%%
% Calculate ligament length change using the
% change_length FUNCTION. The output of the function is
% the lchg (ligament length change) and strain (the
% calculated strain for each ligament). Following the
% calling of the function the output matrices are split
% into the 3 ligament components.
%%%%%%%%%%%%%%%%%%%%%%%%%%%%%%%%%%%%%%%%%%%%%%%%%%


    [lchg, strain]=change_length2( Lacl, Lpcl, Llcl);

    Dacl=lchg(1);
    Dpcl=lchg(2);
    Dlcl=lchg(3);

    Sacl(it)=strain(1);
    Spcl(it)=strain(2);
    Slcl(it)=strain(3);

    %%%%%%%%%%%%%%%%%%%%%%%%%%%%%%%%%%%%%%%%%%%%
    % Calculation of ligament forces using the lig_force
    % FUNCTION. The output contains the forces for each
    % of the 3 ligamens.
    %%%%%%%%%%%%%%%%%%%%%%%%%%%%%%%%%%%%%%%%%%%%


    [Facl, Fpcl, Flcl]=lig_force2(lchg, modelratio);

    Fa(it)=Facl;

    Fp(it)=Fpcl;

    Fl(it)=Flcl;



    e3y=e3y_all(it);        % Definition of Z axis for internal moments to be
                            calculated about same true axis as external moments.
                            See before the loop for definition of e3y_all variable.
```

```
%%%%%%%%%%%%%%%%%%%%%%%%%%%%%%%%%%%%%%%%%%%%%%%%%%%
% Calculation of internal moments (call function)
%%%%%%%%%%%%%%%%%%%%%%%%%%%%%%%%%%%%%%%%%%%%%%%%%%%

[Maz, Mpz, Mlz, Flx, Fly]=moments(e3y,BW,modelratio,JCx, JCy, angacl,
angpcl, anglcl, Rlacl, Rlpcl, Rllcl, jp, Insertiontacl, Insertiontpcl, Insertiontlcl,
Insertiontlcly, Facl,Fpcl,Flcl);

Mia(it)=Maz(it);

Mip(it)=Mpz(it);
Mil(it)=Mlz(it);

Faclx(it)=Flx(1);
Fpclx(it)=Flx(2);
Flclx(it)=Flx(3);

Facly(it)=Fly(1);
Fpcly(it)=Fly(2);
Flcly(it)=Fly(3);


Fyi=Fy(it);             % Definition of Fy and Fz forces for the given it value
                        % to be used in
Fzi=Fz(it);             % the calculation of the contact force.


end


%%%%%%%%%%%%%%%%%%%%%%%%%%%%%%%%%%%%%%%%%%%%%%%%%%%
% Writing output files.
% Parameters will be read by Mathcad templates for the
% calculation of patello-femoral equilibrium mechanism and
% find the solution for the quasi-static model of the knee
%%%%%%%%%%%%%%%%%%%%%%%%%%%%%%%%%%%%%%%%%%%%%%%%%%%


% Output file 1
fout=fopen('disp_mdl2n.out','w')

for it=1:max(size(tmax)),

  fprintf(fout, '%f %f %f %f %f %f %f %f\n',tmax(it), APdisp(it), roll(it),
lxant(it),dispx(it),dispy(it), JCx(it), JCy(it))
```

```
end


% Output file 2
fout=fopen('moms2n.out','w')

for it=1:max(size(tmax)),

  fprintf(fout, '%f %f %f %f %f %f %f %f %f %f %f %f\n',tmax(it), Mia(it), Mip(it),
Mil(it), M_flex(it), Fa(it), Fp(it), Fl(it),Sacl(it), Spcl(it), Slcl(it),e3y_all(it))
end

% Output file 3

fout=fopen('forces_mdl2n.out','w')

for it=1:max(size(tmax)),

  fprintf(fout, '%f %f %f %f %f %f %f %f %f\n',tmax(it), Faclx(it), Fpclx(it),
Flclx(it),Facly(it),Fpcly(it), Flcly(it), Fy(it), Fz(it))
end


fclose all;



%%%%%%%%%%%%%%%%%%%%%%%%%%%%%%%%%%%%%%%%%%%%%%%%%%%%%%%%%%%%%%%%
% Definition of the ligament parameters for GRAPHING
% purposes only. X and Y coordinates are given for the
% origin and insertion points. tb is defined as the Y
% parameter for the tibia plateau.
%%%%%%%%%%%%%%%%%%%%%%%%%%%%%%%%%%%%%%%%%%%%%%%%%%%%%%%%%%%%%%%%

  aclligx=[Insertiontacl; Rlacl(1)];

  aclligy=[jp; Rlacl(2)];

  pclligx=[Insertiontpcl; Rlpcl(1)];

  pclligy=[jp; Rlpcl(2)];

  lclligx=[Insertiontlcl; Rllcl(1)];
  lclligy=[Insertiontlcly; Rllcl(2)];
  tb=[jp; jp];
```

```
% Patella constant paramenters

   [LPTe, PTalphae, PTbetae, PTi, gama]=patella_ext(lyfdt, lxfant, lypfc, Tratio,
modelratio, jtspace, lxotibia,jp);


%Patella

   [cp, Ppa, Pdp, Ppp, Pda, Ps2d, Ps2p, PTo, PTi, Pcy,
Pcx]=pat_definition(theta,dispx, dispy,lxant, Tratio, modelratio, lxotibia,jp);

   PTox=PTo(1);       PToy=PTo(2);

   PTix=PTi(1);       PTiy=PTi(2);


   comp=90*pi/180;          % To define theta from the vertical
   QTx=Ppa(1)+(cos(comp-theta)*3);
                            % Quadriceps Tendon definition (length of 3 -->
                            arbitrarily picked)

   QTy=Ppa(2)+(sin(comp-theta)*3);


  % Definition of lines for graphing purposes only


  Pdpx=[Ppa(1); Ppp(1)];    % Top X
  Pdpy=[Ppa(2); Ppp(2)];    % Top y
  Pdax=[Pda(1); Pdp(1)];    % Bottom x
  Pday=[Pda(2); Pdp(2)];    % Bottom y
  Pantbx=[Pda(1); Ppa(1)];  % Anterior x
  Pantby=[Pda(2), Ppa(2)];  % Anterior y
  Ppostx=[Pdp(1) Ppp(1)];   % Posterior x
  Pposty=[Pdp(2) Ppp(2)];   % Posterior y
  PTx=[PTix; PTox];         % PT x
  PTy=[PTiy; PToy];         % PT y
  Ps2x=[Ps2d(1) Ps2p(1)];   % 2nd Art. Surface x
  Ps2y=[Ps2d(2) Ps2p(2)];   % 2nd Art. Surface y
  Quadx=[Ppa(1) QTx];            % Quadriceps tendon x
  Quady=[Ppa(2) QTy];        % Quadriceps tendon y
```

```
% Plot of knee

    line(aclligx, aclligy)   % ACL

    title('Squatting - F267 (Norm) 110 Degrees of Flexion (Trial #10- Right)')

     axis([-12 4 -10 6])
    hold on
    line(pclligx, pclligy)  %PCL
    hold on
    line(lclligx, lclligy)  %LCL
    hold on
    plot(lx,ly)  % Involute
    hold on
    line(tibia, tb,'color','r','markersize',2)
                                % Tibia Plateau

    hold on
    plot(Sax,Say, 'o','color','y')
                                 % Sa target
   hold on
    plot(lxo,lyo, 'o','color','r')
                                % First point of involute at full extension

   hold on
    plot(lxtb,lytb, 'o','color','b')
                                % Initial point of rotation at full extension
   hold on
    plot(JCx,JCy, '*','color','g')
                                % Instantaneous center of rotation

      hold on
   plot(lxotibia, lyotibia, '*','color','r')
                                % Most anterior point in the tibial plateau (constant)

    hold on

    plot(Xtc, Ytc, '+','color','b')
                                %Tibial plateau contact point

    hold on
    plot(Pcx, Pcy, '*','color', 'r')
                                % Patello-femoral contact point

   hold on
    plot(Xc, Yc, '+', 'color', 'g')
```

```
                    % Tibio-femoral contact point at full extension

    line(Pdpx, Pdpy)
    hold on
    line (Pdax, Pday)
    hold on
    line (Pantbx, Pantby)
    hold on
    line (Ppostx, Pposty)
    hold on
    line (Ps2x, Ps2y, 'LineStyle',:)
    hold on
    line (Quadx, Quady)
    hold on
    line (PTx, PTy, 'color','g')
    hold on


%%%%%%%%%%%%%%%%%%%%%%%%%%%%%%%%%%%%%%%%%%%%%%%%%%%%%%%%%%%%%%%%%%%%%%%%%%%%
%                              Kneesize Function Code                          %
%%%%%%%%%%%%%%%%%%%%%%%%%%%%%%%%%%%%%%%%%%%%%%%%%%%%%%%%%%%%%%%%%%%%%%%%%%%%

function [pmratio, Smax, Smay]=kneesize


% User input to define the true ratio between the knee and
% the model. Also this values will be use to define the
% position of the Sa target used in the
% calculation of the ICR and in the graphical
% representation of the model

disp('Enter the following target locations in mm from the standing file');
disp(' ');
disp('Enter the X, Y, Z location of the fl-cond target (one at a time)');
flcondx=input('X: ');
flcondy=input('Y: ');
flcondz=input('Z: ');
disp('Enter the Z location of the fm-cond target');
fmcondz=input('Z: ');
disp('Enter the X, Y location of the Sa-prox target (one at a time)');
Saproxx=input('X: ');
Saproxy=input('Y: ');

width=norm(fmcondz-flcondz);
                    % definition of the true knee width
trueratio=0.8636;   % ratio between "normal" knee depth and knee width
```

```
Modellength=9.4248;        % parameter establishing the model's knee depth
                           (from lxant to lxpost)

length=trueratio*width;
                           % Definition of the depth of the patient's knee using
                           the established true ratio between depth and width
pmratio=length/Modellength;
                           % Calculation of the patient's model ratio to be used
                           in any conversion between linear parameters
                           established in inertial or segmental coordinate
                           systems.
Smax=(Saproxx-flcondx)/pmratio;
                           % Position of the Sa target relative to the mid tibial
                            plateau (x)

Smay=(flcondy-Saproxy)/pmratio;
                           % Position of the Sa target relative to the tibial
                           plateau (y)


%%%%%%%%%%%%%%%%%%%%%%%%%%%%%%%%%%%%%%%%%%%%%%%%%%%%%%%%%%%%%%%%%%%%%%%
%                          Contact_Point Function Code                   %
%%%%%%%%%%%%%%%%%%%%%%%%%%%%%%%%%%%%%%%%%%%%%%%%%%%%%%%%%%%%%%%%%%%%%%%

function [Rfcp, lxct, purer]=contact_point(theta, T, phi, maxy, maxx, minx, miny,
b, Tr)

% Function CONTACT_POINT will define the initial contact
% point of the femur/tibia at full extension. lyfdt is the
% distal limit of the femur during full extension Xc is the
% intersection with lyfdt at full extension The Contact
% point will the transformed in the rotated coordinate
% system to follow the movement relative to the rotation of
% the femur.
% The (lxc, lyc) will be used to calculate anterior
% displacement of the femur relative to the tibia (see
% tct_pt function)

lyfdt=b.*sin(T(1)+phi+(-phi+maxy))-b.*(-phi+maxy).* cos(T(1)+phi+(-phi+maxy));

lxc=-b.*cos(T(1)+phi+(-phi+maxy))-b.*(-phi+maxy).* sin(T(1)+phi+(-phi+maxy));

lxct=-b.*cos(T(1)+phi+(-phi-theta+maxy)+theta)-b.*(-phi-
theta+maxy).*sin(T(1)+phi+(-phi-theta+maxy)+theta);
```

```
purer=-(1/2.*(b^2.*(maxy-phi-theta)^2)^(1/2).*(maxy-phi-theta)-1/2.*(b^2.*(maxy-
phi)^2)^(1/2).*(maxy-phi));
Rfcp=Tr*[lxc; lyfdt];


%%%%%%%%%%%%%%%%%%%%%%%%%%%%%%%%%%%%%%%%%%%%%%%%%%%%%%%%%%%%%%%%%%%%%%%%%%%%
%                                    tcp_pt Function Code                                    %
%%%%%%%%%%%%%%%%%%%%%%%%%%%%%%%%%%%%%%%%%%%%%%%%%%%%%%%%%%%%%%%%%%%%%%%%%%%%

function [Rtcp]=tct_pt(T, phi, maxy, maxx, minx, miny, b, jtspace, lydist)


% Function to calculate the tibial contact point at the full
% extension position lydist is the distal femur limit at
% full extension, defined by the maxy variable and dependent
% on the angle of flexion lxc will define the X point
% relative to lydist.
% No transformation is necessary since the TIBIA is taken as
% the FIXED segment the jtspace is the adjustment due to the
% shifting when graphing different angles.

lxc=-b.*cos(phi+(-phi+maxy))-b.*(-phi+maxy).*sin(phi+(-phi+maxy));


Rtcp=[lxc; (lydist-jtspace)];


%%%%%%%%%%%%%%%%%%%%%%%%%%%%%%%%%%%%%%%%%%%%%%%%%%%%%%%%%%%%%%%%%%%%%%%%%%%%
%                                    e_moments Function Code                                    %
%%%%%%%%%%%%%%%%%%%%%%%%%%%%%%%%%%%%%%%%%%%%%%%%%%%%%%%%%%%%%%%%%%%%%%%%%%%%

function [M_flex, M_flex2, BW, ec, Fy, Fz]=e_moments(ICRix, ICRiy)

% Calculation of External moments using as input paraments 3
% components of Forces and 3 componet of Moments as measured
% by the force plate. Need the Xo and Zo offsets from the
% Lab CS to the FP CS. All 8 numbers are input parameters in
% the function. The ICR location should be read in the LAB
% CS. The transformation is written for T to be transformed
% from FP to LAB.
% The output of the moments will be in N/m about the ICR all
% in LAB CS.
% Input parameters necessary in the function. These should
% be modified to read the force file to be able to calculate
% the e-moments for the complete motion trial.
```

```
% Read force  file
force=fopen('a10cs2.frc');
 [f,ff]=fscanf(force,'%f',[7,236]);

% Read condyle location file
cond=fopen('virtual.prn');
[p,pf]=fscanf(cond, '%f',[12,236]);
p=p/10;

% Assign variables to force file columns
Fx=f(3,:);
Fy=f(4,:);
Fz=f(2,:);
mx=f(6,:);
my=f(7,:);
mz=f(5,:);
% Used input of X and Z offsets and BW
Xo=input('Enter the Xo offset: ');
Zo=input('Enter the Zo offset: ');
BW=input('Enter BW in Newtons: ');

% Transpose force variables
Fx=Fx';
Fy=Fy';
Fz=Fz';
mx=mx';
my=my';
mz=mz';

% Assign variables to virtual targets
fm_condx=p(4,:);
fm_condy=p(5,:);
fm_condz=p(6,:);

fl_condx=p(1,:);
fl_condy=p(2,:);
fl_condz=p(3,:);

proxx=p(7,:);
proxy=p(8,:);
proxz=p(9,:);

distx=p(10,:);
disty=p(11,:);
distz=p(12,:);
```

```
% Resultant Force Vector
r=sqrt(Fx.^2+Fy.^2+Fz.^2);

% Unit vectors
rx=Fx./r;
ry=Fy./r;
rz=Fz./r;

w=mx.*rx+my.*ry+mz.*rz;

qx=mx-w.*rx;
qy=my-w.*ry;
qz=mz-w.*rz;

%Position of x and y intercepts
pz=0.0405;  % to center of forceplate in z direction
py=(qx+pz*Fy)./Fz;
px=(pz*Fx-qy)./Fz;


% Change of units from mm to cm
px=100*px;
py=100*py;

% Change units to N for torque vectors
tx=100*w.*rx;
ty=100*w.*ry;
tz=100*w.*rz;

%Transformation from force plate CS to Lab CS
T1=[0 1 0; 0 0 -1; -1 0 0]; % Transformation matrix

COPx=1.0*py+Xo;
COPz=-1.0*px+Zo;
COPy=0;

Rf=-[Fx Fy Fz]*T1';
Rt=-[tx ty tz]*T1';

Fx=Rf(:,1);     Fy=Rf(:,2);       Fz=Rf(:,3);
tx=Rt(:,1);     ty=Rt(:,2);       tz=Rt(:,3);


% Define the z variable of ICR by the middle of the 2 condyles
KJCx=(fm_condx'+fl_condx')/2;
```

```
KJCy=(fm_condy'+fl_condy')/2;
KJCz=(fm_condz'+fl_condz')/2;

% COP to ICR Position Vector
Rcpx=COPx-ICRix';
Rcpy=COPy-ICRiy';
Rcpz=COPz-KJCz;

Rcpx2=COPx-KJCx;
Rcpy2=COPy-KJCy;


%Calculation of Knee moments in Lab CS
Mx=Rcpy.*Fz-Rcpz.*Fy+tx;
My=Rcpz.*Fy-Rcpx.*Fz+tz;
Mz=Rcpx.*Fy-Rcpy.*Fx+tz;

Mx2=Rcpy2.*Fz-Rcpz.*Fy+tx;
My2=Rcpz.*Fy-Rcpx2.*Fz+tz;
Mz2=Rcpx2.*Fy-Rcpy2.*Fx+tz;

for i=1:max(size(Fx))
        % Create vectors containing x,y,z
fl=[fl_condx(i)' fl_condy(i)' fl_condz(i)'];
fm=[fm_condx(i)' fm_condy(i)' fm_condz(i)'];

prox=[proxx(i)' proxy(i)' proxz(i)'];
dist=[distx(i)' disty(i)' distz(i)'];

% Create Y axis of Thigh and Z axis of Shank
Yt=(fm-fl)/norm(fm-fl);
Zs=(prox-dist)/norm(prox-dist);

% Create axis of rotations
e3=Zs';
e2=Yt';
e1=cross(Yt',Zs')/norm(cross(Yt',Zs'));


T=[e1'; e2'; e3'];
M=[Mx(i) My(i) Mz(i)];
M2=[Mx2(i) My2(i) Mz2(i)];


Mm=inv(T)*M';
Mm2=inv(T)*M2';
```

```
m_flex(i)=Mm(2);
m_flex2(i)=Mm2(2);

ecx(i)=e3(1);
ecy(i)=e3(2);
ecz(i)=e3(3);

end

M_flex=m_flex/(100*BW/9.81);

M_flex2=m_flex2/(100*BW/9.81);

ec=[ecx' ecy' ecz'];



%%%%%%%%%%%%%%%%%%%%%%%%%%%%%%%%%%%%%%%%%%%%%%%%%%%%%%%%%%%%%%%%%%%%%%%
%                        change_length2 Function Code                    %
%%%%%%%%%%%%%%%%%%%%%%%%%%%%%%%%%%%%%%%%%%%%%%%%%%%%%%%%%%%%%%%%%%%%%%%

function [lchg, strain]=change_length2( Lacl, Lpcl, Llcl)

% The ligaments are strained at full extension, therefore
% these position should not be taken as the Lo position.
% The strain values were reported in the article, and used
% to calculate the Lo position for all ligaments. The Length
% at full extension was used in combination with the strain
% at full extension to obtain the correct Lo values.

Eacl=.031;    % strain value at full extension (average between anterior and
posterior fibers)
Epcl=.05;             % strain value at full extension
Elcl=.05;             % strain value at full extension

Lfeacl=3.620728;          % value taken from Lacl at 0 degrees of flexion
Lfepcl=3.4352;            % value taken from Lpcl at 0 degrees of flexion
Lfelcl=6.811496;          % value taken from Llcl at 0 degrees of flexion

Loacl=Lfeacl/(Eacl+1);  % Calculation of the original "unstrained" length
Lopcl=Lfepcl/(Epcl+1);
Lolcl=Lfelcl/(Elcl+1);

Dacl=Lacl-Loacl;                  % Calculation of the change in length
Dpcl=Lpcl-Lopcl;
```

```
Dlcl=Llcl-Lolcl;

if Dacl> 0
  Sacl=Dacl/Loacl;
else
  Sacl=0;

end

if Dpcl>0
  Spcl=Dpcl/Lopcl;
else
  Spcl=0;
end

 if Dlcl>0
  Slcl=Dlcl/Lolcl;
else
  Slcl=0;
end

lchg=[Dacl; Dpcl; Dlcl];
strain=[Sacl; Spcl; Slcl];


%%%%%%%%%%%%%%%%%%%%%%%%%%%%%%%%%%%%%%%%%%%%
%                    lig_force2 Function Code                         %
%%%%%%%%%%%%%%%%%%%%%%%%%%%%%%%%%%%%%%%%%%%%

function [Facl, Fpcl, Flcl]=lig_force2(lchg, modelratio)


% Function lig_force calculated the resolved force at the
% ACL, PCL and LCL. The stiffness parameter is constant
% Change in length is read from the main script
% A negative change in length of the ligament indicates
% buckling resulting in F=0 Force Units will be in Newtons.


kacl=20; % Stiffness units are in N/mm2
kpcl=17.5;
klcl=15;

Dacl=lchg(1)*modelratio/10;   % Change in length units are in "Real" units (mm)
Dpcl=lchg(2)*modelratio/10;
Dlcl=lchg(3)*modelratio/10;
```

```
if Dacl> 0
  Facl=kacl*(Dacl^2);
  while Facl>1700
    kacl=kacl-0.01;
    Facl=kacl*(Dacl^2);
  end

else
  Facl=0;

end

if Dpcl>0
  Fpcl=kpcl*(Dpcl^2);
  while Fpcl>2840
    kpcl=kpcl-0.01;
    Fpcl=kpcl*(Dpcl^2);
  end

else
  Fpcl=0;
end

 if Dlcl>0
   Flcl=klcl*(Dlcl^2);
   while Flcl>1000
     klcl=klcl-0.01;
     Flcl=klcl*(Dlcl^2);
  end

else
  Flcl=0;
end


%%%%%%%%%%%%%%%%%%%%%%%%%%%%%%%%%%%%%%%%%%
%                 moments Function Code                    %
%%%%%%%%%%%%%%%%%%%%%%%%%%%%%%%%%%%%%%%%%%

function [Maz, Mpz, Mlz, Flx,Fly]=moments (e3y,BW, modelratio,JCx, JCy,
angacl, angpcl, anglcl, Rlacl, Rlpcl, Rllcl, jp, Insertiontacl, Insertiontpcl,
Insertiontlcl, Insertiontlcly, Facl,Fpcl,Flcl)


% Set X-parameters for the point of application of the
% ligament force at the tibial plateau
```

```
aclpx=Insertiontacl;
pclpx=Insertiontpcl;
lclpx=Insertiontlcl;

% Estimation of the perpendicular distance in the X-
% direction from the  ligament's force point of application
% to the JC.  Multiply by modelratio to convert to real
% units (mm). Divide by 10 to convert to cm. (same units as
% e-moments calculation)

dpxacl=(JCx-aclpx)*(modelratio/10);
dpxpcl=(pclpx-JCx)*(modelratio/10);
dpxlcl=(lclpx-JCx)*(modelratio/10);


% Set Y-parameters for the point of application of the
% ligament force at the tibial plateau for the ACL and PCL.
% The LCL has point of application lower on the tibia.

aclpy=jp;
pclpy=jp;
lclpy=Insertiontlcly;

% Estimation of the perpendicular distance in the Y-
% direction from the ligament to the JC.

dpyacl=(JCy-aclpy)*(modelratio/10);
dpypcl=(JCy-pclpy)*(modelratio/10);
dpylcl=(JCy-lclpy)*(modelratio/10);


% + Fy --> Superior pull from the tibia (origin of forces
% taken at tibia plateau)
% + Fx --> Posterior pull from the tibia for ACL and LCL --
% Anterior Pull for PCL (origin of forces taken at tibia
% plateau)

Faclx=Facl*(cos(angacl));      Facly=Facl*(sin(angacl));
Fpclx=Fpcl*(cos(angpcl));      Fpcly=Fpcl*(sin(angpcl));
Flclx=Flcl*(cos(anglcl));      Flcly=Flcl*(sin(anglcl));

% - CW and + CCW
% Units for the moments Nmm
```

```
Macl=-(Facly*dpxacl)+(Faclx*dpyacl);
Mpcl=(Fpcly*dpxpcl)-(Fpclx*dpypcl);
Mlcl=(Flcly*dpxlcl)-(Flclx*dpylcl);


% Transformation of the calculated moments about the true
% medial-lateral axis of the knee joint.

  Maclz=Macl*e3y;
  Mpclz=Mpcl*e3y;
  Mlclz=Mlcl*e3y;

 %Normalize to %BW for comparison
Maz=Maclz/(100*BW/9.81);
Mpz=Mpclz/(100*BW/9.81);
Mlz=Mlclz/(100*BW/9.81);


Flx=[Faclx Fpclx Flclx];
Fly=[Facly Fpcly Flcly];
```

APPENDIX B

APPENDIX B

Mathcad Template 1

Mathcad Template used for the calculation of the ICR

Reading Thigh and Shank Target location from KTA file (modified).

Thigh Targets

Ta := C:\..\a5.xls Tb := C:\..\a5.xls Tc := C:\..\a5.xls

Shank Targets

Sa := C:\..\a5.xls Sb := C:\..\a5.xls Sc := C:\..\a5.xls

Transpose Matrix to allow long vector format

$Tar := Ta^T$ $Tbr := Tb^T$ $Tcr := Tc^T$ $Sar := Sa^T$ $Sbr := Sb^T$ $Scr := Sc^T$

Calculations for Frame 1

Definition of i and delta t

$i := 0$ Define the first frame to calculate the second forward difference

$\Delta t := 0.01$ Sampling rate of cameras (100 Hz.)

Calculation of Linear Velocity for 2 targets per segment using Forward Difference Equations - (Burington, 1973)

$$Vtc(i) := \left(\frac{1}{12\cdot\Delta t}\right)\cdot\left(-25\cdot Tcr^{\langle i\rangle} + 48\cdot Tcr^{\langle i+1\rangle} - 36\cdot Tcr^{\langle i+2\rangle} + 16\cdot Tcr^{\langle i+3\rangle} - 3\cdot Tcr^{\langle i+4\rangle}\right)$$

$$Vtb(i) := \left(\frac{1}{12\cdot\Delta t}\right)\cdot\left(-25\cdot Tbr^{\langle i\rangle} + 48\cdot Tbr^{\langle i+1\rangle} - 36\cdot Tbr^{\langle i+2\rangle} + 16\cdot Tbr^{\langle i+3\rangle} - 3\cdot Tbr^{\langle i+4\rangle}\right)$$

$$Vsa(i) := \left(\frac{1}{12\cdot\Delta t}\right)\cdot\left(-25\cdot Sar^{\langle i\rangle} + 48\cdot Sar^{\langle i+1\rangle} - 36\cdot Sar^{\langle i+2\rangle} + 16\cdot Sar^{\langle i+3\rangle} - 3\cdot Sar^{\langle i+4\rangle}\right)$$

$$Vsb(i) := \left(\frac{1}{12\cdot\Delta t}\right)\cdot\left(-25\cdot Sbr^{\langle i\rangle} + 48\cdot Sbr^{\langle i+1\rangle} - 36\cdot Sbr^{\langle i+2\rangle} + 16\cdot Sbr^{\langle i+3\rangle} - 3\cdot Sbr^{\langle i+4\rangle}\right)$$

Definition of position vectors between targets in the same segment

$$r_{tba}(i) := Tcr^{\langle i \rangle} - Tbr^{\langle i \rangle} \qquad r_{sba}(i) := Sbr^{\langle i \rangle} - Sar^{\langle i \rangle}$$

Definition of relative velocity between the velocities of targets in the dame segment

$$vtba(i) := Vtc(i) - Vtb(i) \qquad vsba(i) := Vsb(i) - Vsa(i)$$

Calculation of angular velocity of the thigh and shank respectively

$$\omega_t(i) := \frac{r_{tba}(i) \times vtba(i)}{r_{tba}(i) \cdot r_{tba}(i)} \qquad \omega_s(i) := \frac{r_{sba}(i) \times vsba(i)}{r_{sba}(i) \cdot r_{sba}(i)}$$

Calculation of Joint's angular velocity

$$\omega_j(i) := \omega_s(i) - \omega_t(i)$$

Definition of relative vectors and linear velocities between targets in different segments

$$vts(i) := Vtb(i) - Vsa(i) \qquad r_{ts}(i) := Tbr^{\langle i \rangle} - Sar^{\langle i \rangle}$$

$$vst(i) := Vsa(i) - Vtb(i) \qquad r_{st}(i) := Sar^{\langle i \rangle} - Tbr^{\langle i \rangle}$$

Calculation of position vector from thigh and shank targets to ICR
(Class Notes MSM442, 1998)

$$r_{jct}(i) := \left[\frac{\left(\omega_j(i) \times vts(i)\right) + r_{ts}(i) \cdot \left(\omega_j(i) \cdot \omega_s(i)\right)}{\left(\omega_j(i) \cdot \omega_j(i)\right)} \right] \cdot -1$$

$$r_{jcs}(i) := \left[\frac{\omega_j(i) \times vst(i) + r_{st}(i) \cdot \left(\omega_j(i) \cdot \omega_t(i)\right)}{\omega_j(i) \cdot \omega_j(i)} \right]$$

Transformation of ICR into Lab Coordinate System

$$ICR(i) := Tbr^{\langle i \rangle} + r_{jct}(i) \qquad ICR_{20} := Sar^{\langle i \rangle} + r_{jcs}(i)$$

Calculations for Frame 2

$i := 1$ Identification of Frame 2

Calculation of Linear Velocity for 2 targets per segment
using Forward Difference Equations - (Burington, 1973)

$$Vtc(i) := \left(\frac{1}{12 \cdot \Delta t}\right) \cdot \left(-3 \cdot Tcr^{\langle i-1 \rangle} - 10 \cdot Tcr^{\langle i \rangle} + 18 \cdot Tcr^{\langle i+1 \rangle} - 6 \cdot Tcr^{\langle i+2 \rangle} + Tcr^{\langle i+3 \rangle}\right)$$

$$Vtb(i) := \left(\frac{1}{12 \cdot \Delta t}\right) \cdot \left(-3 \cdot Tbr^{\langle i-1 \rangle} - 10 \cdot Tbr^{\langle i \rangle} + 18 \cdot Tbr^{\langle i+1 \rangle} - 6 \cdot Tbr^{\langle i+2 \rangle} + Tbr^{\langle i+3 \rangle}\right)$$

$$Vsa(i) := \left(\frac{1}{12 \cdot \Delta t}\right) \cdot \left(-3 \cdot Sar^{\langle i-1 \rangle} - 10 \cdot Sar^{\langle i \rangle} + 18 \cdot Sar^{\langle i+1 \rangle} - 6 \cdot Sar^{\langle i+2 \rangle} + Sar^{\langle i+3 \rangle}\right)$$

$$Vsb(i) := \left(\frac{1}{12 \cdot \Delta t}\right) \cdot \left(\left(-3 \cdot Sbr^{\langle i-1 \rangle} - 10 \cdot Sbr^{\langle i \rangle} + 18 \cdot Sbr^{\langle i+1 \rangle} - 6 \cdot Sbr^{\langle i+2 \rangle} + Sbr^{\langle i+3 \rangle}\right)\right)$$

Definition of position vectors between targets in the same segment

$$r_{tba}(i) := Tcr^{\langle i \rangle} - Tbr^{\langle i \rangle} \qquad r_{sba}(i) := Sbr^{\langle i \rangle} - Sar^{\langle i \rangle}$$

Definition of relative velocity between the velocities of targets in the dame segment

$$vtba(i) := Vtc(i) - Vtb(i) \qquad vsba(i) := Vsb(i) - Vsa(i)$$

Calculation of angular velocity of the thigh and shank respectively

$$\omega_t(i) := \frac{r_{tba}(i) \times vtba(i)}{r_{tba}(i) \cdot r_{tba}(i)} \qquad \omega_s(i) := \frac{r_{sba}(i) \times vsba(i)}{r_{sba}(i) \cdot r_{sba}(i)}$$

Calculation of Joint's angular velocity

$$\omega_j(i) := \omega_s(i) - \omega_t(i)$$

Definition of relative vectors and linear velocities between targets in different segments

$$vts(i) := Vtb(i) - Vsa(i) \qquad r_{ts}(i) := Tbr^{\langle i \rangle} - Sar^{\langle i \rangle}$$

$$vst(i) := Vsa(i) - Vtb(i) \qquad r_{st}(i) := Sar^{\langle i \rangle} - Tbr^{\langle i \rangle}$$

Calculation of position vector from thigh and shank targets to ICR

(Class Notes MSM442, 1998)

$$r_{jct}(i) := \left[\frac{\left(\omega_j(i) \times vts(i)\right) + r_{ts}(i) \cdot \left(\omega_j(i) \cdot \omega_s(i)\right)}{\left(\omega_j(i) \cdot \omega_j(i)\right)} \right] - 1$$

$$r_{jcs}(i) := \left[\frac{\omega_j(i) \times vst(i) + r_{st}(i) \cdot \left(\omega_j(i) \cdot \omega_t(i)\right)}{\omega_j(i) \cdot \omega_j(i)} \right]$$

Transformation of ICR into Lab Coordinate System

$$ICR(i) := Tbr^{\langle i \rangle} + r_{jct}(i) \qquad ICR_{21} := Sar^{\langle i \rangle} + r_{jcs}(i)$$

Calculations for Rest of the file

$i := 2, 3 .. 500$ Definition of frames - Upper limit can be adjusted according to file length.

Calculation of Linear Velocity for 2 targets per segment
using Forward Difference Equations - (Burington, 1973)

$$Vtc(i) := \left(\frac{1}{12 \cdot \Delta t}\right) \cdot \left(Tcr^{\langle i-2 \rangle} - 8 \cdot Tcr^{\langle i-1 \rangle} + 8 \cdot Tcr^{\langle i+1 \rangle} - Tcr^{\langle i+2 \rangle}\right)$$

$$Vtb(i) := \left(\frac{1}{12 \cdot \Delta t}\right) \cdot \left(Tbr^{\langle i-2 \rangle} - 8 \cdot Tbr^{\langle i-1 \rangle} + 8 \cdot Tbr^{\langle i+1 \rangle} - Tbr^{\langle i+2 \rangle}\right)$$

$$Vsa(i) := \left(\frac{1}{12 \cdot \Delta t}\right) \cdot \left(Sar^{\langle i-2 \rangle} - 8 \cdot Sar^{\langle i-1 \rangle} + 8 \cdot Sar^{\langle i+1 \rangle} - Sar^{\langle i+2 \rangle}\right)$$

$$Vsb(i) := \left(\frac{1}{12 \cdot \Delta t}\right) \cdot \left(Sbr^{\langle i-2 \rangle} - 8 \cdot Sbr^{\langle i-1 \rangle} + 8 \cdot Sbr^{\langle i+1 \rangle} - Sbr^{\langle i+2 \rangle}\right)$$

Definition of position vectors between targets in the same segment

$$r_{tba}(i) := Tcr^{\langle i \rangle} - Tbr^{\langle i \rangle} \qquad r_{sba}(i) := Sbr^{\langle i \rangle} - Sar^{\langle i \rangle}$$

Definition of relative velocity between the velocities of targets in the dame segment

$$vtba(i) := Vtc(i) - Vtb(i) \qquad vsba(i) := Vsb(i) - Vsa(i)$$

Calculation of angular velocity of the thigh and shank respectively

$$\omega_t(i) := \frac{r_{tba}(i) \times vtba(i)}{r_{tba}(i) \cdot r_{tba}(i)} \qquad \omega_s(i) := \frac{r_{sba}(i) \times vsba(i)}{r_{sba}(i) \cdot r_{sba}(i)}$$

Calculation of Joint's angular velocity

$$\omega_j(i) := \omega_s(i) - \omega_t(i)$$

Definition of relative vectors and linear velocities between targets in different segments

$$vts(i) := Vtb(i) - Vsa(i) \qquad r_{ts}(i) := Tbr^{\langle i \rangle} - Sar^{\langle i \rangle}$$

$$vst(i) := Vsa(i) - Vtb(i) \qquad r_{st}(i) := Sar^{\langle i \rangle} - Tbr^{\langle i \rangle}$$

Calculation of position vector from thigh and shank targets to ICR
(Class Notes MSM442, 1998)

$$r_{jct}(i) := \left[\frac{\left(\omega_j(i) \times vts(i)\right) + r_{ts}(i) \cdot \left(\omega_j(i) \cdot \omega_s(i)\right)}{\left(\omega_j(i) \cdot \omega_j(i)\right)} \right] - 1$$

$$r_{jcs}(i) := \left[\frac{\omega_j(i) \times vst(i) + r_{st}(i) \cdot \left(\omega_j(i) \cdot \omega_t(i)\right)}{\omega_j(i) \cdot \omega_j(i)} \right]$$

Transformation of ICR into Lab Coordinate System

$$ICR(i) := Tbr^{\langle i \rangle} + r_{jct}(i) \qquad ICR_2(i) := Sar^{\langle i \rangle} + r_{jcs}(i)$$

Mathcad Template used in the Transformation of ICR to the Shank Coordinate System

Read ICR (in Lab CS) from previous Mathcad file

Reference:C:\Dissertation\ICR-LCS.mcd

Reading target locations from modified KTA file

Thigh Targets

Ta := C:\..\a5n.xls Tb := C:\..\a5n.xls Tc := C:\..\a5n.xls

Shank Targets

Sa := C:\..\a5n.xls Sb := C:\..\a5n.xls Sc := C:\..\a5n.xls

Transpose of matrix

$Tar := Ta^T$ $Tbr := Tb^T$ $Tcr := Tc^T$ $Sar := Sa^T$ $Sbr := Sb^T$ $Scr := Sc^T$

Reading Force values from FRC file

$F_e :=$ C:\..\a5cs.frc

Transpose of Matric

$F_{er} := F_e^T$

Definition of frames in the file

$i := 0, 1 .. 499$

Definition of position vectors between segment targets

$rtab(i) := Tar^{\langle i \rangle} - Tbr^{\langle i \rangle}$ $rsba(i) := Sbr^{\langle i \rangle} - Sar^{\langle i \rangle}$

$rtcb(i) := Tcr^{\langle i \rangle} - Tbr^{\langle i \rangle}$ $rsca(i) := Scr^{\langle i \rangle} - Sar^{\langle i \rangle}$

Definition of segmental coordinate system for thigh and shank respectively

$$k_t(i) := \frac{rtab(i) \times rtcb(i)}{|rtab(i) \times rtcb(i)|} \qquad k_s(i) := \frac{rsba(i) \times rsca(i)}{|rsba(i) \times rsca(i)|}$$ k + medial

$$i_t(i) := \frac{rtab(i) \times k_t(i)}{|rtab(i) \times k_t(i)|} \qquad i_s(i) := \frac{k_s(i) \times rsba(i)}{|k_s(i) \times rsba(i)|}$$ i + posterior

$$j_t(i) := k_t(i) \times i_t(i) \qquad j_s(i) := k_s(i) \times i_s(i)$$ j + superior

Definition of Transformation matrix

Thigh

$$T_t(i) := \begin{bmatrix} i_t(i)_0 & i_t(i)_1 & i_t(i)_2 \\ j_t(i)_0 & j_t(i)_1 & j_t(i)_2 \\ k_t(i)_0 & k_t(i)_1 & k_t(i)_2 \end{bmatrix}$$

Shank

$$T_s(i) := \begin{bmatrix} i_s(i)_0 & i_s(i)_1 & i_s(i)_2 \\ j_s(i)_0 & j_s(i)_1 & j_s(i)_2 \\ k_s(i)_0 & k_s(i)_1 & k_s(i)_2 \end{bmatrix}$$

Calculation of Relative position between ICR and
Shank Target.

$$R_{isa}(i) := \begin{bmatrix} ICR(i)_0 - (Sar^{\langle i \rangle})_0 \\ ICR(i)_1 - (Sar^{\langle i \rangle})_1 \\ (Sar^{\langle i \rangle})_2 - (Sar^{\langle i \rangle})_2 \end{bmatrix}$$

Transformation of ICR location to Shank CS

$$ICR_s(i) := T_s(i) \cdot R_{isa}(i)$$

Break down of components of ICR location for export to excel file

$$ICR_x(i) := ICR_s(i)_0 \qquad ICR_y(i) := ICR_s(i)_1 \qquad ICR_z(i) := ICR_s(i)_2$$

$$ICRt_x(i) := ICR(i)_0 \qquad ICRt_y(i) := ICR(i)_1$$

Transformation of Force values to Shank CS

$$F_{em}(i) := \begin{bmatrix} \left(F_{er}^{\langle i \rangle}\right)_2 \\ \left(F_{er}^{\langle i \rangle}\right)_0 \\ \left(F_{er}^{\langle i \rangle}\right)_1 \end{bmatrix}$$

$$F_{es}(i) := T_s(i) \cdot F_{em}(i)$$

$$F_{ex}(i) := F_{es}(i)_0 \quad F_{ey}(i) := F_{es}(i)_1 \quad F_{ez}(i) := F_{es}(i)_2$$

Variables read in excel.

$$ICR_x(i) = \qquad ICR_y(i) =$$

$$ICRt_x(i) = \qquad ICRt_y(i) =$$

$$F_{ex}(i) = \qquad F_{ey}(i) =$$

APPENDIX C

APPENDIX C

Mathcad Template 3

Mathcad Template used in the solution of patello-femoral equilibrium, and in the final solution of the quasi-static model

Input Variables - (Taken from Matlab script)

dis_values := C:\..\disp_mdl2n.out

lig_force_v := C:\..\forces_mdl2n.out

dis_vr := dis_values^T

lig_vr := lig_force_v^T

ext_force := C:\..\forces_scs.xls

eforce_vr := ext_force^T

mom_values := C:\..\moms2n.out

cont_value := C:\..\Cont_mdl.out

mom_vr := mom_values^T

cont_vr := cont_value^T

i := 25 Frame from motion file - Calculations can be executed 1 frame at a time

Definition of input variables

Ixant := (dis_vr <i>)

dispx := (dis_vr <i>)

dispy := (dis_vr <i>)

Xct := (cont_vr <i>)

Constant Variables of the Tibio-femoral and Patello-femoral models

$Ptx := 4 \cdot \frac{1.644}{6.6285}$

$Pty := 15 \cdot \frac{1.644}{6.6285}$

$w2 := \frac{7}{6.6285}$

Ptyinser := -4.7124 – Pty

Ptxinser := -7.0686 – Ptx

Tryf := 1.5

$ptwidth := 9 \cdot \frac{1.644}{6.6285}$

$ptlength := \frac{39.4}{6.6285}$

ptwidth2 := ptwidth – w2

$trochr := \frac{22}{6.6285}$

Trx := | -7.0686 | – trochr

Trxtf := Ixant + trochr

$LPTe := \frac{47.3}{6.6285}$ $jp := -4.7124$

$Trxt := Trxtf + dispx$

$Try := Tryf + dispy$

Knee Flexion Angle

$theta := (dis\_vr^{\langle i \rangle})_0 \cdot deg$

Ligament forces

$L_{aclx} := (lig\_vr^{\langle i \rangle})_1$ $L_{pclx} := (lig\_vr^{\langle i \rangle})_2$ $L_{lclx} := (lig\_vr^{\langle i \rangle})_3$

$L_{acly} := (lig\_vr^{\langle i \rangle})_4$ $L_{pcly} := (lig\_vr^{\langle i \rangle})_5$ $L_{lcly} := (lig\_vr^{\langle i \rangle})_6$

Ligament Moments

$M_{acl} := (mom\_vr^{\langle i \rangle})_1$ $M_{pcl} := (mom\_vr^{\langle i \rangle})_2$ $M_{lcl} := (mom\_vr^{\langle i \rangle})_3$

External Forces

$F_{eh} := (eforce\_vr^{\langle i \rangle})_0$ $F_{ev} := (eforce\_vr^{\langle i \rangle})_1$

External Moment

$M_e := (mom\_vr^{\langle i \rangle})_4$

Input paramenters - From Matlab script

$\Sigma F_{lx} := L_{aclx} - L_{pclx} + L_{lclx}$ Horizontal Internal Forces $BW := 850.7$ Body Weight

$\Sigma F_{ly} := (L_{acly} + L_{pcly} + L_{lcly})$ Vertical Internal Forces $norm := \frac{BW}{9.81}$

$\Sigma F_{ex} := F_{eh}$ Horizontal External Forces $\Sigma F_{ey} := F_{ev}$ Vertical External Forces

$\Sigma M_l := (M_{acl} + M_{pcl} + M_{lcl}) \cdot norm$ Internal Moments

$\Sigma M_e := M_e \cdot norm$ External Moments (Moments caused by extrenal forces)

$Ppax := -10.1846$ $JCx := (dis\_vr^{\langle i \rangle})$

$Ppay := 3.0058$ $JCy := (dis\_vr^{\langle i \rangle})$

Initial Values for Calculated parameters

beta := 5·deg anga := 1

alpha := .1 angc := 1

a := 1 cc := 1 pl := 0.1

Set of Simultaneous equations

Due to Margins limitations the set of similtaneous equations used at this point are presented at the end of the Appendix.

Calculations beyond this point can only be performed after obtaining values for beta, pl, alpha, a, cc, anga, angc after solving the simultaneous equations.

$$y := (Ptyinser + \cos(beta)\cdot LPTe)$$

$$x := (Ptxinser - \sin(beta)\cdot LPTe)$$

$$C_x := (x - \sin(anga - alpha)\cdot cc) \qquad C_y := (y + \cos(anga - alpha)\cdot cc)$$

$$\gamma := \begin{bmatrix} (alpha + (90\cdot deg - theta)) & \text{if } 90\cdot deg - theta > alpha \\ ((alpha)) & \text{otherwise} \end{bmatrix} \qquad \delta := (90\cdot deg - beta - alpha)$$

Definition of unit vectors for the 3 patello-femoral forces

$q_{xi} := x + ptlength\cdot\sin(alpha)$ $q_{yi} := y + ptlength\cdot\cos(alpha)$ Insertion of QT on the Patella

Unit vectors

$$e_q := \frac{\begin{bmatrix} q_{xi} - C_x \\ q_{yi} - C_y \\ 0 \end{bmatrix}}{\left\| \begin{bmatrix} q_{xi} - C_x \\ q_{yi} - C_y \\ 0 \end{bmatrix} \right\|} \quad e_{pt} := -\frac{\begin{bmatrix} Ptxinser - C_x \\ Ptyinser - C_y \\ 0 \end{bmatrix}}{\left\| \begin{bmatrix} Ptxinser - C_x \\ Ptyinser - C_y \\ 0 \end{bmatrix} \right\|} \quad e_n := \frac{\begin{bmatrix} PFCx - C_x \\ PFCy - C_y \\ 0 \end{bmatrix}}{\left\| \begin{bmatrix} PFCx - C_x \\ PFCy - C_y \\ 0 \end{bmatrix} \right\|}$$

Perpendicular Distances used in the calculation of moments

$PT_{pery} := (Ptyinser - JCy) \cdot 0.66285$

$PT_{perx} := (Ptxinser - JCx) \cdot 0.66285$

$FC_{pery} := (jp - JCy) \cdot 0.66285$

$FC_{perx} := (Xct - JCx) \cdot 0.66285$

$FH_{perx} := (.7972 - JCx) \cdot 0.66285$

Inverse Matrix solution method - solving for Fpt and Fqt

$$R := \begin{bmatrix} \Sigma F_{ly} + \Sigma F_{ey} \\ \Sigma F_{lx} + \Sigma F_{ex} \\ -\Sigma M_{e} + \Sigma M_{l} \\ 0 \end{bmatrix} \qquad X := \begin{bmatrix} F_{pt} \\ F_{c} \\ F_{hx} \\ F_{qt} \end{bmatrix}$$

$$C := \begin{bmatrix} \cos(beta) & -1 & 0 & 0 \\ \sin(beta) & 0 & -1 & 0 \\ (\sin(beta)) \cdot PT_{pery} - (\cos(beta)) \cdot PT_{perx} & -FC_{perx} & -FC_{pery} & 0 \\ (\sin(\delta)) & 0 & 0 & \sin(\gamma) \end{bmatrix}$$

$$X := \left(C^{T} \cdot C\right)^{-1} \cdot C^{T} \cdot R$$

$$\begin{bmatrix} F_{pt} \\ F_{c} \\ F_{hx} \\ F_{qt} \end{bmatrix} := X$$

$$PFCF := \left(-\cos(\gamma) \cdot F_{qt} - \cos(\delta) \cdot F_{pt}\right)$$

$$\begin{bmatrix} F_{qtx} \\ F_{qty} \end{bmatrix} := \begin{bmatrix} |F_{qt}| \cdot e_{q_0} \\ |F_{qt}| \cdot e_{q_1} \end{bmatrix} \qquad \begin{bmatrix} PFCFx \\ PFCFy \end{bmatrix} := \begin{bmatrix} |PFCF| \cdot e_{n_0} \\ |PFCF| \cdot e_{n_1} \end{bmatrix} \qquad \begin{bmatrix} F_{ptx} \\ F_{pty} \end{bmatrix} := \begin{bmatrix} |F_{pt}| \cdot e_{pt_0} \\ |F_{pt}| \cdot e_{pt_1} \end{bmatrix}$$

$$rtb := \frac{theta}{beta} \qquad rta := \frac{theta}{alpha}$$

Solutions to the simultaneous equations

$$\begin{bmatrix} x \\ y \end{bmatrix} = \begin{bmatrix} -8.683 \\ -1.324 \end{bmatrix}$$

Position of distal-anterior corner of patella

$$\begin{bmatrix} C_x \\ C_y \end{bmatrix} = \begin{bmatrix} -9.466 \\ -0.702 \end{bmatrix}$$

Point of intersection of PF forces

$$\begin{bmatrix} PFCx \\ PFCy \end{bmatrix} =$$

Position of the Patello-femoral contact point

$$\begin{bmatrix} q_{xi} \\ q_{yi} \end{bmatrix} = \begin{bmatrix} -8.089 \\ 4.59 \end{bmatrix}$$

Point of insertion of QT

$$\frac{\delta}{deg} = 79.27$$

Angle between PT force and PFCF

$$\frac{\gamma}{deg} =$$

Angle between QT force and PFCF

$$\frac{beta}{deg} = 5$$

Angle of PT from vertical

$$\frac{alpha}{deg} = 5.73$$

Angle of patella inclination

$$F_{pt} = \begin{bmatrix} F_{ptx} \\ F_{pty} \end{bmatrix} =$$

Patello-femoral mechanism forces

$$F_{qt} = \begin{bmatrix} F_{qtx} \\ F_{qty} \end{bmatrix} =$$

Patello-femoral mechanism forces

$$PFCF = \begin{bmatrix} PFCFx \\ PFCFy \end{bmatrix} =$$

Patello-femoral mechanism forces

$F_c =$ Tibio-femoral Contact Force

$F_{hx} =$ Horizontal Force

$pl = 0.1$ Position of Patello-femoral contact point r.t. patellar length

$LPTe = 7.136$ Length of Patellar Tendon

rtb =

rta =

ratios of beta and alpha relative to the angle of flexion

$$M_c := (FC_{perx} \cdot F_c) - (FC_{pery} \cdot F_{hx})$$

$$\frac{M_c}{norm} =$$

$$M_{pt} := (F_{ptx} \cdot PT_{pery}) - (F_{pty} \cdot PT_{perx})$$

$$\frac{M_{pt}}{norm} =$$

Set of Simlutaneous Equations

Given

$$Ptyinser + \cos(beta)\cdot LPTe = \begin{cases} ((Try + \sin(alpha)\cdot trochr + \sin(alpha)\cdot ptwidth) - (\cos(alpha)\cdot(pl\cdot ptlength))) & \text{if } theta < 100\cdot deg \\ ((Try + \sin(alpha)\cdot trochr + \sin(alpha)\cdot ptwidth2) - (\cos(alpha)\cdot(pl\cdot ptlength))) & \text{otherwise} \end{cases}$$

$$Ptxinser - \sin(beta)\cdot LPTe = \begin{cases} ((Trxt - \cos(alpha)\cdot trochr - (\cos(alpha)\cdot ptwidth)) - (\sin(alpha)\cdot pl\cdot ptlength)) & \text{if } theta < 100\cdot deg \\ ((Trxt - \cos(alpha)\cdot trochr - \cos(alpha)\cdot ptwidth2) - (\sin(alpha)\cdot pl\cdot ptlength)) & \text{otherwise} \end{cases}$$

$$\frac{cc}{\sin(angc)} = \frac{ptlength}{\sin(beta + theta)}$$

$$cc\cdot\sin(90\cdot deg - beta - alpha) = pl\cdot ptlength$$

$$\frac{a}{\sin(anga)} = \frac{ptlength}{\sin(beta + theta)}$$

$$ptlength^2 = a^2 + cc^2 - 2\cdot a\cdot cc\cdot\cos(beta + theta)$$

$$beta + theta = anga + angc$$

$$\begin{bmatrix} beta \\ pl \\ alpha \\ a \\ cc \\ anga \\ angc \end{bmatrix} := Find(beta, pl, alpha, a, cc, anga, angc)$$

APPENDIX D

APPENDIX D

Ligament Forces

Presented in this appendix are the graphs of ligament forces obtained with the model. The graphs (Figure 1A-3B) are presented for each tested condition to allow comparison of the interaction between the ligaments throughout the range of motion. The pattern of tensile forces sustained by the ligaments closely resembles the pattern of ligament strain.

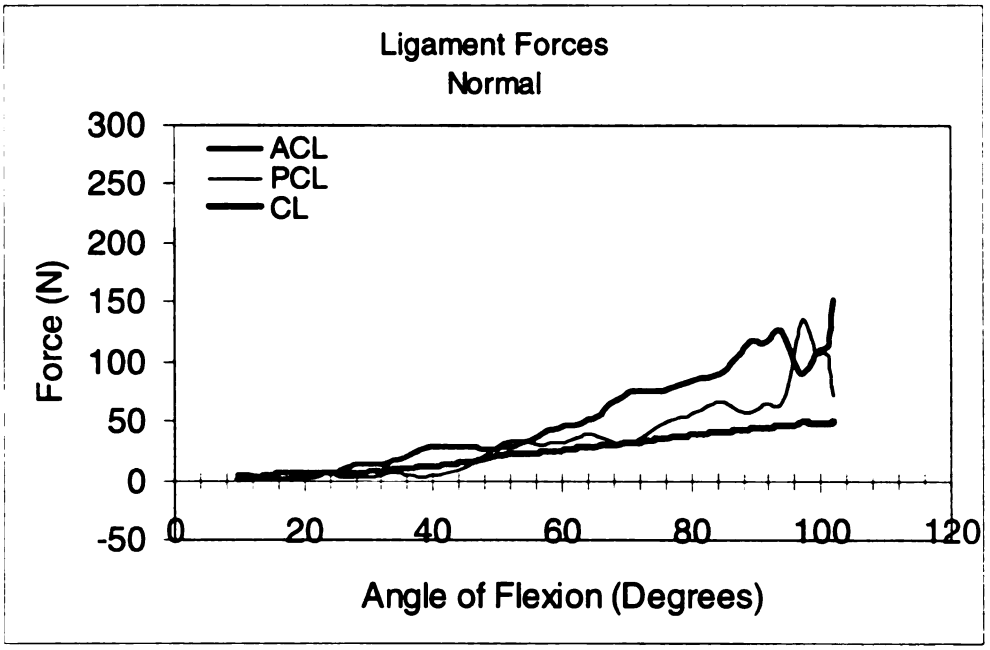

Figure 1A: Ligament forces for the normal knee.

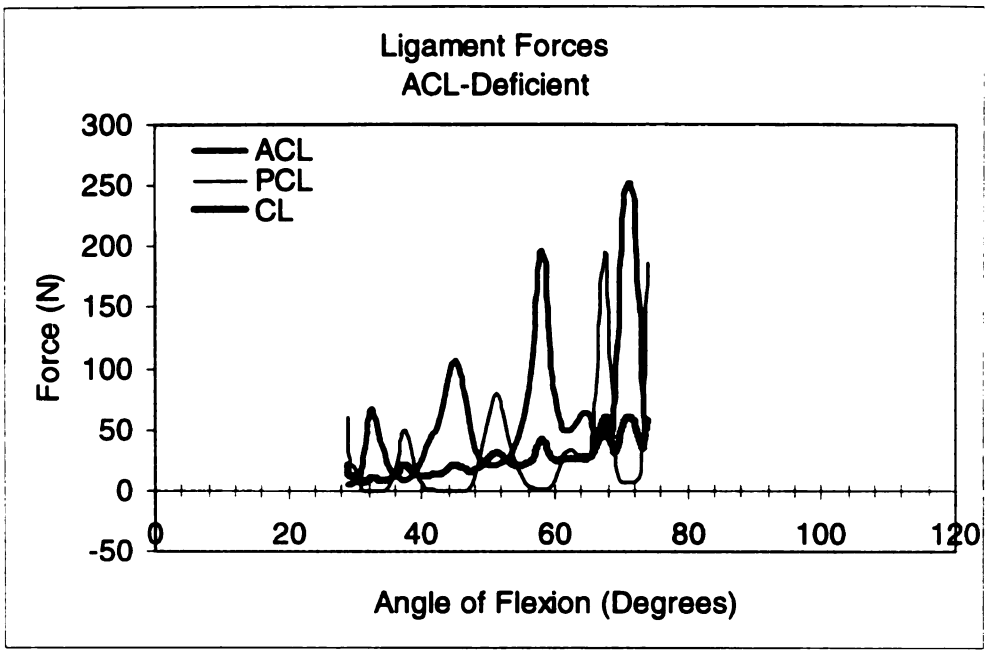

Figure 2A: Ligament Force for the ACL-deficient knee.

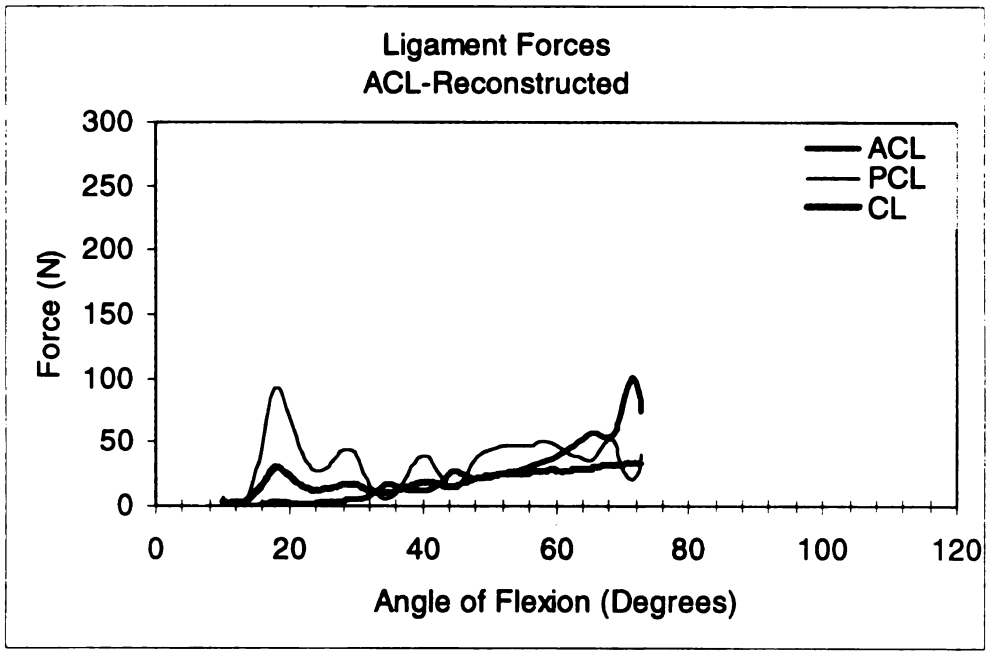

Figure 3A: Ligament forces for the ACL-reconstructed knee.

REFERENCES

REFERENCES

Abdel-Rahman, E., & Hefzy, M. (1993). A two-dimensional dynamic anatomical model of the human knee joint. Journal of Biomechanical Engineering, 115, 357-365.

Aune, A., Nordsletten, L., Skjeldal, S., Madsen, J. & Ekeland, A. (1995). Hamstrings and gastrocnemius co-contraction protects the anterior cruciate ligament against failure: an in vivo study in the rat. Journal of Orthopaedic Research, 13, 147-150.

Balint, D. (1998). A two-dimensional analytical kinematic model for the quantification of rolling and sliding in the human knee joint. Unpublished bachelor's thesis, Michigan State University, East Lansing.

Blackevoort, L., & Huiskes, R. (1991). Ligament-bone interaction in a three-dimensional model of the knee. Journal of Biomechanical Engineering, 113, 263-269.

Burington, R. (1973). Handbook of Mathematical Tables and Formulas (5^{th} ed.). New York: McGraw-Hill.

Butler, D., Noyes, F., & Grood, E. (1980). Ligamentous restrains to anterior-posterior drawer in the human knee. The Journal of Bone and Joint Surgery, 62-A(2), 250-270.

Chan, S., & Seedhom, B. (1995). The effect of the geometry of the tibia on prediction of the cruciate ligament forces: a theoretical analysis. Proceedings of the Institution of Mechanical Engineers [H], (209), 17-30.

Chan, S., & Seedhom, B. (1999). 'Equivalent geometry' of the knee and the prediction of tensions along the cruciates: an experimental study. Journal of Biomechanics, 32, 35-48.

Collins, J., & O'Connor, J. (1991). Muscle-ligament interactions at the knee during walking. Proceedings of the Institution of Mechanical Engineers [H], (205), 11-18.

Daniel, D., Akeson, W., & O'Connor, J. (1990). Knee Ligaments: Structure, Function, Injury, and Repair. Raven Press: New York.

Fuss, F. (1989). Anatomy of the cruciate ligaments and their function in extension and flexion of the human knee joint. The American Journal of Anatomy, 184, 165-176.

Gill, H., & O'Connor, J. (1996). Biarticulating two-dimensional computer model of the human patellofemoral joint. Clinical Biomechanics, 11, 81-89.

Haut, R., & Little, R. (1972). A constitutive equation for collagen fibers. Journal of Biomechanics, 5, 423-430.

Hefty, M., & Grood, E. (1983). An analytical technique for modelling knee joint stiffness. Part II: Ligamentous geometric nonlinearities. Journal of Biomechanical Engineering, 105, 145-153.

Hirokawa, S., & Tsuruno, R. (1997). Hyper-elastic model analysis of anterior cruciate ligament. Medicine and Engineering Physics, 19:7, 637-651.

Hsieh, H., & Walker, P. (1976). Stabilizing mechanisms of the loaded and unloaded knee joint. The Journal of Bone and Joint Surgery, 58-A(1), 87-93.

Hsieh, Y., & Draganich, L. (1998). Increasing quadriceps loads affect the lengths of the ligaments and the kinematics of the knee. Journal of Biomechanics Engineering, 120, 750-756.

Hurschler, C., Loitz-Ramage, B., & Vanderby, R. (1997). A structurally based stress-stretch relationship for tendon and ligament. Journal of Biomechanical Engineering, 119, 392-399.

Imran, A., & O'Connor, J. (1997). Theoretical estimates of cruciate ligament forces: effects of tibial surface geometry and ligament orientations. Proceedings of the Institution of Mechanical Engineers [H], (211), 425-439.

Lanir, Y. (1983). Constitutive equations for fibrous connective tissues. Journal of Biomechanics, 16, 1-12.

Li, G., Rudy, T., Sakane, M., Kanamori, A., Ma, C., & Woo, S. (1999). The importance of quadriceps and hamstring muscle loading on knee kinematics and in-situ forces in the ACL. Journal of Biomechanics, 32, 395-400.

Liao, H.,& Belkoff, S. (1999). A failure model for ligaments. Journal of Biomechanics, 32, 183-188.

Lu, T., & O'Connor, J. (1996). Lines of action and moment arms of the major force-bearing structures crossing the human knee joint: comparison between theory and experiment. Journal of Anatomy, 189, 575-585.

Macnicol, M. (1986). The problem knee- Diagnosis and management in the younger patient. Rockville: Aspen Publishers.

Matsuda, S., Miura, H., Nagamine, R., Urabe, K., Ikenoue, T., Okazaki, K., & Iwamoto, Y. (1999). Posterior tibial slope in the normal and varus knee. The American Journal of Knee Surgery, 12, 165-168.

Meister, K., Talley, M., Horodyski, M., Indelicato, P., Hartzel, J., & Batts, J. (1998). Caudal slope of the tibia and its relationship to noncontact injuries to the ACL. The American Journal of Knee Surgery, 11, 217-219.

Mommersteeg, T., Blackvoort, L., Huiskes, R., Kooloos, G., & Kauer, J. (1996b). Characterization of the mechanical behavior of human knee ligaments: A numerical-experimental approach. Journal of Biomechanics, 29, 151-160.

Mommersteeg, T., Huiskes, R., Blackvoort, L., Kooloos, G., & Kauer, J. (1997). An inverse dynamics modeling approach to determine the restraining function of human knee ligament bundles. Journal of Biomechanics, 30 (2), 139-146.

Mommersteeg, T., Huiskes, R., Blackvoort, L., Kooloos, G., Kauer, J., & Maathuis, P. (1996a). A global verification study of a quasi-static knee model with multi-bundle ligaments. Journal of Biomechanics, 29 (12),1659-1664.

Nicholas, J., & Hershman, E. (1995). The lower extremity ans spine in sports medicine Vol. 2. St Louis: Mosby.

O'Connnor, J., Shercliff, T., Biden, E., Goodfellow, J. (1989). The geometry of the knee in the sagittal plane. Proceedings of the Institution of Mechanical Engineers [H], (203), 223-233.

Pioletti, D., Rakotomanana, L., Benvenuti, J. & Layvraz, P. (1998). Viscoelastic constitutive law in large deformations: application to human knee ligaments and tendons. Journal of Biomechanics, 31, 753-757.

Piziali, R., Seering, W., Nagel, D., & Schurman, D. (1980). The function of the primary ligaments of the knee in anterior-posterior and medial-lateral motions. Journal of Biomechanics, 13, 777-784.

Sakane, M., Fox, R., Woo, S., Livesay, G., Li, G., & Fu, F. (1997). In situ forces in the anterior cruciate ligament and its bundles in response to anterior tibial loads. Journal of Orthopaedic Research, 15, 285-293.

Shelburne, K., & Pandy, M. (1997). A musculoskeletal model of the knee for evaluating ligament forces during isometric contractions. Journal of Biomechanics, 30, 163-176.

Singerman, R., Berilla, J., Archdeacon, M., & Peyser, A. (1999). In vitro forces in the normal and cruciate deficient knee during simulated squatting motion. Journal of Biomechanical Engineering, 121, 234-242.

Solomonow, M., Baratta, R., Zhou, B., Shoji, H., Bose, W., Beck, C., & D'Ambrosia, R. (1987). The synergistic action of the anterior cruciate ligament and thigh

muscles in maintaining joint stability. The American Journal of Sports Medicine, 15, 207-213.

Takai, S., Woo, S., Livesay, G., Adams, D., & Fu, F. (1993). Determination of the in situ loads on the human anterior cruciate ligament. Journal of Orthopaedic Research, 11, 686-695.

Wismans, J., Veldpaus, F., & Janssen, J. (1980). A three-dimensional mathematical model of the knee joint. Journal of Biomechanics, 13, 677-685.

Woo, S., Johnson, G., & Smith, B. (1993). Mathematical modeling of ligaments and tendons. Journal of Biomechanical Engineering, 115, 468-473.

Zavatsky, A., Beard, D., & O'Connor, J. (1994). Cruciate ligament loading during isometric muscle contractions: A theoretical basis for rehabilitation. The American Journal of Sports Medicine, 22, 418-423.

Zavatsky, A., & O'Connor, J. (1992). A model of human knee ligaments in the sagittal plane, Part1 : response to passive flexion. Proceedings of the Institution of Mechanical Engineers [H], (206), 125-134.